2016

Deposits Emplaced In Upper Regime

Ricardo Rafael Hernández Moreira
University of South Carolina

DEPOSITS EMPLACED IN UPPER REGIME

by

Ricardo Rafael Hernández Moreira

Bachelor of Science
Instituto Tecnológico de Santo Domingo, 2003

Master of Science
University of Illinois at Urbana-Champaign, 2007

Submitted in Partial Fulfillment of the Requirements

For the Degree of Doctor of Philosophy in

Civil Engineering

College of Engineering and Computing

University of South Carolina

2016

Accepted by:

Enrica Viparelli, Major Professor

Hanif Chaudrhy, Committee Member

Jasim Imran, Committee Member

Christopher G. St. C. Kendall, Committee Member

Cheryl L. Addy, Vice Provost and Dean of the Graduate School

DEDICATION

I dedicate this dissertation to my family and my friends, teachers and professors, my mentors and advisers, colleagues and peers, whether far or near in time and space. They have been my support system and have been instrumental, in one way or another, in shaping me into who I am. This dissertation is a testament to their belief in me. To them I say thank you.

I also dedicate this work to the engineers and scientists of past and present, who saw it fit to pry into the fundamentals of nature and ask the questions that have shaped my academic and professional life. This work is an effort to both answer some of those questions and come up with many more.

Finally, I dedicate this dissertation to you, the reader. Your life choices have put you in front of it, hopefully through no fault of your own. I hope you find answers to your questions here and enjoy the process. Best of luck to you.

ACKNOWLEDGEMENTS

The author thanks their adviser, Dr. Enrica Viparelli, fully admitting that their expression of gratitude is a gross understatement, for all the support throughout the duration of the doctoral studies from which this body of work is produced—from before day 1 through the end—for their advise, mentorship and friendship.

The author acknowledges the countless tons of sediment moved, dried and bagged by Bradley Huffman and Drew Vautin, as well as all the construction works and data collection. They made difficult tasks look and feel easy.

The dataset resulting from this work has been made publicly available through the assistance of the Sediment Experimentalist Network (SEN) (NSF 1324660). The author further thanks Theo Jeremiah, Rachel Kuprenas, Melissa Bresko, Simran Matthews, Alex Nettles and Christian Pellot for the help in the laboratory during the performance of the experimental work The majority of the students participating in the experiments were supported by the NSF grant EAR-1250641, the others by Dr. Viparelli's start-up fund. The University of South Carolina Support for Minority Advancement in Research Training (SMART) Program supported Sydney Sanders, to whom the author also extends their gratitude.

ABSTRACT

Relatively common to the submarine setting are depositional sequences that begin with a lower erosional boundary, followed in ascending order by a either a graded or an inherently massive basal unit, a relatively coarse parallel laminated unit, a cross laminated unit, a relatively fine parallel laminated unit, and a capping layer of massive mud. These sequences are present in turbidity current, coastal storm and tsunami deposits, and their study is the key to understanding the physical processes governing sediment transport, erosion and deposition in submarine settings, to the reconstruction of global paleoclimate and paleoflow, to the exploration of hydrocarbon reservoirs and to the prediction of natural hazards associated with earthquake and landslide induced tsunamis. A common feature of these deposits is a basal erosional layer underlying a sandy massive unit, i.e. a unit lacking internal structure. Previous studies have shown that these sequences were deposited from waning energy flows, and the mechanism for the emplacement of the basal massive unit is thought to be associated with rapid deposition of suspended sediment. Here we present the results of laboratory experiments specifically designed to test the hypothesis that these massive units can also be emplaced by very intense bedload transport conditions corresponding to what is commonly called sheet flow in the engineering literature. The experiments clearly show that in bedload dominated systems 1) the transition from upper regime plane bed with standard bedload transport to upper regime plane bed with bedload transport in sheet flow mode is gradual

and occurs with the formation of downstream migrating antidunes and thus can be representative of waning energy flows, and 2) in the presence of bedload transport in sheet flow mode, the internal fabric of the emplaced deposits is massive. Noting that in systems transporting medium to coarse sand bedload transport in sheet flow mode occurs for less intense flows than suspended transport, the results of this work demonstrate that the use of current suspension-based models may result in an overestimation of the flow velocities and bed shear stresses of extreme events. Finally, the analysis of time series of bed elevations reveals that the gradual transition from upper regime plane bed with standard bedload transport to upper regime plane bed with bedload transport in sheet flow mode can be modeled in terms of normal probability functions of bed elevations with mean equal to the mean bed elevation and standard deviation that varies with the flow properties. The definition of probability density functions of bed elevations as a function of the flow conditions represents the first and necessary step towards the implementation of a continuous morphodynamic modeling framework for non-uniform bed material that is able to numerically reproduce the internal fabric of the emplaced deposit.

TABLE OF CONTENTS

LIST OF TABLES

LIST OF FIGURES

CHAPTER 1

OVERVIEW OF THE RESEARCH WORK

The interpretation of the stratigraphic record, field studies of modern sedimentary systems and laboratory experiments reveal that the upper regime plane bed is representative of flow and sediment transport conditions, such as river floods [Simons and Richardson, 1962; Nnadi and Wilson, 1995], coastal storms [Bourgeois, 1980; Ribberink and Al-Salem, 1995] and turbidity currents [Middleton, 1967; Sohn, 1999; Kostic, 2014], that are relevant to describe the evolution of sedimentary systems. The study of this regime is thus fundamental to understanding the physical processes governing the morphodynamics of subaerial and submarine settings, to the reconstruction of global paleoclimate and paleoflow, to the exploration of hydrocarbon reservoirs and to the prediction of natural hazards.

A perusal of the literature on sediment transport and depositional fabric reveals that two conflicting definitions of upper regime plane bed are proposed, one with long wavelength and small amplitude downstream migrating bedforms, the other with nearly flat beds under a transport layer of colliding grains few tens of grain diameters thick – the sheet flow layer.

Upper regime units are characteristics of depositional sequences of turbidites and tempestite, i.e. deposits respectively emplaced by turbidity currents and storms (Bouma, 1962; Walker et al., 1983). These sequences present two common features that are relevant for the present study 1) they are characterized by a basal erosional surface

underlying, in ascending order, a coarse basal unit and a parallel laminated unit, and 2) they are deposited by waning energy flows. Field and laboratory studies demonstrated that these parallel laminated units are deposited under upper regime plane bed conditions with long wavelength and small amplitude bedforms (e.g. Cheel and Middleton, 1986, Paola et al., 1989). Thus, recalling that the sequences of interest are deposited by waning energy flows, the basal massive unit has to be emplaced by more intense flow conditions than the overlying parallel laminated unit and these should be able to suppress parallel lamination.

Several mechanisms have been proposed to describe the emplacement of massive turbidites and tempestites (e.g. Lowes, 1982; Breien et al., 2010; Shanmungam, 1996; Cartigny et al., 2014). All the proposed mechanisms associate the emplacement of massive units with a rapid deposition of suspended sediment. None of the proposed mechanisms, however, fully explains how the same sustained event can deposit both the basal massive and the overlying parallel laminated unit. In addition, the proposed mechanisms cannot entirely justify how massive turbidites, which extend long distances in the dip direction and may contain coarser particles as floating clasts, can be emplaced 10's – 100's km downstream of the source (Leeder, 1999).

The central hypothesis of this dissertation is that the basal massive unit of tempestite and turbidite deposits can be emplaced under very intense bedload transport conditions corresponding to what has been called sheet flow in the engineering literature on sediment transport (e.g. Wilson, 1966; Nnadi and Wilson, 1995; Hassan and Ribberink, 2005). The sheet flow is a near bed layer of colliding grains with thickness of the order of10s of grain diameters (Gao, 2008).

For this hypothesis to hold, the transition from upper regime plane bed with bedload transport in sheet flow mode to upper regime plane bed with long wavelength and small amplitude bedforms has to be gradual. A gradual transition only can fully explain the deposition of a basal massive unit underlying a parallel laminated deposit by waning energy flows.

Two groups of laboratory experiments were performed in the Hydraulic Laboratory of the University of South Carolina at Columbia. Noting that he experimental modeling of turbidity currents powerful enough to produce sheet flow conditions has proved elusive, we followed the lead of McBride et al. (1975) and Vrolijk and Southard (1997), and performed the laboratory experiments in open-channel mode, under conditions that are specifically designed to model intense, net-depositional subaqueous flows.

The first group of experiments was performed with uniform sand to study the transition from upper regime plane bed with bedload transport in sheet flow mode to upper regime plane bed with long wavelength and small amplitude bedforms. The second group of experiments was done with a mixture of sediments differing in grain size to observe the internal fabric upper regime deposits.

Main outcome of the first group of experiments is that in bedload dominated systems the transition from upper regime plane bed with long wavelength and small amplitude bedforms to upper regime plane bed with bedload transport in sheet flow mode is gradual and is characterized by the formation of downstream migrating bedforms called antidunes. The antidunes have smaller wavelengths and larger amplitudes than the upper regime plane bed bedforms responsible for the emplacement of parallel laminated deposits. The mode of bedload transport in presence of long wavelength and small

amplitude bedforms is what we refer to as *standard bedload transport*, i.e. a mode of bedload transport in which sediment grains move in a 2-3 grain diameters thick near bed layer with negligible particle-particle interactions. Thus, the transition from one upper regime plane bed to the other is associated with a change in the mode of bedlaod transport. Downstream migrating antidunes form at the transition from one mode of bedload transport to the other.

The second objective of this thesis is to explore the possibility of the implementation of a mathematical framework to quantitatively model at field scale the internal fabric of deposits emplaced by waning energy flows in the upper regime. The modeling hypothesis is that the continuous probabilistic morphodynamic framework proposed by Parker, Paola and Leclair (2000) for mixtures of sediments differing in size is able to reproduce the internal fabric of the deposit. The Parker, Paola and Leclair (PPL) framework, however, cannot yet be fully implemented due to the lack of information describing how particle entrainment and deposition vary in the vertical direction in an alluvial deposit (Blom et al., 2008, Blom, 2008, Viparelli et al., 2016). The definition of the spatial variability of entrainment and deposition in the vertical direction goes well beyond the scope of the present work, thus the test of the modeling hypothesis was approached in two phases.

The one-dimensional form of the PPL framework was implemented to study the response of a gravel bed river to changes in flow regime and sediment supply. This exercise demonstrated that, if the spatial variability of entrainment and deposition is modeled with continuous probability density functions, the computational costs of the

PPL framework are comparable with those of the commonly used layer-based models (Viparelli et al., 2016).

Starting from the work of Wong et al. (2007) on the dispersal of tracer stones in lower regime plane bed experiments, the analysis of time series of bed elevations was performed to characterize the changes in bed elevation associated with bedform migration and to relate them to the characteristics of the flow. This analysis represented the first and necessary step for a physically-based implementation of the PPL framework to predict the internal fabric of upper regime deposits. The results demonstrated that the variability of bed elevation around the mean in the laboratory experiments could be reasonably described with normal probability functions. Further, the standard deviation of the time series of bed elevation resulted to be a function of the flow characteristics. In particular, the standard deviation of the bed elevation, and thus the height of the bed elevation changes, decrease as the mode of bedload transport transitions from standard bedload transport to sheet flow.

Finally, a modified version of the PPL framework is proposed to model tracer stones dispersal in the case of uniform sediment. The time series of bed elevation are used to estimate the net rates of particle entrainment and deposition at different elevations in the alluvial bed. Future research effort is needed to identify the dependence of the elevation specific net entrainment and deposition rates with the characteristics of the flow and the bedload transport and to explore how these rates change in the case of a mixture of sediment particles differing in grain size.

This thesis is organized in three separate studies respectively presented in Chapter 2, 3 and 4. The uniform sediment experiments are described and analyzed in Chapter 2.

The experiments with non-uniform sediment are illustrated and the results are summarized in Chapter 3. The analysis of the time series of bed elevation change and the proposed modeling framework of tracer stones dispersal are presented in Chapter 4. The relevant results of the research effort and future research needs are summarized in Chapter 5.

CHAPTER 2

BEDLOAD TRANSPORT, BEDFORM GEOMETRY AND FLOW RESISTANCE OF UPPER REGIME PLANE BEDS[1]

ABSTRACT

Upper regime plane bed-forms are important to the interpretation of the stratigraphic record and the study of river floods, coastal storms and turbidity currents but how they form remains poorly defined. Two different upper plane bed configurations are described in the literature, one with long wavelength and small amplitude downstream migrating bedforms, the other with nearly flat beds under a transport layer of colliding grains few tens of grain diameters thick – the sheet flow layer. Our laboratory experiments studying the interactions between flow hydrodynamics, mode of bedload transport and bedform geometry characterize these upper regime plane bed configurations. The experiments showed that in the absence of suspended load two upper plane bed configurations exist for increasing values of the bed material transport capacity. The upper plane bed with long wavelength and small amplitude bedforms occurs for a relatively small bed material transport capacity. As the bed material transport capacity increases, downstream

---

1 Ricardo Hernandez Moreira, Bradley J. Huffman, Drew Vautin, Christopher G. St. C. Kendall and Enrica Viparelli. Submitted to *Journal of Geophysical Research – Earth Surface*

migrating antidunes form as a stable bed configuration. Further increasing the bed material transport capacity, the bed flattens out and the sheet flow layer forms. This change in bed configuration is associated with a change in the mode of bedload transport, from *standard bedload transport* with a two-three grain diameter thick bedload layer to *bedload transport in sheet flow mode*. Downstream migrating antidunes form during the sheet flow layer development. Significant form drag is associated with the upper regime bedforms observed in this study.

KEY POINTS

- Two stable upper regime plane bed conditions exist and they differ for the bed configuration and the mode of bedload transport
- Downstream migrating antidunes represent a stable bed configuration in bedload dominated systems
- Significant form drag is associated with upper regime long wavelength and small amplitude bedforms

2.1. INTRODUCTION

The interpretation of the stratigraphic record, field studies of modern sedimentary systems and laboratory experiments reveal that the upper regime plane bed is representative of flow and sediment transport conditions, such as river floods (Simons and Richardson, 1962; Nnadi and Wilson, 1995), coastal storms [Bourgeois, 1980; Ribberink and Al-Salem, 1995] and turbidity currents [Middleton, 1967; Sohn, 1999;

Kostic, 2014], that are relevant to describe the evolution of sedimentary systems. However the main characteristics of the upper regime plane bed are still poorly defined and a represent a matter of debate.

Simons and Richardson [1962] defined the upper regime plane bed as the bed configuration at the transition between the formation of dunes and antidunes. This upper plane bed was associated with a relatively flat bed configuration and small flow resistances compared to bed configurations with dunes and antidunes. Subsequent laboratory experiments [e.g. McBride et al., 1975; Bridge and Best, 1988; Paola et al., 1989; Cheel, 1990; Best and Bridge, 1992] demonstrated that, as dunes were washed out, downstream migrating long wavelength and small amplitude bedforms appeared on the channel bed. In other words laboratory experiments revealed that the bed deposit of the upper regime plane bed at the transition between dunes and antidunes was covered with downstream migrating, long wavelength and small amplitude bedforms that were responsible for the emplacement of parallel laminated units [Paola et al., 1989; Best and Bridge, 1992].

According to Nnadi and Wilson [1995] and Sumer et al. [1996] among others, an upper regime plane bed occurs when the bed is flat and the bed material is transported in a sheet flow layer, which is a tens of grain diameters thick layer of colliding grains [Wilson, 1987, 2005; Nnadi and Wilson, 1992, 1995; Bennett et al., 1997; Sumer et al., 1996; Pugh and Wilson, 1999; Dohmen-Janssen et al., 2001; Dohmen-Janssen and Hanes, 2002; Abrahams and Gao, 2006; Gao, 2008]. The sheet flow layer resembles the expanded bed [Middleton, 1967] and the traction carpet [Sohn, 1997 and references therein] introduced to describe the deposition of massive sandy turbidites.

In summary, notwithstanding the numerous studies on bedforms in sedimentary systems [see Southard, 1991 and Garcia 2008 for thorough reviews] the upper regime plane bed remains poorly defined. In particular, two conflicting definitions have been proposed, one describing a bed configuration with long wavelength and small amplitude bedforms and the other with a sheet flow layer over a nearly flat bed [Bennett and Best, 1997; Nnadi and Wilson, 1997].

Noting that 1) in the Paola et al. [1989] and Best and Bridge [1992] upper regime plane bed experiments part of the bed material was transported in suspension and part as bedload transport in a layer that was few grain diameters thick and with negligible particle-particle interaction; 2) in the Nnadi and Wilson [1995] and Sumer et al. [1996] experiments the bed material was transported in a sheet flow layer; and 3) sheet flow is expected to occur for values of the Shields number greater than 0.5-0.8 [Gao, 2008], we hypothesize that the two upper regime plane bed conditions described in the literature correspond to two different bed configurations associated with different modes of bedload transport.

In particular, upper plane bed conditions with long wavelength and small amplitude bedforms are associated with *standard bedload transport*, i.e. a mode of bedload transport with negligible particle-particle interaction and a bedload layer that is few grain diameter thick, while upper regime plane bed conditions with a flat bed are associated with *bedload transport in sheet flow mode*, i.e. a mode of bedload transport with a near bed layer of colliding particles that is tens of grain diameters thick. Further, we expect that the transition from standard bedload transport to bedload transport in sheet flow mode occurs for increasing values of the bed material transport capacity and, thus, of the

bed shear stress associated with skin friction [Fernandez Luque and Van Beek, 1975; Parker, 2008].

To test this hypothesis we performed laboratory experiments to study the interactions between the flow, the mode of bedload transport and the bed configuration in upper regime plane bed conditions, and to document the transition from upper regime with standard bedload transport [e.g. Paola et al., 1989] to upper regime with bedload transport in sheet flow mode [e.g. Sumer et al., 1996]. The experiments were performed in a sediment feed flume with increasing values of the bedload transport capacity and with medium sand to prevent bed material transport in suspension.

In the experiments the transition from upper plane bed with standard bedload transport to upper plane bed with bedload transport in sheet flow mode occurred with the formation of stable downstream migrating antidunes. In particular, the transition from upper regime plane bed with standard bedload transport to upper regime plane bed with sheet flow transport in sheet flow mode was characterized by a gradual increase in the bedload layer thickness, corresponding to the development of the sheet flow layer. The formation of the sheet flow layer was associated with a change in bedform geometry from downstream migrating, long wavelength and small amplitude bedforms, to downstream migrating antidunes, to a nearly flat bed.

This change in bedform geometry was associated with a gradual change in the flow resistances. The roughness height was highest in the upper regime plane bed experiments with standard bedload transport and was smallest in the upper regime plane bed experiments with bedload transport in sheet flow mode. This change in roughness height

was due to the decrease in form drag during the transition from one upper regime configuration to the other.

2.2. Background information on small scale bedforms relevant to the present study

Following Engelund and Hansen [1967] for a general review on the evolution of small scale bedforms, i.e. bedforms with a height that is small compared to the water depth, we consider an idealized unidirectional laboratory flume in which the velocity is gradually increased. When the flow velocity is close to the threshold for the initiation of motion and the sediment is finer than ~0.6 mm [Parker, 2004] ripples may form and travel in the downstream direction. Ripple are few centimeters high and their wavelengths are few tens of centimeters long. Due to the relatively small wave height, these bedforms do not interact with the water surface. When the sediment is coarser than ~0.6 mm, ripples do not form and the bed is said to be plane.

As the flow velocity increases, dunes form. In general, dunes are asymmetrical bedforms with a relatively long and gently sloping stoss face and a steep downstream migrating lee face [Blom et al., 2003; Kennedy, 1963]. Dunes are present in the vast majority of sand bed rivers, they may be up to several meters high [Nittrouer et al., 2008] and hundreds of meters long [Best, 2005]. Dunes weakly interact with the water surface, with the flow accelerating on the crests with a reduction in the water surface elevation, i.e. the water surface is out of phase with the bed [e.g. Parker, 2004].

If we further increase the flow velocity, the height of the sediment waves decreases and the bed tends to flatten out [Kennedy, 1963] with the formation of downstream

migrating long wavelength and small amplitude bedforms [McBride et al., 1975; Bridge and Best, 1988; Paola et al., 1989; Best and Bridge, 1992]. For another increase in flow velocity nearly symmetrical bedforms called antidunes form [Kennedy, 1963; Engelund and Hansen, 1967]. Antidunes heights and wavelengths are such that the bedforms interact strongly with the water surface. The water surface is in phase with the sediment waves, i.e. it is highest on the crest and lowest on the troughs. As the flow velocity increases, the deformation of the water surface becomes so strong that breaking waves may form [e.g. Kennedy, 1963].

Antidunes can migrate in the upstream and downstream direction [Reynolds, 1965; Engelund, 1970; Fredsøe, 1974]. The observation of downstream migrating antidunes is relatively common in experiments on density and turbidity currents [Spinewine et al., 2009; Sequeiros et al., 2010] but, aside from the works of Kennedy [1960], Carling and Shvidchenko [2002], Nunez-Gonzalez and Martin-Vide [2010; 2011] and Yokokawa et al.[2011], we are not aware of other open channel flow experiments in which downstream migrating antidunes represented a stable configuration of the alluvial deposit.

Cartigny et al. [2014] performed experiments with uniform fine sands (grain diameters of 0.16 mm, 0.265 mm and 0.35 mm) in a sediment recirculating flume to study the evolution of upper regime bedforms for increasing Froude numbers (flow velocity) over a mobile bed. For the lowest Froude number (~0.7) upper regime plane bed formed, but the authors do not describe the bed configuration or the mode of bedload transport. However, the authors follow Simons and Richardson [1962] and define the upper plane bed as a transitional region between dune and antidune bed configurations,

we thus interpret their upper plane bed condition as upper plane bed with standard bedload transport.

At relatively low Froude numbers trains of upstream migrating antidunes formed, with the smallest wavelength bedforms occurring for the highest Froude numbers. Further increasing the Froude number, antidunes evolved into chutes and pools and cyclic steps, i.e. upstream migrating long wavelength and large amplitude bedforms characterized by a hydraulic jump downstream of the lee face. In summary, these experiments showed that as the bed shear stress increases the bed configuration transitions from upper plane bed with standard bedload transport, to downstream migrating antidunes to cyclic steps.

In the chute and pools and cyclic step configurations Cartigny et al. [2014] observed sediment transport in a traction carpet on the stoss side of the bedforms. This observation suggests that bedload transport in sheet flow mode (sheet flow layer = traction carpet) occurred at high Froude numbers and was associated with significant suspended bed material transport and long wavelength upstream migrating bedforms. In other words, upper regime plane bed with bedload transport in sheet flow mode was not observed in upper regime experiments with fine sand and significant suspended transport.

Yokokawa et al. [2011] compiled a large series of experimental data to propose an upper regime bedform phase diagram for antidunes and cyclic steps. The bedform existence regions were defined as functions of the suspension index, equal to the ratio between the shear velocity and the settling velocity, and the Froude number. When the suspension index was smaller than 0.8-1 the bed material was preferentially transported as bedload and downstream migrating antidunes formed. Upstream migrating antidunes

occurred for slightly higher Froude numbers (Fr = 1.3-2.5) than downstream migrating antidunes (Fr = 1-2) and for significant suspended transport of bed material, i.e. suspension index greater than 1. Finally, cyclic steps formed in the case of suspended bed material transport and very large Froude numbers (Fr = 2.5-3.5).

2.3. EXPERIMENTAL SETUP

The experiments were performed in the Hydraulics Laboratory of the Department of Civil and Environmental Engineering of the University of South Carolina, in a 13 m long, 0.50 m wide and 0.70 m deep sediment feed flume with glass sidewalls (Figure 2.1). A 6.9 m long and 0.19 m wide test reach was built with plywood. The flume cross section was gradually reduced from 0.5 m to 0.19 m in the upstream most 2.0 m of the flume. This width reduction was necessary to obtain upper regime conditions with high, but still feasible, feed rates. The test reach started 2.0 m downstream of the flume entrance and ended at the sediment trap.

The constant head tank of the laboratory supplied the flow to the flume. Flow rates were measured with a calibrated orifice plate and a Dwyer 490-1 wet/wet digital differential manometer. The water surface elevation downstream of the sediment trap was controlled with a tailgate. Dry sediment was fed at a constant rate with a Schenck Accurate 600 feeder. Water surface and bed surface elevation profiles were captured with ruler readings through the glass flume wall. Bed configurations were characterized by means of still photographs, time lapses and videos taken with a Nikon d3000 camera. Details on the experimental setup are available through the wiki page of the Sediment

Experimentalist Network (SEN) at *http://sedexp.net/experiment/setting-hydraulics-laboratory-limited-resources*.

2.3.1. EXPERIMENTAL DESIGN

The experimental design consisted in the identification of the sediment type, the flow and the sediment feed rates that would have resulted in the upper regime plane bed configuration characterized by standard bedload transport. Noting that 1) bedload transport in sheet flow mode occurs at higher bed shear stresses than standard bedload transport, 2) threshold conditions for the initiation of bedload transport in sheet flow mode are poorly constrained, and 3) the available relations to predict bedload transport rates underestimate the bedload transport in sheet flow mode [Wilson, 1987] and thus cannot be used in the experimental design, we determined the flow rate that would have resulted in upper plane bed with standard bedload transport for sediment feed rates up to 4 kg/min. We then gradually increased the sediment feed rate to 20 kg/min to document the transition from standard bedload transport to bedload transport in sheet flow mode, which occurs at higher transport capacities than the standard bedload transport.

2.3.1.1. Sediment design

We chose uniform sand with density equal to 2632 kg/m^3, geometric mean diameter, D_g, of 1.11 mm and geometric standard deviation of 1.44 mm. The sediment grain size distribution is shown in Figure 2.2. This material was coarse enough to prevent the

formation of ripples and limit the amount of suspended sediment at the relatively high bed shear stresses typical of the upper regime.

Significant suspended sediment transport occurs when the ratio between the shear velocity, and the fall velocity is greater than ~0.8 [e.g. Sumer et al., 1996]. The shear velocity is defined as $u^* = \sqrt{\tau^* RgD}$, where τ^* is the Shields number defined as $\tau_b/\rho RgD$, with τ_b denoting the bed shear stress, ρ the water density, R the submerged specific gravity of the sediment, g the acceleration of gravity and D the characteristic sediment size. The fall velocity of the 1.11 mm sand in still water estimated with the Dietrich [1982] relation is v_s = 17 cm/s, and the threshold Shields number for significant suspension is equal to 1.03. This value, which is larger than the threshold for the initiation of bedload transport in sheet flow mode, 0.5-0.8 [Gao, 2008], allows us to obtain bedload transport in sheet flow mode with negligible suspension.

2.3.1.2. Design of the experimental conditions

The design of the experiments was performed for mobile bed equilibrium conditions, i.e. conditions of null net erosion or deposition on time scales that were long compared to those of channel bed aggradation and degradation [Parker, 2008]. At mobile bed equilibrium the flow could be approximated as steady and uniform and the calculation of the flow parameters was relatively straightforward [Parker, 2004].

We used the Engelund [1966] and Vanoni [1974] bedform diagrams to identify the flow rates and the sediment feed rates that would have resulted in upper regime plane bed equilibrium conditions with standard bedload transport. In the Engelund [1966] bedform

diagram, the bed configuration was predicted based on the ratio between the average flow velocity U and u^* and the Froude number defined as $Fr = U/\sqrt{gH}$, with H denoting the flow depth. In the Vanoni [1974] diagram, the bed configuration was predicted based on the Froude number and the ratio between the flow depth H and the characteristic sediment size D.

For different combinations of flow and sediment feed rate, the parameters Fr, H/D, U and u^* were estimated as follows.

At mobile bed equilibrium in a sediment feed flume the sediment feed rate was equal to the bedload transport capacity, thus u^* was estimated from the Meyer-Peter and Muller relation modified by Wong and Parker [2006] and the Ashida and Michiue relation [Parker, 2008], which related the volumetric bedload transport capacity q_b to the excess Shields number $\left(\tau^* - \tau^*_{ref}\right)$, with τ^*_{ref} denoting a reference value of the Shields number that varied from one bedload relation to the other [Parker, 2008].

In a 19 cm wide flume the different roughness between the smooth sidewalls and the rough bed was likely to be significant, thus u^* had to be interpreted as a sidewall corrected shear velocity [Vanoni and Brooks, 1957]. It could thus be used to enter the Engelund [1966] diagram, but could not be directly used to estimate U and H.

We estimated U and H following the inverse of the Vanoni and Brooks [1957] sidewall correction procedure as outlined in Viparelli et al. [2015]. These calculations were performed with a roughness height k_s equal to $2D_g$ (i.e. no form drag) in the Manning-Strickler formulation for the flow resistances on the rough bed, and with the Nikuradse relation to compute the friction coefficient for the smooth flume sidewalls. The assumption of negligible form drag was justified in the experimental design because

1) predictors to compute the partition between skin friction and form drag in the upper regime plane bed were not available in the literature [Best and Bridge, 1992], and 2) it is commonly assumed that form drag is negligible in upper regime plane bed configurations [e.g. Parker, 2004].

This exercise showed that we expected upper plane bed conditions with standard bedload transport for values of the mass sediment feed, G_s, rate between 0.5 kg/min and 4 kg/min and a flow rate, Q, of 30 l/s.

We thus performed 13 experimental runs with a flow rate of 30 l/s and sediment feed rates varying between 0.5 kg/min and 20 kg/min to study the transition from upper regime plane bed with standard bedload transport ($G_s \leq 4$ kg/min) to upper regime plane bed with bedload transport in sheet flow mode. To further investigate the effect of the flow depth on the bed configuration we performed three runs with a flow rate of 20 l/s and feed rates equal to 1.5 kg/min, 8 kg/min and 16 kg/min.

To unambiguously refer to each experimental run in the continuing of this paper we use the shorthand G_{sQ}; for example, to refer to the 30 l/s, 8 kg/min run we use the notation 8_{30}.

2.4. Experimental procedure

The study of the upper regime bed configurations for increasing values of the bedload transport capacity presented herein is performed at mobile bed equilibrium, i.e. when the flow hydrodynamics, the bed configuration and the mode of bed material transport did not change in space and time over time scales that are long compared to those that characterize bedform migration. The measurements of water depth, bed slope and

bedform geometry reported below have to be interpreted as temporal averages over a series of bedforms.

Noting that in a sediment-feed flume mobile bed equilibrium was independent from the initial conditions [Parker and Wilcock, 1993], the initial condition of each experiment was either the equilibrium deposit obtained at the end of the previous experiment or a non-equilibrium deposit obtained by eroding the topmost part of an equilibrium bed. These initial conditions were chosen to reduce the duration of each experiment and to control the sediment volumes that had to be dried in the laboratory and they did not have any influence on the measurements and the observation discussed below.

Water surface and bed elevation profiles were periodically measured with ruler readings at 15 to 30 minute intervals, with higher feed rate experiments warranting more frequent measurements. Due to the presence of a column next to the flume, we imposed a maximum distance of 15 cm and a minimum distance of 5 cm between two consecutive readings. When the elevations and slopes of the water surface and of the bed profiles did not change significantly in time, we assumed that the system had reached conditions of mobile bed equilibrium.

Example of equilibrium profiles for the experiments 1.5_{30}, 8_{30} and 16_{30} are presented in Figure 2.3a, b and c respectively, where the blue dots and lines pertain to water surface elevation data and the black dots and lines describe the bed elevations. As expected, the higher the sediment feed rate, the steeper the bed slope was and the shallower the water depth became. A careful look at Figure 2.3 reveals that the scatter between the measurements of bed elevation is larger than the scatter of the water surface elevation measurements. This is only partially due to the difficult measurement of the mobile bed

elevation, it is also the consequence of the presence of downstream migrating bedforms on the bed deposit.

When the system reached conditions of mobile bed equilibrium, water temperature was measured as an input for the jsr sonar system [Wong et al., 2007], with which instantaneous measurements of bed surface elevations were taken at six locations along the centerline of the flume. The analysis of the time series of bed elevation goes well beyond the scope of the present paper and will be presented in a separate manuscript. Photographs were taken through the glass side-windows of the flume, sometimes during the experiment and other times after the flow had been stopped. Videos and time lapse images were recorded for some experiment runs through the glass side windows as well. The complete dataset is available through the SEAD repository through the assistance of SEN and the temporary doi is *http://doi.org/10.5072/FK2G44PS74*.

2.5. Experimental results

The experimental results presented herein refer to conditions of mobile bed equilibrium. In other words, data describing the evolution from one equilibrium state to the other are not discussed because they do not necessarily represent a stable bed configuration. In the interpretation of the experimental results it has to be born in mind that two runs with the same feed rate have the same the bed shear stresses associated with skin friction, but the form drag may be different because it depends on the bed configuration [e.g. Parker, 2008 and references therein].

2.5.1. EXPERIMENTS WITH A FLOW RATE OF 30 L/S

Photographs of the equilibrium bed deposit for the experiments with flow rate of 30 l/s are shown in Figure 2.4. In the experiments 0.5_{30} - 4_{30}, the bed configuration was characterized by mostly asymmetrical triangular bedforms with a long, mildly sloping stoss face and a short, steep lee face (Figure 2.4a-b). The sediment transport mode was standard bedload transport with a bedload layer about $3D_g$ thick.

Due to the relatively high bed shear stresses, the bedload transport at the brinkpoint, i.e. the point separating the stoss face from the lee face, was not entirely trapped on the lee face, as observed dune experiments [e.g. Blom et al., 2003]. Part of the brinkpoint bedload transport was deposited on the stoss face of the next bedform downstream. As the transport rate increased, the portion of the brinkpoint bedload transport deposited on the lee face became smaller. A flow separation region was clearly visible immediately downstream of the lee face (video 1a - 0.5_{30} - and 1b – 4_{30} - of the online supplementary material). In this region, as well as slightly downstream of it, bedload transport was greatly reduced.

The bedforms migrated downstream in trains of varying size and celerity. Small bedforms superimposed on the large bedforms were observed in these runs. The small bedform celerity was significantly higher than the celerity of the large bedform, so that the small bedform relatively rapidly reached the large bedform brinkpoint and merged into an even larger bedform. The observed celerity of the largest bedforms was in the order of several millimeters per second.

As the bedload transport rate increased to 8 kg/min, the mode of bedload transport changed. Standard bedload transport was observed in the runs up to 4_{30}. The thickness

of the bedload transport layer rapidly increased in the 6_{30} and 8_{30} runs, identifying the transition from the standard bedload transport to bedload transport in sheet flow mode.

The transition from standard bedload transport to bedload transport in sheet flow mode was associated with a change in bedform shape (Figure 2.4c-d). The bedform wavelength decreased and the separation between the stoss and the lee face became more gradual resulting in more rounded bedforms, i.e. bedforms with a somewhat poorly defined brinkpoint. The flow separation zone downstream of the rounded bedforms was less evident than in the case of triangular bedforms and the majority of the sediment reaching the bedform crest was deposited on the next bedform downstream (video 2 of the online supplementary material).

As we further increased the sediment transport rate from 8 kg/min to 20 kg/min, the bedforms flattened out. Undulations with heights on the order of $2D_g$ and wavelengths on the order of several tens of centimeters characterized the bed surface (Figure 2.4e-f). The mode of bedload transport was sheet flow with a transport layer several grain diameters thick. The maximum bedload layer thickness was approximately $18D_g$ and it was observed during the highest feed rate run.

In all the runs with a flow rate of 30 l/s the bedforms migrated downstream, and the water surface sometimes was in phase with the channel bed. When bedforms were present, there were observable zones of flow separation that became less evident as either the height of the bedforms decreased and/or their shape became more rounded and symmetric.

2.5.2. EXPERIMENTS WITH A FLOW RATE OF 20 L/S

This set of experiments was characterized by three feed rates, each deemed to be representative of upper regime conditions with mode of bedload transport ranging from standard bedload transport to bedload transport in sheet flow mode. These experiments were performed to study the effects of a reduction in water depth on the equilibrium bed configuration.

Photographs of equilibrium bed configurations are shown in Figure 2.5a–c. In the 1.5_{20} experiment, the bedforms were asymmetrical with a long, mild sloped stoss, a short steep lee face and a rounded transition between the two (Figure 2.5a). A zone of flow separation was visible downstream of the lee face (video 3 of the online supplementary material). Sediment was transported in standard bedload transport mode on the stoss faces and the thickness of the bedload transport layer was about $2D_g$. As in the 30 l/s runs with triangular bedforms, part of the sediment was trapped on the lee faces and part was deposited on the stoss side of the next bedform downstream.

In the 8_{20} run symmetric, rounded bedforms formed and migrated downstream (Figure 2.5b). These bedforms had larger amplitudes but smaller wavelength than the bedforms observed in experiment 1.5_{20}. Flow separation seldom occurred downstream of the highest bedforms. In the 8_{20} experiment the water surface was consistently in phase with the bed surface, as documented in video 4 of the online supplementary material. The thickness of the bedload layer was approximately $7D_g$, denoting a transition from standard bedload transport to bedload transport in sheet flow mode.

At the highest transport rate the bed was undulated with wavelengths of about 70 cm, and heights of about $5D_g$ (Figure 2.5c). The thickness of bedload layer was approximately $15D_g$ with the main mode of transport being sheet flow.

The long wavelength, small amplitude bedforms described herein for feed rates smaller than 4 kg/min and flow rates of 30 l/s and 20 l/s are similar to those observed and described by Guy et al. [1966] at the transition between dunes and antidunes, by Paola et al. [1989] and by Bridge and Best [1988]. The comparison between the bedforms observed in the 1.5_{20}, 1.5_{30}, 8_{20} and 8_{30} experiments suggests that as the flow depth decreases, the bedforms become rounder and their interaction with the free surface becomes more evident than in experiments with the same bedload transport capacity and larger flow depths.

2.5.3. QUANTIFICATION OF THE EXPERIMENTAL OBSERVATIONS

The experiments are quantitatively summarized in Table 2. 1. The experiment name is reported in column 1. Columns 2 through 6 summarize the observed parameters. Mean flow depth H and slope S (column 2 and 3) are computed averaging the measurements over the equilibrium profiles. The bedform height Δ, wavelength λ, and the thickness of the bedload transport layer Lt are reported in columns 4, 5, and 6, respectively. They were measured from ruler readings or from videos and photographic documentation. Columns 7 and 8 show respectively the mean flow velocity $U = Q/BH$ and the Froude number Fr. Columns 9 and 10 summarize the sidewall corrected flow parameters [Vanoni and Brooks, 1957; Viparelli et al., 2015] in terms of the composite roughness height k_c and the sidewall corrected Shields number τ_b^*. Columns 10 through 14

summarize the flow parameters associated with skin friction, the Shields number τ_{bs}^{*}, the flow depth H_o, i.e. the flow depth on a flat bed having the same microscopic roughness and slope of the measured bed profile, the dimensionless bedform wave number $k = 2\pi H_o/\lambda$, and the Froude number associated with the equivalent flat bed Fr_o.

2.5.3.1. Flow Resistances

The experiments presented herein, as well as those performed by Guy et al. [1966], McBride et al. [1975], Bridge and Best [1988], Paola et al. [1989], Cheel [1990] and Best and Bridge [1992] among others, reveal that the bed configuration known as upper plane bed associated with standard bedload transport is characterized by downstream migrating, small amplitude and long wavelength bedforms. As shown in the supplementary videos 1a, 1b, and 2, flow separation occurs on the lee face of the asymmetrical bedforms that characterized the equilibrium deposits at relatively low transport rates. It is thus reasonable to expect that form drag should not be neglected in the calculation of the flow resistances. In other words, due to the presence of the small amplitude and long wavelength bedforms, the common assumption that in upper plane bed regime the flow resistances are associated with the presence of a granular bed only, i.e. no form drag [e.g. Simons and Richardson, 1962; Engelund and Hansen, 1967; Julien and Raslan, 1998; Nnadi and Wilson, 1995], may not be appropriate [Best and Bridge, 1992].

To our knowledge, the only attempt to quantify the form drag associated with the long wavelength and small amplitude bedforms in upper plane bed is that of Kishi [1979] who used some of Guy et al. [1966] data to identify two flow resistance regimes at the transition from dunes to antidunes. One regime was characterized by negligible form drag

and the other regime had a form drag that varied with τ_b^* and the non-dimensional flow depth H/D. The analysis by Kishi [1979], however, was performed for values of $H/D >$ 200 and for experiments with significant suspended transport. This analysis did not strictly apply to the experimental conditions considered herein, where $H/D < 200$ and the mode of bed material transport was bedload.

To determine if form drag was significant in the upper regime when $H/D < 200$, we performed a decomposition between skin friction and form drag for our experimental data, for Kennedy [1960] and Guy et al. [1966] antidune, plane bed and transitional experiments. The plane bed Guy et al. [1966] data with $Fr < 0.6$ were not considered in the analysis because they pertained to lower regime conditions [Carling and Shvidchenko, 2002].

We estimated the hydraulic radius for the bed region R_{hb}, the sidewall corrected bed friction coefficient C_{fb} following the Vanoni and Brooks [1957] procedure to remove the sidewall effects. The roughness height was then computed with the Keulegan relation as $k_c = 11R_{hb}/\exp\{\kappa C_{fb}^{-0.5}\}$, where the subscript c denoted a composite (skin friction and form drag) roughness height and the von Karman constant κ was set equal to 0.41 [Parker, 2004]. The non-dimensional roughness height, k_c/D is plotted against the Froude number in Figure 2.6a where the black diamonds refer to our experiments (Table 2. 1, columns 9 and 10), the white diamonds refer to the Guy et al. [1966] experiments at the transition between dunes and upstream migrating antidunes, the white circles denote Guy et al. [1966] plane bed configurations, the grey triangles pertain to Guy et al. [1966] antidune beds, the white squares and triangles are the Kennedy [1960] data for plane bed and for downstream migrating dunes weakly coupled with the water surface (interpreted

here as transitional between dunes and antidunes) and the grey squares are Kennedy [1960] antidune data. In Figure 2.6a k_c/D varies over several orders of magnitude, decreases for increasing Fr and it is generally larger than $2D_g$. Thus, following Engelund and Hansen [1967] and Sumer et al. [1996], we assumed a roughness height associated with skin friction equal to $2D_g$ in the calculation to partition the flow resistances between skin friction and form drag.

The results of the flow resistance partition between skin friction and form drag are reported in Figure 2.6b with the same symbols of Figure 2.6a to distinguish between different experimental datasets. Figure 2.6b is analogous to the Engelund and Hansen [1967] resistance diagram for the flow partition in the dune and antidune regimes. The sidewall corrected Shields number associated with skin friction τ_{bs}^* is on the horizontal axis and the total sidewall corrected Shields number τ_b^* is on the vertical axis. For reference, the Engelund and Hansen criterion to partition between skin friction and form drag in the dune regime is represented with a continuous line, and the dashed line denotes the condition with no form drag, $\tau_b^* = \tau_{bs}^*$. Engelund and Hansen also provide a graphic criterion to estimate the form drag in the case of antidunes but due to the lack of a functional relation we do not report it in Figure 2.6b.

The difference between Figure 2.6b and the Engelund and Hansen [1967] diagram is that our figure contains the Guy et al. [1966] experimental data at the dune/antidune transition, which were neglected in the Engelund and Hansen [1967] study, the Kennedy [1960] data and it focuses on the upper regime only.

The skin friction/form drag partition in our experiments is similar to the partition of Guy et al. [1966] and Kennedy [1960] transitional and plane bed experiments, confirming

that these experiments had similar bed configurations and that, as observed by Best and Bridge [1992], form drag is non-negligible in upper regime plane bed at the transition between dunes and antidunes.

Following observations by Kishi [1979] that the flow resistances in upper plane bed depend on the flow depth H and the grain diameter D, and noting that the non-dimensional roughness height decreases with increasing Froude numbers (Figure 2.6a), we found a reasonable collapse of our upper plane bed data when the fraction of bed shear stress associated with skin friction $\varphi = \tau_{bs}^{*}/\tau_{b}^{*}$ is computed as a function of the non dimensional group $Fr(H/D)^{0.25}$. The data collapse is presented in Figure 2.6c where we used the same symbols of Figure 2.6a-b to distinguish between our experiments, the Guy et al. and the Kennedy experiments. The continuous black line of Figure 2.6c represents a linear function linking the fraction of the bed shear stress associated with skin friction with the Froude number and the ratio H/D. This function takes the form

$$\varphi = \begin{cases} 0.2Fr(H/D)^{0.25} & \text{if} \quad Fr(H/D)^{0.25} < 5 \\ 1 & \text{if} \quad Fr(H/D)^{0.25} \geq 5 \end{cases} \tag{2.1}$$

The dot lines in Figure 2.6c represent the ±30 % interval around equation (2.1). Equation (2.1) predicts the fraction of bed shear stress associated with skin friction reasonably well for all our experimental runs but 10_{30}, which was characterized by relatively high bedforms.

The Guy et al. [1966] and the Kennedy [1969] points were not used in the regression analysis, and are used to test equation (2.1) with upper regime conditions (Figure 2.6c). The majority of Guy et al. [1966] and Kennedy [1960] transitional and plane bed points fall between the ±30 % interval showing that equation (2.1) provides a reasonable estimate of the form drag for upper regime downstream migrating bedforms. As

expected, equation (2.1) does not interpret the points representing bed configurations with upstream migrating antidunes. In particular, equation (2.1) tends to systematically underestimate the flow resistances associated with form drag in the case of upstream migrating antidunes.

2.5.3.2. Mode of bedload transport and bedform geometry

The variability in bedload transport layer thickness and bedform geometry for increasing bedload transport rates is quantitatively described in Figure 2.7, where we present the bedload layer thickness, *Lt* (Figure 2.7a), the bedform height Δ (Figure 2.7b), the bedform wavelength, λ (Figure 2.7c), and the bedform aspect ratio Δ/λ (Figure 2.7d) as functions of τ_{bs}^*, which is the primary non-dimensional hydraulic parameter in the majority of the bedload transport relations [Fernandez Luque and Van Beek, 1976; Parker, 2008] and thus is a reasonable parameter to describe the transition from standard bedload transport to bedload transport in sheet flow mode.

In this figure the black squares denote the 20 l/s experiments, the black diamonds the 30 l/s experiments and the dashed lines identify the transition region between the upper plane bed with standard bedload transport and the upper plane bed with bedload transport in sheet flow mode. The lower limit of this transition region corresponds to τ_{bs}^* = 0.3 and the upper limit is defined for τ_{bs}^* = 0.5.

For τ_{bs}^* < 0.3 the bedload layer thickness is constant and equal to 2-3D_g (Figure 2.7a), the bedform height remains nearly constant (Figure 2.7b) and the wavelength decreases for increasing values of τ_{bs}^* (Figure 2.7c). For τ_{bs}^* > 0.3 the bedload layer thickness and the bedform wavelength monotonically increase, with the bedload layer thickness

reaching ~10D_g when $\tau_{bs}^* = 0.5$, i.e. Gao's [2008] threshold for the initiation of bedload transport in sheet flow mode. The bedform height slightly increases when $0.3 < \tau_{bs}^* < 0.5$ and the bedforms rapidly flatten out when τ_{bs}^* approaches the value of 0.5. The aspect ratio Δ/λ (Figure 2.7d) increases when $\tau_{bs}^* < 0.3$ due to the reduction in bedform wavelength with nearly constant height, remains constant in the transition region and suddenly decreases when $\tau_{bs}^* \geq 0.5$ and a well defined sheet flow layer forms.

The observed change in bedform geometry associated with the development of the sheet flow layer documented in Figure 2.7 confirms that form drag decreases for increasing transport capacities. As τ_{bs}^* increases, $Fr(H/D)^{0.25}$ increases, the sheet flow layer develops, the bed surface flattens out and the fraction of the flow resistances associated with form drag tends to zero.

2.6. Discussion on bedform classification

To classify the bedforms observed during our experiments we plotted our data using the Engelund [1970] stability diagram and we compare them with the experiments of Guy et al. [1966] and Kennedy [1960]. The Engelund [1970] stability diagram Figure 2.8, has the non-dimensional wave number k on the horizontal axis and the Froude number Fr_o on the vertical axis. As in Figure 2.6, the black diamonds represent our experimental points, the white diamonds and circles respectively are Guy et al. [1966] transitional and plane bed experiments and the grey triangles and squares respectively refer to the Guy et al. [1966] and the Kennedy [1960] antidune data. The dashed line with equation $Fr_o = \sqrt{\tanh(k)/k}$ separates the lower regime from the upper regime. The continuous line

with equation $Fr_o = \sqrt{1/k\tanh(k)}$, separates upper regime configurations with upstream and downstream migrating bedforms [Engelund, 1970].

The experiments with feed rates smaller than 3 kg/min and the transitional experiments performed by Guy et al. [1966] are in proximity of the curve separating the lower from the upper regime. This confirms our interpretation that in our low feed rate runs the bed configuration was at the transition from the dune to the antidune regime, and that these runs were representative of upper plane bed with standard bedload transport [Simons and Richardson, 1962].

As the feed rate increase from 3 kg/min to 12 kg/min the experimental points occupy an area of the stability diagram that corresponds to downstream migrating upper regime bedforms and, to our knowledge, these conditions were not observed in many other open channel flow laboratory experiments [Carling and Shvidchenko, 2003, Nunes-Gonzales and Martin-Vide, 2010, 2011; Yokokawa et al., 2011]. The small amplitude bedforms in this region are downstream migrating antidunes [Engelund and Fredsøe, 1982].

The comparison between our downstream migrating antidunes with the Guy et al. [1966] and the Kennedy [1960] antidunes reveals that

1) The Froude numbers are in the same range, 0.77–1.25 for our experiments, 0.83–1.7 for Guy et al. [1966] and 0.70-2.34 for Kennedy [1960];

2) The ratio between the water depth and the sediment size H/D is larger in the Guy et al. [1966] experiments (190-1075) and in the Kennedy [1960] experiments (52-455) than in our experiments (81–147);

3) Downstream migrating antidunes form for values of $u^*/v_s < 1$, i.e. negligible suspended bed material transport, while upstream migrating antidunes in experiments with significant bed material transport in suspension;

4) The ratio between the average flow depth and the antidune height is slightly larger in our experiments (2-5.9 with an average of 3.8) than in the Guy et al. [1966] experiments (1.24-12.6 with an average of 3 and 90% of the runs with H/Δ smaller than 2.7); and

5) The aspect ratio λ/Δ of our antidunes (10-24) is smaller than λ/Δ of Guy et al. [1966] antidunes (14.3–68).

In summary, the comparison between upstream and downstram migrating antidunes in open channel flow experiments reveals that 1) they occur for the same range of Froude numbers, 2) antidunes migrate downstream in the case of negligible suspension of bed material, 3) H/Δ is, on average, smallest in the case of upstream migrating antidunes, and 4) λ/Δ is largest in the case of upstream migrating antidunes. The same differences between upstream and downstream migrating antidunes were observed in experiments on bedload transport driven by saline currents [Spinewine et al., 2009; Sequeiros et al., 2010].

Finally, the points pertaining to the experiments with bedload transport in sheet flow mode - 20_{30}, 16_{30} and 16_{20} - fall on the curve separating upstream and downstream migrating antidunes, suggesting that the upper plane bed with bedload transport in sheet flow mode can be interpreted as a stable bed configuration separating the region with upstream migrating bedforms from the region with downstream migrating bedforms.

Additional experiments on sheet flow transport are needed to thoroughly test this hypothesis.

2.7. CONCLUSIONS

The flume experiments we performed were specifically designed to study the transition from upper regime plane bed with standard bedload transport to upper regime plane bed with bedload transport in sheet flow mode. The main experimental are summarized as follows:

1) The transition is characterized by a gradual increase in the thickness of the bedload layer for $\tau_{bs}^{*} > 0.3$. The development of the sheet flow layer is associated with changes in bedform geometry. Bedform wavelengths gradually decrease when $\tau_{bs}^{*} \leq 0.3$, and gradually increase for $\tau_{bs}^{*} > 0.3$. Bedform heights rapidly drop when the sheet flow layer is fully developed - $\tau_{bs}^{*} > 0.5$;

2) In the transition region, i.e. when $0.3 < \tau_{bs}^{*} < 0.5$, downstream migrating antidunes represent a stable bed configuration in open channel flow experiments with mobile bed and negligible suspended transport;

3) In the upper plane bed regime with standard bedload transport, form drag should not be neglected in the calculations of flow resistances;

4) The comparison between downstream and upstream migrating antidunes in open channel flow experiments reveals that a) they occur in the same range of Froude numbers, b) they migrate downstream when suspended bed material transport is negligible, c) downstream migrating antidunes are characterized by larger values of the ratio between flow depth and bedform height, and d) the aspect ratio of the dowsntream

migrating antidunes is smaller than in the case of upstream migrating bedforms. The same qualitative observations characterized downstream and upstream migrating antidunes observed in laboratory experiments on bedload transport driven by density currents [Spinewine et al., 2009; Sequeiros et al., 2010];

5) Upper plane bed with bedload transport in sheet flow mode can be interpreted as a stable bed configuration that separates upstream and downstream migrating antidunes in systems with relatively coarse bed material [Yokokawa et al., 2011; Cartigny et al., 2014]

The results presented herein represent the foundational step to characterize and quantify the bed configuration and the bedload transport regime at the relatively high bed shear stress in terms of flow resistances, bed configuration and modes of bedload transport. The high stress conditions considered herein are representative of events that may characterize river floods, coastal storms and turbidity currents. Future work is needed to investigate how the bed configuration and the mode of bedload transport change in the presence of sediment mixtures and how bedform geometry and mode of bedload transport influence the fine structure of the deposit.

2.8. ACKNOWLEDGMENTS

The dataset has been made publicly available through the assistance of the Sediment Experimentalist Network (SEN) (NSF 1324660). The authors thank Theo Jeremiah, Rachel Kuprenas, Melissa Bresko, Simran Matthews and Alex Nettles for the help in the laboratory during the performance of the experimental work. The last author thanks Gary Parker for the discussions during the performance of preliminary experiments. The

majority of the students participating in the experiments were supported by the NSF grant EAR-1250641, the others by the last author's start-up fund.

2.9. REFERENCES

Abrahams, A. D. and P. Gao (2006), A bed-load transport model for rough turbulent open-channel flows on plane beds, Earth Surface Processes and Landforms, 31 (7), 910–928.

Bennett, S., and J. Best, (1997), Discussion and closure: Bed-load motion at high shear stress: Dune washout and plane-bed flow, Journal of Hydraulic Engineering, 123 (4), 375–376.

Best, J., and J. Bridge (1992), The morphology and dynamics of low amplitude bedwaves upon upper stage plane beds and the preservation of planar laminae, Sedimentology, 39 (5), 737–752.

Best, J. (2005), The fluid dynamics of river dunes: A review and some future re- search directions, Journal of Geophysical Research: Earth Surface, 110 (F4), doi:10.1029/2004JF000218, f04S02.

Blom, A., J. S. Ribberink, and H. J. de Vriend (2003), Vertical sorting in bed forms: Flume experiments with a natural and a trimodal sediment mixture, Water Resources Research, 39 (2), doi:10.1029/2001WR001088, 1025.

Bourgeois, J. (1980), A transgressive shelf sequence exibiting hummocky stratification: the Cape Sebastian sandstone (Upper Cretaceous), Southwestern Oregon, Journal of Sedimentary Petrology, 50 (3), 681–702.

Bridge, J. S., and J. L. Best (1988), Flow, sediment transport and bedform dynamics over the transition from dunes to upper-stage plane beds: implications for the formation of planar laminae, Sedimentology, 35 (5), 753–763.

Carling, P. A., and A. B. Shvidchenko (2002), A consideration of the dune : antidune tran- sition in fine gravel, Sedimentology, 49 (6), 1269–1282, doi:10.1046/j.1365-3091.2002.00496.x.

Cartigny, M. J. B., D. Ventra, G. Postma, and J. H. Van den Berg (2014), Morphodynamics and sedimentary structures of bedforms under supercritical-flow conditions: New insights from flume experiments, Sedimentology, 61, 712-748, doi: 10.1111/sed.12076

Cheel, R. J. (1990), Horizontal lamination and the sequence of bed phases and stratification under upper-flow-regime conditions, Sedimentology, 37 (3), 517–529, doi: 10.1111/j.1365-3091.1990.tb00151.x.

Dietrich, W. E. (1982), Settling velocity of natural particles, Water Resources Research, 18 (6), 1615–1626, doi: 10.1029/WR018i006p01615.

Dohmen-Janssen, C. M., W. N. Hassan, and J. S. Ribberink (2001), Mobile-bed effects in oscillatory sheet flow, Journal of Geophysical Research: Oceans (1978–2012), 106 (C11), 27,103–27,115.

Dohmen-Janssen, C. M., and D. M. Hanes (2002), Sheet flow dynamics under monochromatic nonbreaking waves, Journal of Geophysical Research: Oceans, 107 (C10), 13–1– 13–21, doi:10.1029/2001JC001045, 3149.

Engelund, F. (1966), Hydraulic resistance of alluvial streams, Journal of the Hydraulic Division, 92 (2), 315–326.

Engelund, F., and E. Hansen (1967), A monograph on sediment transport in alluvial streams, Tech. rep., TEKNISKFORLAG Skelbrekgade 4 Copenhagen V, Denmark.

Engelund, F. (1970), Instability of erodible beds, Journal of Fluid Mechanics, 42, 225–244, doi: 10.1017/S0022112070001210.

Engelund, F., and J. Fredsøe (1982), Sediment ripples and dunes, Annual Review of Fluid Mechanics, 14 (1), 13–37, doi: 10.1146/annurev.fl.14.010182.000305.

Fernandez Luque, R., and R. Van Beek (1976), Erosion and transport of bed-load sediment, Journal of Hydraulic Research, 14 (2), 127–144, doi: 10/d35fjs.

Fredsøe, J. (1974), On the development of dunes in erodible channels, Journal of Fluid Mechanics, 64, 1–16, doi:10.1017/S0022112074001960.

Gao, P. (2008), Transition between two bed-load transport regimes: Saltation and sheet flow, Journal of Hydraulic Engineering, 134 (3), 340–349.

Garcia, M. H. (2008), Sediment transport and morphodynamics, in M. H. Garcia ed. Sedimentation engineering processes: Measurements, modeling and practice, chapter 2, ASCE, Reston, VA [2008], doi: 10.1061/9780784408148.ch02.

Guy, H., D. Simons, and E. Richardson (1966), Summary of alluvial channel data from flume experiments, 1956-61, no. 462-I in Geological Survey Professional Paper, U.S. Government Printing Office.

Kennedy, J. F. (1960), Stationary waves and antidunes in alluvial channels, Ph.D. thesis, California Institute of Technology.

Kennedy, J. F. (1963), The mechanics of dunes and antidunes in erodible-bed channels, Journal of Fluid Mechanics, 16 (04), 521–544, doi:10.1017/S0022112063000975.

Kishi, T. (1979), Bed forms and hydraulic relations for alluvial streams, in Application o Stochastic Processes in Sediment Transport, edited by H. W. Shen and H. Kikkawa, pp. 1–32, Water Resources Publications, LLC, Littleton, CO, doi: 10.1061/9780784408148, ISBN: 0918334314, 9780918334312.

Kostic, S. (2014), Upper flow regime bedforms on levees and continental slopes: Turbidity current flow dynamics in response to fine-grained sediment waves, Geosphere, 10 (6), 1094–1103, doi:10.1130/GES01015.1.

McBride, E. F., R. G. Shepherd, and R. A. Crawley (1975), Origin of parallel, near-horizontal laminae by migration of bed forms in a small flume, Journal of Sedimentary Petrology, 45 (1), 132–139.

Middleton, G. V. (1967), Experiments on density and turbidity currents: Iii. deposition of sediment, Canadian Journal of Earth Sciences, 4 (3), 475–505, doi:10.1139/e67-025.

Nittrouer, J. A., M. A. Allison, and R. Campanella (2008), Bedform transport rates for the lowermost Mississippi River, Journal of Geophysical Research: Earth Surface, 113 (F3), doi:10.1029/2007JF000795, f03004.

Nnadi, F. N., and K. C. Wilson (1992), Motion of contact-load particles at high shear stress, Journal of Hydraulic Engineering, 118 (12), 1670–1684, doi:10.1061/(ASCE) 0733-9429(1992)118:12(1670).

Nnadi, F. N., and K. C. Wilson (1995), Bed-load motion at high shear stress: Dune washout and plane-bed flow, Journal of Hydraulic Engineering, 121 (3), 267–273.

Nnadi, F. N., and K. C. Wilson (1997), Closure Bed-load motion at high shear stress: Dune washout and plane-bed flow, Journal of Hydraulic Engineering, 123 (4), 376–377.

Nunez-Gonzalez, F., and J. P. Martin-Vide (2010), Downstream-migrating antidunes in sand, gravel and sand-gravel mixtures, Dittrich, Koll, Aberle & Geisenhainer (eds), Proceedings River Flow 2010, International Conference on Fluvial Hydraulics, September 8-10, Braunschweig, Germany, Bundesanstalt für Wasserbau ISBN 978-3-939230-00-7

Nunez-Gonzalez, F. and J. P. Martin-Vide (2011), Analysis of antidune migration direction, Journal of Geophysical Research, Earth Surface, 116, doi:10.1029/2010JF001761.

Paola, C., S. M. Wiele, and M. A. Reinhart (1989), Upper-regime parallel lamination as the result of turbulent sediment transport and low-amplitude bed forms, Sedimentology, 36 (1), 47–59.

Parker, G., and P. R. Wilcock (1993), Sediment feed and recirculating flumes: Fundamental difference, Journal of Hydraulic Engineering, 119 (11), 1192–1204.

Parker, G. (2004), 1D sediment transport morphodynamics with applications to rivers and turbidity currents. Copyrighted e-book. [Available at *http://vtchl.uiuc.edu/people/parkerg/*.]

Parker, G. (2008), Transport of gravel and sediment mixtures, in M. H. Garcia ed. Sedimentation engineering processes: Measurements, modeling and practice, chapter 3, pp. 165 – 251, ASCE, Reston, VA Garcia [2008], pp. 165– 251, doi: 10.1061/9780784408148.ch03.

Pugh, F. J., and K. C. Wilson (1999), Velocity and concentration distributions in sheet flow above plane beds, Journal of Hydraulic Engineering, 125 (2), 117–125, doi: 10.1061/ (ASCE)0733-9429(1999)125:2(117).

Reynolds, A. J. (1965), Waves on the erodible bed of an open channel, Journal of Fluid Mechanics, 22, 113–133, doi: 10.1017/S0022112065000630.

Ribberink, J. S., and A. A. Al-Salem (1995), Sheet flow and suspension of sand in oscillatory boundary layers, Coastal Engineering, 25 (34), 205–225.

Sequeiros, O. E., B. Spinewine, R. T. Beaubouef, T. Sun, M. H. Garcia, and G. Parker (2010), Bedload transport and bed resistance associated with density and turbidity currents, Sedimentology, 57 (6), 1463–1490.

Simons, D. B., and E. V. Richardson (1962), The effect of bed roughness on depth-discharge relations in alluvial channels, Geological Survey Water-Supply Paper 1498-E, U.S. Government Printing Office.

Sohn, Y. K. (1997), On traction-carpet sedimentation, Journal of Sedimentary Research, 67 (3), 502-509.

Sohn, Y. K. (1999), Discussion rapid development of gravelly high-density turbidity currents in marine Gilbert-type fan deltas, Loreto Basin, Baja California Sur, Mexico, Sedimentology, 46 (4), 757–761, doi:10.1046/j.1365-3091.1999.00241.x.

Southard, J. B. (1991), Experimental determination of bed-form stability, Annual Review of Earth and Planetary Sciences, 19, 423-455.

Spinewine, B., O. E. Sequeiros, M. H. Garcia, R. T. Beaubouef, T. Sun, B. Savoye, and G. Parker (2009), Experiments on wedge-shaped deep sea sedimentary deposits in minibasins and/or on channel levees emplaced by turbidity currents. Part ii. morphodynamic evolution of the wedge and of the associated bedforms, Journal of Sedimentary Research, 79 (8), 608–628.

Sumer, B. M., A. Kozakiewicz, J. Fredsøe, and R. Deigaard (1996), Velocity and concentration profiles in sheet-flow layer of movable bed, Journal of Hydraulic Engineering, 122 (10), 549–558.

Vanoni, V. A. (1974), Factors determining bed forms of alluvial streams, Journal of the Hydraulics Division, 100 (3), 363–377.

Vanoni, V. A., and N. H. Brooks (1957), Laboratory studies of the roughness and suspended load of alluvial streams, Tech. rep., California Institute of Technology, Pasadena, CA, report No. E-68.

Viparelli, E., L. Solari, and K. M. Hill (2015), Downstream lightening and upward heavy- ing: Experiments with sediments differing in density, Sedimentology, 62 (5), 1384–1407, doi:10.1111/sed.12187.

Wilson, K. C. (1987), Analysis of bed-load motion at high shear stress, Journal of Hydraulic Engineering, 113 (1), 97–103.

Wilson, K. C. (2005), Rapid increase in suspended load at high bed shear, Journal of Hydraulic Engineering, 131 (1), 46–51, doi:10.1061/(ASCE)0733-9429(2005)131:1(46).

Wong, M., and G. Parker (2006), Reanalysis and correction of bed-load relation of Meyer-Peter and Muller using their own database, Journal of Hydraulic Engineering, 132 (11), 1159–1168, doi:10.1061/(ASCE)0733-9429(2006)132:11(1159).

Wong, M., G. Parker, P. De Vries, T. M. Brown, and S. J. Burges (2007), Experiments on dispersion of tracer stones under lower-regime plane-bed equilibrium bed load transport, Water Resources Research, 43 (3).

Yokokawa, M., Y. Takahashi, H. Yamamura, Y. Kishima, G. Parker and N. Izumi (2011), Phase diagram for antidunes and cyclic steps based on suspension index, non-dimensional Chezy resistance coefficient and Froude number, Proceedings River, Coastal and Estuarine Morphodynamics RCEM 2011.

2.10. FIGURE CAPTIONS

Figure 2.1. Schematic drawing, not to scale, of the experimental flume.

Figure 2.2. Sediment size distribution.

Figure 2.3. Equilibrium longitudinal profiles of water surface (blue triangles) and bed (black triangles) elevation measured in runs 1.5_{30}, 8_{30} and 16_{30}. The lines are the trend lines used to estimate the slopes.

Figure 2.4. Pictures of the equilibrium bed deposit in the 30 l/s experiments.

Figure 2.5. Pictures of the equilibrium bed deposit in the 20 l/s experiments.

Figure 2.6. Quantification of the flow resistances. a) Non-dimensional composite roughness height, the continuous line corresponds to $k_c/D = 2$. b) Partition between skin friction and form drag, the continuous line is the Engelund and Hansen dune form drag predictor and the dashed line denotes *no form drag* conditions. c) Proposed form drag predictor for upper plane bed conditions, the continuous line represents equation (1), the dotted lines identify a ±30% region around the proposed predictor. The black diamonds are our experimental data, the white diamonds and triangles respectively are the Guy et al. [1966] and Kennedy [1960] transitional data, the white circles and squares are the Guy et al. [1966] and the Kennedy [1960] plane bed data, the grey triangles are the Guy et al. [1966] antidune data and the grey squares are the Kennedy [1960] antidune data.

Figure 2.7. Quantification of the bedform geometry as a function of the Shields number associated with skin friction. The diamonds refer to the 30 l/s experiments and the squares to the 20 l/s experiments. The vertical dashed lines at $\tau_{bs}^{*} = 0.3$ and at $\tau_{bs}^{*} = 0.5$ identify the limits of the transition zone from standard bedload transport to bedload transport in sheet flow mode. a) Non-dimensional bedload layer thickness. b) Bedform height. c) Bedform wavelength. d) Bedform aspect ratio.

Figure 2.8. Bedform stability diagram [Engelund, 1970]. The black diamonds represent our experimental data, the white diamonds and triangles are the Guy et al. [1966] and the Kennedy [1960] transitional data, the white circles are the Guy et al. [1966] upper plane bed data, the grey triangles are the Guy et al. [1966] antidune data and the grey squares are the Kennedy [1960] antidune data.

2.11. FIGURES

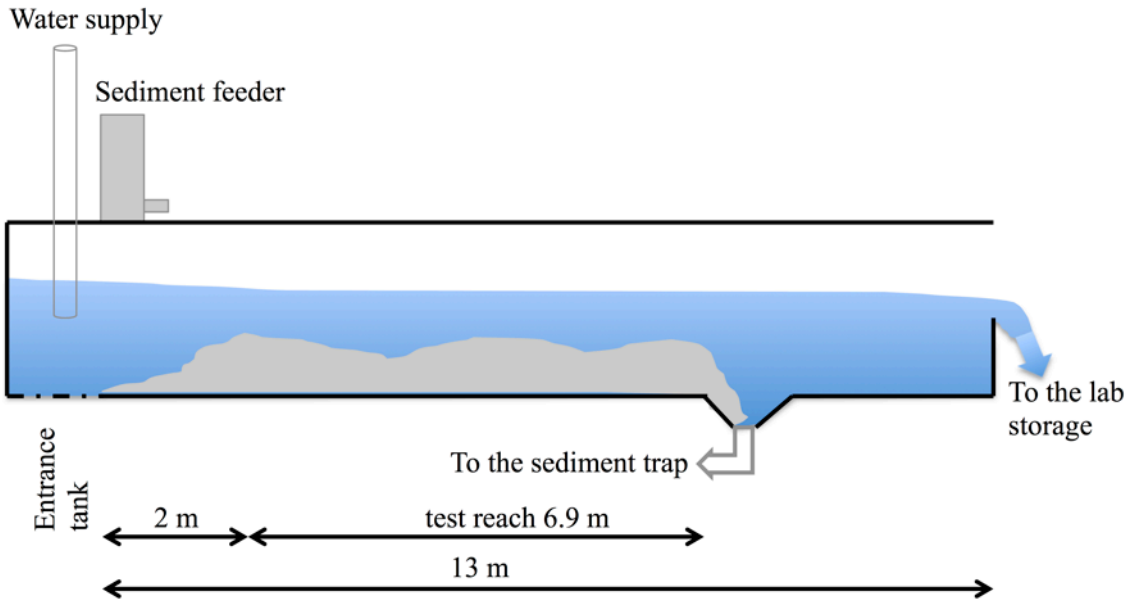

Figure 2.1. Schematic drawing, not to scale, of the experimental flume.

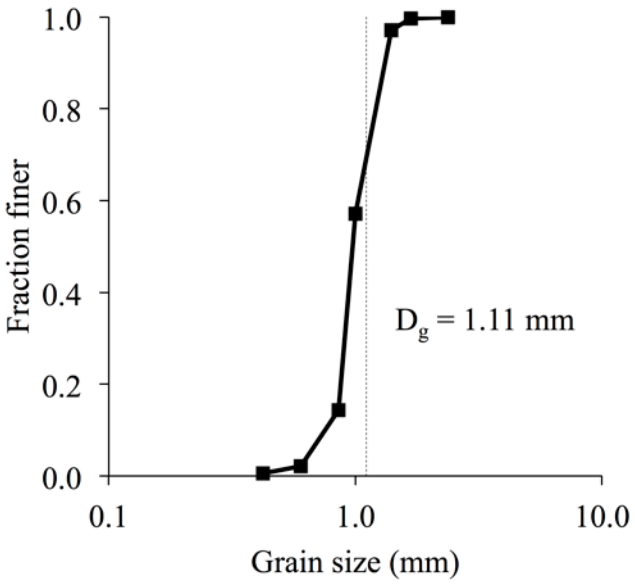

Figure 2.2. Sediment size distribution.

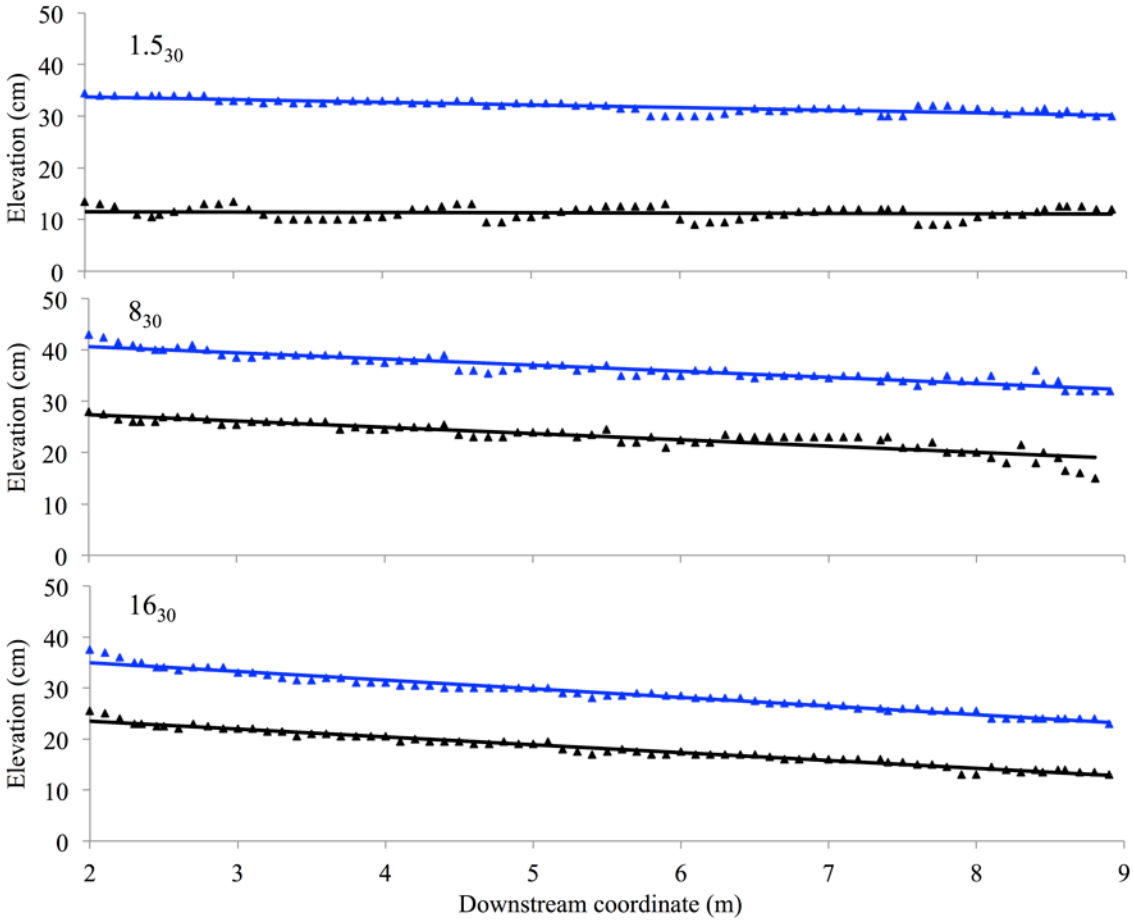

Figure 2.3. Equilibrium longitudinal profiles of water surface (blue triangles) and bed (black triangles) elevation measured in runs 1.5_{30}, 8_{30} and 16_{30}. The lines are the trend lines used to estimate the slopes.

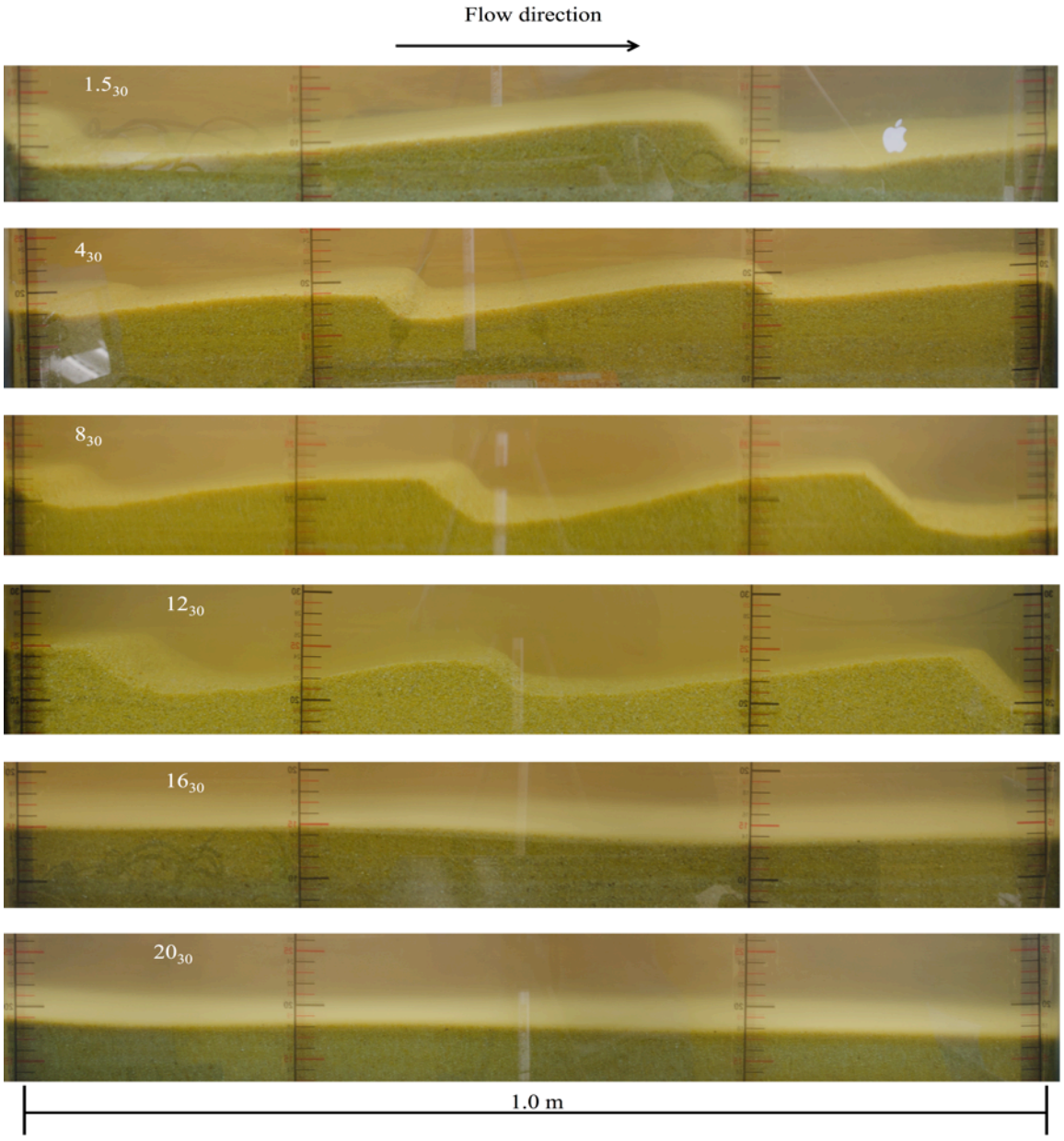

Figure 2.4. Pictures of the equilibrium bed deposit in the 30 l/s experiments.

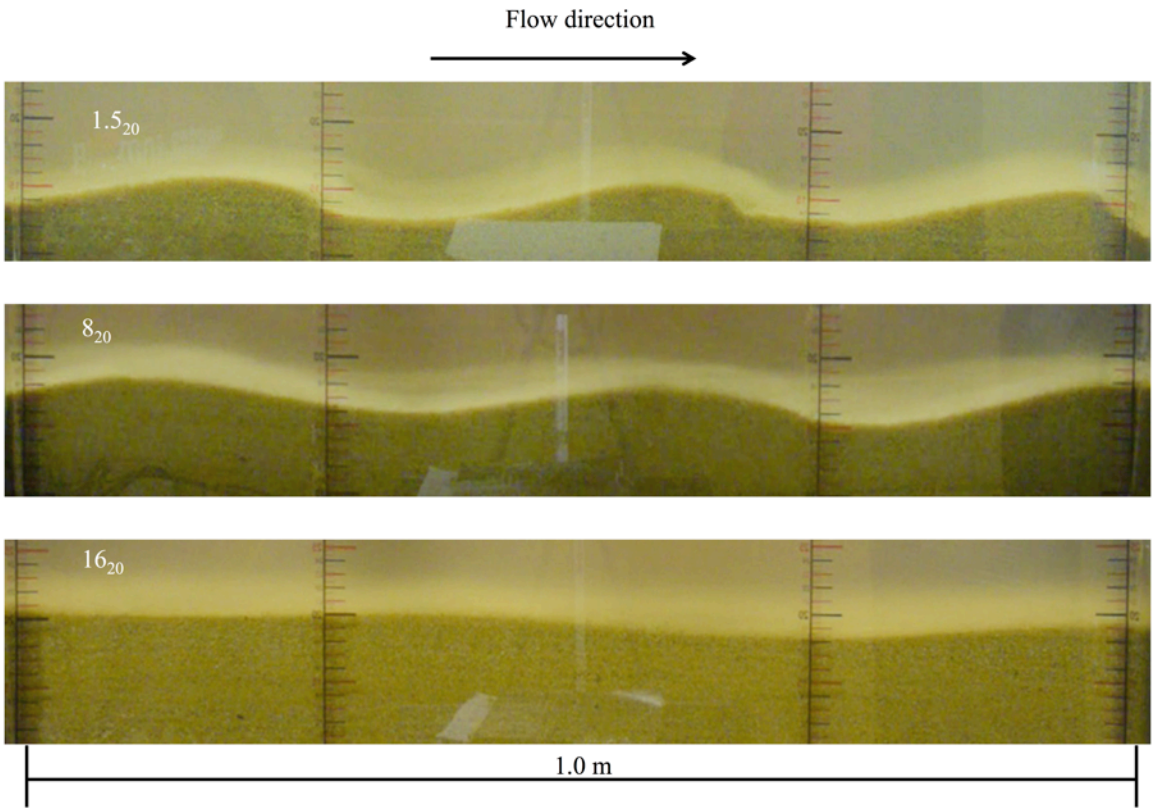

Figure 2.5. Pictures of the equilibrium bed deposit in the 20 l/s experiments.

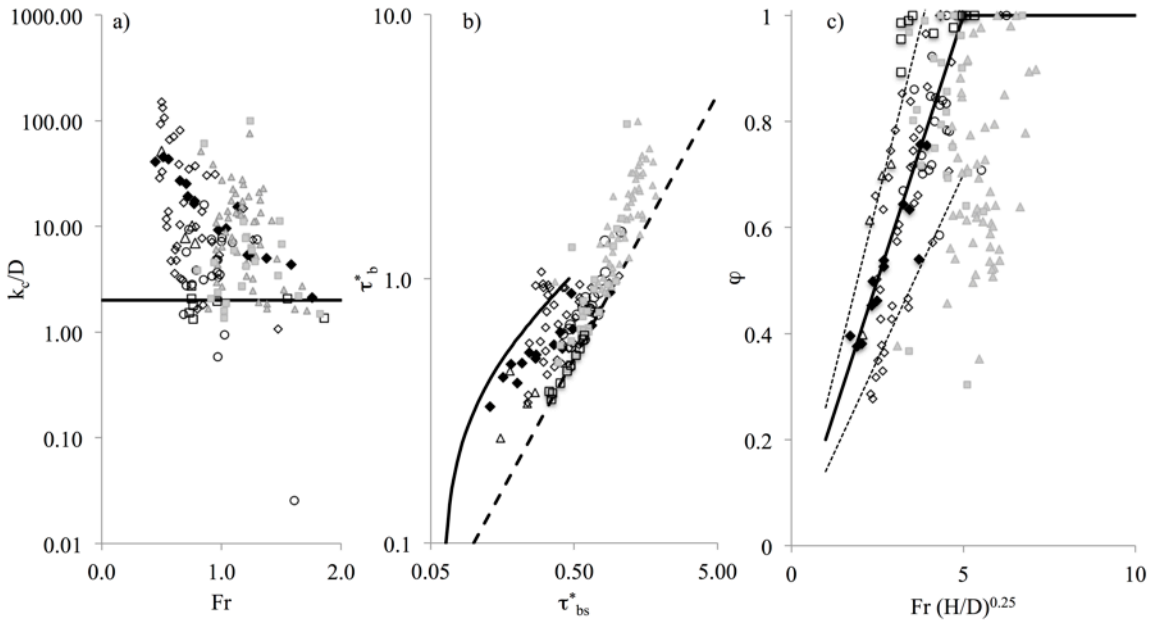

Figure 2.6 Quantification of the flow resistances. a) Non-dimensional composite roughness height, the continuous line corresponds to $k_c/D = 2$. b) Partition between skin friction and form drag, the continuous line is the Engelund and Hansen dune form drag predictor and the dashed line denotes *no form drag* conditions. c) Proposed form drag predictor for upper plane bed conditions, the continuous line represents equation (1), the dotted lines identify a ±30% region around the proposed predictor. The black diamonds are our experimental data, the white diamonds and triangles respectively are the Guy et al. [1966] and Kennedy [1960] transitional data, the white circles and squares are the Guy et al. [1966] and the Kennedy [1960] plane bed data, the grey triangles are the Guy et al. [1966] antidune data and the grey squares are the Kennedy [1960] antidune data.

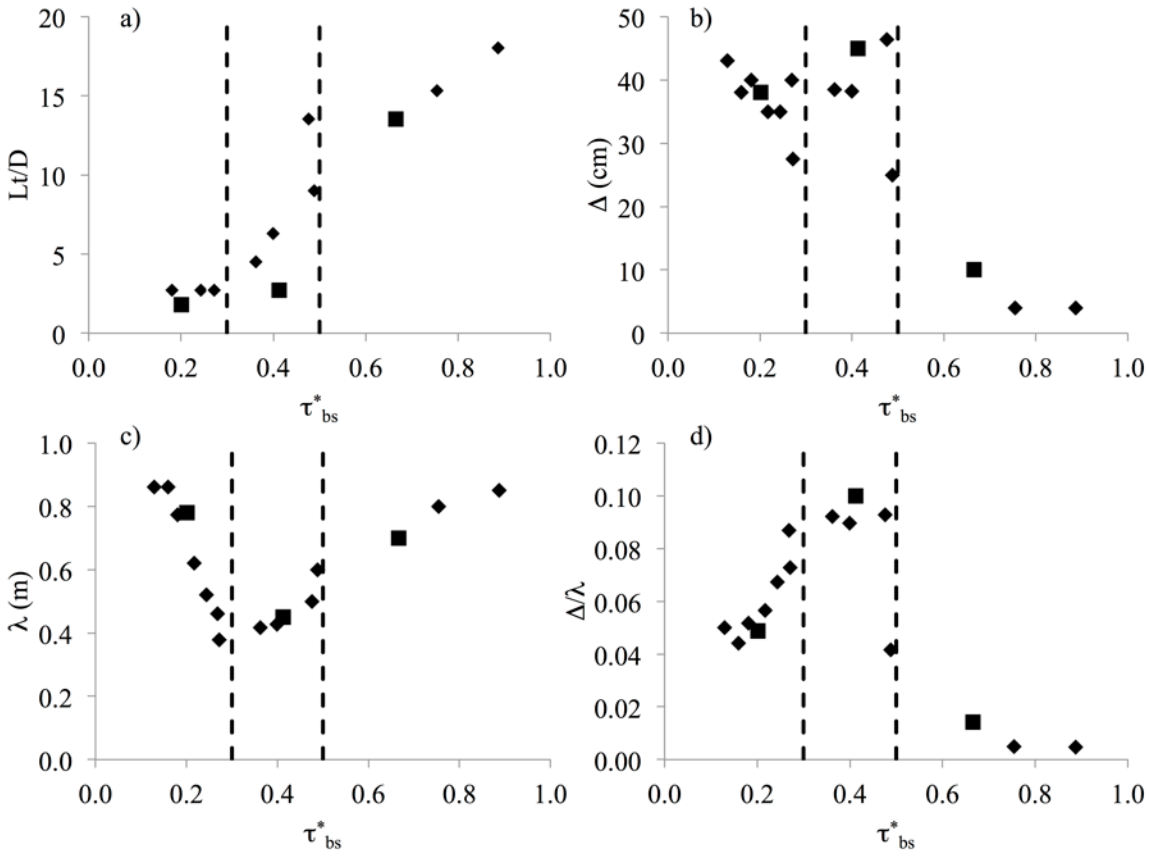

Figure 2.7. Quantification of the bedform geometry as a function of the Shields number associated with skin friction. The diamonds refer to the 30 l/s experiments and the squares to the 20 l/s experiments. The vertical dashed lines at $\tau_{bs}^{*} = 0.3$ and at $\tau_{bs}^{*} = 0.5$ identify the limits of the transition zone from standard bedload transport to bedload transport in sheet flow mode. a) Non-dimensional bedload layer thickness. b) Bedform height. c) Bedform wavelength. d) Bedform aspect ratio.

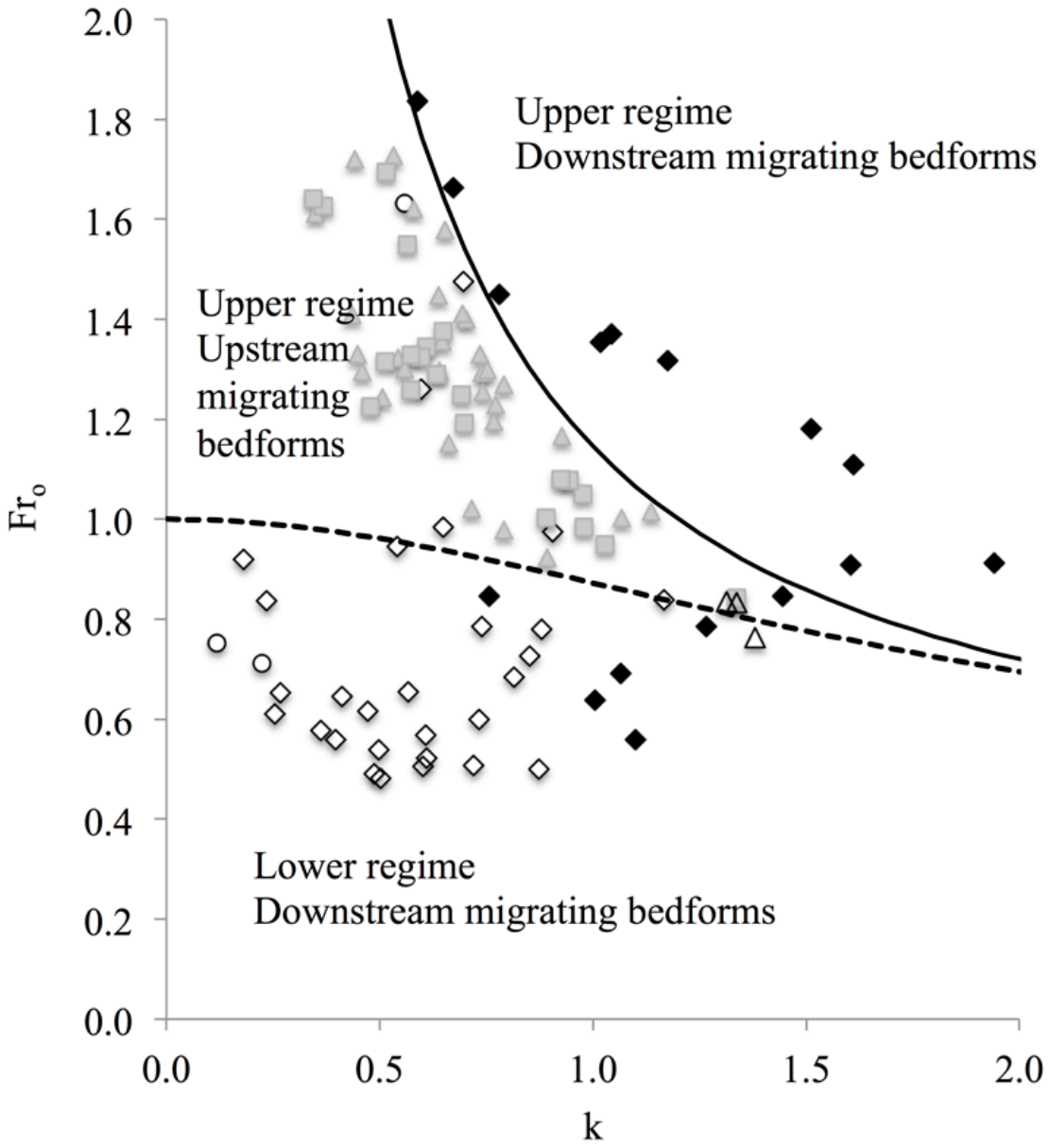

Figure 2.8. Bedform stability diagram [Engelund, 1970]. The black diamonds represent our experimental data, the white diamonds and triangles are the Guy et al. [1966] and the Kennedy [1960] transitional data, the white circles are the Guy et al. [1966] upper plane bed data, the grey triangles are the Guy et al. [1966] antidune data and the grey squares are the Kennedy [1960] antidune data.

2.12. TABLE

Table 2.1. Summary of the experimental observations at equilibrium with H denoting the flow depth, S the bed slope, Δ the bedform height, λ the bedform wavelength, Lt the thickness of the bedload layer, U the mean flow velocity, Fr the Froude number, k_c the composite roughness height, τ^*_b the sidewall corrected Shields number, τ^*_{bs} the sidewall corrected Shields number associated with skin friction, H_o the water depth of the associated flat bed with skin friction ($k_s = 2D_g$), k is the non-dimensional wave number and Fr_o is the Froude number of the associated flat bed.

Run	H	S	Δ	λ	Lt	U	Fr	k_c	τ^*_b	τ^*_{bs}	H_o	k	Fr_o
	cm		mm	m	mm	m/s		mm			cm		
1.5_{20}	13.0	0.0074	38	0.78	2	0.81	0.72	21.3	0.40	0.20	9.4	0.76	0.85
8_{20}	9.0	0.0144	45	0.45	3	1.17	1.25	5.7	0.55	0.41	7.5	1.04	1.37
16_{20}	7.2	0.0219	10	0.70	15	1.47	1.76	2.4	0.67	0.67	6.6	0.59	1.84
0.5_{30}	23.3	0.0037	43	0.86	-	0.68	0.45	45.6	0.33	0.13	15.0	1.10	0.56
1_{30}	21.3	0.0050	38	0.86	-	0.74	0.51	50.7	0.42	0.16	13.8	1.01	0.64
1.5_{30}	20.1	0.0059	40	0.77	3	0.79	0.56	48.4	0.47	0.18	13.1	1.07	0.69
2_{30}	18.2	0.0067	35	0.62	-	0.87	0.65	30.1	0.48	0.22	12.5	1.27	0.79
2.5_{30}	17.2	0.0076	35	0.52	3	0.92	0.71	28.2	0.53	0.24	12.0	1.45	0.85
3_{30}	16.2	0.0079	40	0.46	-	0.97	0.77	18.2	0.50	0.27	11.7	1.60	0.91
4_{30}	16.2	0.0081	28	0.38	3	0.98	0.78	19.4	0.52	0.27	11.7	1.94	0.91
6_{30}	13.9	0.0103	39	0.42	5	1.14	0.97	10.2	0.56	0.36	10.7	1.61	1.11
8_{30}	13.3	0.0119	38	0.43	7	1.19	1.04	10.7	0.63	0.40	10.3	1.51	1.18
10_{30}	11.9	0.0138	25	0.60	10	1.32	1.22	6.0	0.65	0.49	9.7	1.02	1.35
12_{30}	12.5	0.0166	46	0.50	15	1.26	1.14	17.1	0.88	0.48	9.3	1.17	1.32
16_{30}	11.0	0.0170	4	0.80	17	1.43	1.37	5.6	0.75	0.75	9.9	0.78	1.45
20_{30}	10.1	0.0215	4	0.85	20	1.57	1.58	4.9	0.89	0.89	9.1	0.67	1.66

CHAPTER 3

MASSIVE UNITS EMPLACED BY BEDLOAD TRANSPORT IN SHEET FLOW MODE[2]

ABSTRACT

The study of turbidity current, coastal storm and tsunami deposits is the key to understanding the physical processes governing sediment transport, erosion and deposition in submarine settings, to the reconstruction of global paleoclimate and paleoflow, to the exploration of hydrocarbon reservoirs and to the prediction of natural hazards associated with earthquake and landslide induced tsunamis. Although generated by very different flows, a common feature of these deposits is a basal erosional layer underlying a sandy massive unit, i.e. a unit lacking internal structure including parallel or cross lamination. The emplacement of these basal massive units was thought to be the result of a relatively rapid deposition of suspended sediment. Here we present the results of laboratory experiments that demonstrate these basal massive units are not necessarily deposited by suspended transport. A thick bedload layer of colliding grains – the sheet flow layer – can also deposit sandy massive units in shallow and deep water settings. In systems transporting medium to coarse sand and pea gravel, bedload transport in sheet flow mode occurs for bed shear stresses that are significantly smaller than those predicted

---

[2] Ricardo Hernandez Moreira, Sadegh Jafarinik, Sydney Sanders, Bradley Huffman, Christopher G. St. C. Kendall, Gary Parker, Enrica Viparelli. In preparation for submission.

with suspension-based models. Thus, suspension-based models may overestimate the bed shear stresses and misrepresent the characteristics of the flow.

3.1. INTRODUCTION

Relatively common to the submarine setting are depositional sequences that begin with a lower erosional boundary followed in ascending order by a either a graded or an inherently massive basal unit, a relatively coarse parallel laminated unit, a cross laminated unit, a relatively fine parallel laminated unit, and a capping layer of massive mud. These sequences contain sediments deposited during storms in relatively shallow water settings[1,2], tempestites, or sediments deposited by turbidity currents, turbidites[3,4]. In the case of turbidites the sequence corresponds to the classical Bouma sequence[3], which is characteristic of deposits emplaced under decelerating flow conditions[5]. A very similar sequence was defined by Walker et al.[6] to interpret storm deposits emplaced under "*decreasing rates of deposition and increasing importance of wave reworking in a waning flow*"[6]. In the same paper, Walker et al.[6] note that the basal parallel laminated unit of their turbidite sequence and of the Bouma sequence are most likely deposited under conditions that they define as upper flat bed. However, they do not propose any mechanism for the formation of the basal massive unit. In summary, studies have shown that the sequences considered herein were deposited from waning energy flows[7,8] but the physical processes the emplacement of the basal massive unit (Figure 3.1) are still not fully understood[9,10].

Studies of depositional fabrics in the field[11-13] and in the laboratory[14-16] demonstrate that the basal parallel laminated units are deposited when the bed configuration is at the transition between the dune and the antidune regime – upper regime plane bed[17].

Recalling that the depositional sequences considered herein are emplaced from waning energy flows[7,8], with the basal massive unit accumulating under more intense flow conditions than the overlying parallel laminated unit, as the basal parallel laminated unit is deposited in upper plane bed conditions, the basal massive unit should be emplaced under even stronger transport conditions and these should be able to suppress parallel lamination.

Several mechanisms have been proposed to describe the emplacement of massive turbidites, high-density turbidity currents with sediment sizes ranging from clay to gravel[18,19], dense subaqueous gravity flows[20], sandy debris flow[21], internal hydraulic jump[22-24], damping of near-bed turbulence[9]. None of those, however, fully explains how the same sustained event can deposit both the basal massive and the overlying units. In addition, these mechanisms cannot entirely justify how massive turbidites, which extend long distances in the dip direction and may contain coarser particles as floating clasts, can be emplaced 10's – 100's km downstream of the source[5].

Numerical simulations of high-density turbidity currents suggest that primary deposition most likely generates stratified turbidites rather than massive deposits[25]. Laboratory experiments on sandy debris flows[26] show that the presence of mud nevertheless plays a fundamental role in maintaining the excess pore pressure that sustains the debris flow. In other words, it does not appear that a purely sandy debris

flow moving under its own weight can travel long distances on slopes of a degree or less that are typical of submarine canyons. An internal hydraulic jump effectively reduces the basal shear stress and rapid deposition of bed material occurs in relatively short distances[23, 24]. Finally, the dumping or freezing of near-bed turbulence is characterized by the lack (or great suppression) of entrainment of sand into suspension, causing the sand to be depleted over a few 100's km to a few km. In addition, the collapse of near-bed turbulence should nearly totally suppress bedload transport, and clasts or pea gravel cannot be emplaced in the deposits.

Here we present the results of laboratory experiments specifically designed to test the hypothesis that relatively coarse, massive tempestites and turbidites can be deposited under very intense bedload transport corresponding to what has been called laminar sheared layer[27], sheet flow[28-30], expanded bed[31], traction carpet[32] or flowing grain layer[33]. This mode of bedload transport is characterized by a near bed layer of colliding grains that is 10s of grain diameters thick and it has been observed for both oscillatory flows[29] and unidirectional flows[28,30].

The major factor controlling the formation of a sheet flow layer is the dimensionless Shields number, τ^*, characterizing particle mobility[29,34,35]. Laboratory experiments performed by the authors[36] with 1.11 mm sand demonstrated that bedload transport remains within a layer of 1-3 grain thickness for values of the Shields number associated with skin friction τ_s^* smaller than 0.3. For values of τ_s^* between 0.3 and 0.5 the sheet flow layer develops with a gradual increase of the bedload layer thickness. When τ_s^* is greater than 0.5 the sheet flow layer is fully developed[34,37] and its thickness increases for increasing bed shear stresses. The observed change in the mode of bedload transport is

associated with a change in bedform geometry. Downstream migrating long wavelength and small amplitude[14-16] bedforms characterize the deposit for $\tau_s^* < 0.3$. As the sheet flow layer develops - $0.3 < \tau_s^* < 0.5$ - downstream migrating antidunes form and represent a stable configuration[38]. For $\tau_s^* > 0.5$, the deposit can be considered for all practical purposes flat.

Sheet flow conditions are commonly observed on the continental shelf during storms[35,39-41], it is thus reasonable to expect the emplacement of storm and tsunami deposits in these transport conditions. On the contrary, it is important to ask whether or not turbidity currents can drive sheet flow bedload transport.

Pirmez and Imran[42] reconstructed the formative flows in a channel on the Amazon Submarine Fan. Based over their estimates of current thickness, H = 40 m, channel slope, S = 0.003, and volumetric concentration of suspended sediment, C = 0.01, over a reach of 300 km, a reasonable scale for the bed shear stress, τ_b, is obtained by balancing bed resistance against the downstream pull of gravity acting on the suspended sediment, i.e. $\tau_b = \rho RgCHS$, with ρ denoting the density of the water, R the specific gravity of the suspended sediment and g the acceleration of gravity. The Shields number, estimated as $\tau_b/(\rho RgD)$, ranges from 2.4 to 4.8, as grain size D declines from 0.5 mm to 0.25 mm. Thus, the strong, sustained currents that can be effective in the formation of long submarine channels are likely well into the sheet flow regime. In addition, Sequeiros et al.[43] and Spinewine et al.[44] observed antidunes and cyclic steps with Froude-supercritical turbidity currents in laboratory experiments, showing that it is possible to have a sustained turbidity current over a mobile sand bed under upper regime conditions[17]. The assumption of a turbidity current-driven sheet flow layer is thus a reasonable inference,

which has been partially confirmed by the experiments of Middleton[31] for high concentrated turbidity currents.

3.2. Experimental results

We performed the laboratory experiments in the 13 m long and 0.5 m wide sediment feed flume of the hydraulic laboratory in the Department of Civil and Environmental Engineering at the University of South Carolina. The flume cross section was narrowed to 0.19 m in the upstream most 9 m of the flume to obtain a 7 m long test reach. Details on the characteristics of the experimental facility are available through the wiki page of the Sediment Experimentalists Network http://sedexp.net/experiment/setting-hydraulics-laboratory-limited-resources. Five experiments were performed with a flow rate of 30 l/s and sediment feed rates varying between 1.5 kg/min to 20 kg/min corresponding to bed configurations ranging from upper regime plane bed[17] to plane bed with bedload transport in sheet flow mode (Supplementary Figure 3.4). The sediment was a mixture of three components, purple fine sand with D = ~0.5 mm, medium white sand with D = 1.11 mm and the coarse brown sand with D = ~1.4 mm. The geometric mean diameter, D_g, of the sediment mixture was 0.95 mm and the geometric standard deviation was 1.65.

Each experiment was characterized by two phases, the equilibrium phase, in which we waited for the system to reach conditions null net erosion and deposition over time scales that are long compared to the time scales of bedform migration[45], and the aggradation phase, in which the water surface base level was slowly raised to induce channel bed aggradation under the transport conditions observed on the equilibrium bed.

At the end of the aggradation run, stratigraphic sections were cut (one dip section in the center of the test reach and several strike sections) and photographed, core samples were taken and to measure the spatial variation of grain sizes. Details on the experimental procedure and protocol are presented in the Methods section. The dataset is available at the SEN repository. Experimental results are quantitatively summarized in Table 3. 1 in terms of equilibrium bedload transport capacity, G_s, flow depth H, bed slope S, characteristic diameters of the bed surface D_{sg} and D_{s90}, Shields number associated with skin friction, bedform height and wavelength, Δ and λ, bedload layer thickness, Lt, and bed configuration. The bed surface is here defined as the portion the deposit that exchanges sediment with the bedlaod transport with thickness roughly equal to the bedform height[45]. In agreement with our uniform sediment observations, as τ_s^* increases the bed configuration transitions from upper regime plane bed (G_s = 1.5 kg/min) to downstream migrating antidunes (G_s = 6 kg/min and 10 kg/min) to flat bed with bedload transport in sheet flow mode (G_s = 16 kg/min and 20 kg/min).

Pictures of the stratigraphic sections are presented in Figure 3.2, where the white continuous line identifies the surface of the equilibrium deposit and the yellow arrows highlight the two laminae emplaced in the 1.5 kg/min experiment. The stratigraphic sections show that parallel laminated deposit are emplaced in upper regime plane bed (1.5 kg/min)[11-16]. The downstream migrating antidune deposit of the 6 kg/min experiment presents parallel laminae that are thinner than those deposited in the upper plane bed regime experiment. The preservation of thin laminae in the 6 kg/min experiment is only in part due to a change in bed configuration. It is also due to the relatively high aggradation rate (~0.5 mm/min) compared with the 1.5 kg/min experiment (~0.1

mm/min), as noted by Best and Bridge[16]. As the Shields number associated with skin friction increases, the antidunes flatten out (10 kg/min experiment), the sheet flow layer develops and the deposits become massive (10 kg/min – 20 kg/min experiments).

We explain the observed change in deposit fabric noting that a region of flow separation forms downstream of the upper regime plane bed bedforms and downstream migrating antidunes[16,36]. Part of the fine sediment that is entrained in transport on the stoss face of the next bedform downstream is transported upstream in the separation zone. This fine sediment is trapped under the lee face of the migrating bedform and the fine part of a parallel lamina forms. The coarse portion of the parallel lamina is associated with the normal grading that occurs on the bedform lee face (Supplementary video 1).

As the Shields number associated with skin friction increases, antidunes flatten out, flow separation does not occur and the sheet flow develops[36]. In the stratigraphic record this change in bed configuration corresponds to the transition from a parallel laminated to a massive unit.

In our experiments the transition from a parallel laminated to a massive unit is associated with a change in the grain size distribution of the deposit with the massive deposits being significantly finer than the laminated units. The vertical variation of the geometric mean in the deposits obtained in the aggradation phase of the experiments is presented in Figure 3.3, where the ratio between the geometric mean diameter of the deposit and the geometric mean diameter of the bedload transport is on the horizontal axis and the non-dimensional elevation of the deposit sample is on the vertical axis. In Figure 3.3 the elevation of the sample above the equilibrium deposit surface, z, is made

non-dimensional with the thickness of the deposit emplaced in the aggradation phase, $\Delta\eta$. Thus $z/\Delta\eta = 0$ corresponds to the surface of the equilibrium deposit and $z/\Delta\eta = 1$ corresponds to the surface of the final deposit. It is important to note here that significant spatial – vertical and streamwise - variation of deposit grain size distribution was not observed, confirming that the aggradation rate occurred with negligible changes in bed configuration and bedload transport characteristics.

The observed fine D_g of the massive deposit compared to the parallel laminated unit D_g is likely due to particle segregation in dense sheared flows – the sheet flow layer. This segregation results in the preferential concentration of fine particles in the lowest part of the sheared layers (near the bed) with the coarse particles transported in the highest part of the sheared layers (far from the bed)[35,46,47]. The aggradation rates in the experiments with a developing (10 kg/min) or fully developed sheet flow layer (16 kg/min and 20 kg/min) were relatively low to prevent significant changes in bed configuration (0.84 mm/min – 1.7 mm/min). Thus, the lowermost and fine part of the sheet flow layer only contributed to the formation of the aggrading deposit. In the 16 kg/min experiment the aggradation rate was the lowest (0.84 mm/min) and the emplaced deposit was the finest because the likelihood of trapping coarse sediment in the deposit was smaller than in the other experiments.

To illustrate how the results of these experiments may impact the interpretation of the stratigraphic record, we consider a basal massive unit with characteristics sand size of 1 mm, which is typical of channel deposits in the present Congo channel[48]. In suspension-based models, the shear velocity has to be larger than the threshold for significant suspension, which can be estimated by imposing that the ratio between shear velocity and

settling velocity is equal to one[49]. Using the Dietrich relation to estimate the settling velocity of sand particles[50], the threshold shear velocity for significant suspension is 15.5 cm/s corresponding to a threshold Shields number of 1.5. On the contrary, if we use the results of the present study, a massive unit can be emplaced when the Shields number associated with skin friction is greater than ~0.5 and a threshold shear velocity of 9 cm/s, which corresponds to a significantly less intense flow than the flow estimated from a suspension-dominated model.

3.3. REFERENCES

1) Duke, W. L. Hummocky cross-stratification, tropical hurricanes, and intense winter storms. *Sedimentology* 32, 167-194 (1985)

2) Pomar, L. & Kendall, G. St. C. Carbonate-platform architecture: a response to hydrodynamics and evolving ecology. *Controls on Carbonate Platform and Reef Development*, SEPM Special Publication 89, 55-84 (2007)

3) Bouma, A. H. *Sedimentology of some flysh deposits: A graphic approach to facies interpretations*, Elsevier, Amsterdam (1962)

4) Prave, A. R. & Duke, W. L. Small-scale hummocky cross-stratification in turbidites: a form of antidune stratification? *Sedimentology* 37, 531-539 (1990)

5) Leeder, M. *Sedimentology and Sedimentary Basins*, Blackwell Science Ltd., Oxford, U. K, 592p. (1999),

6) Walker, R. G., Duke, W. L. & Leckie, D. A. Hummocky stratification: Significance of its variable bedding sequences: Discussion. *Geological Society of America Bulletin* 94, 1245-1251 (1983)

7) Dott, R. H. Jr. & Bourgeois, J. Hummocky stratification: Significance of its variable bedding sequences. *Geological Society of America Bulletin* 93, 663-680 (1982)

8) Kneller, B. Beyond the turbidite paradigm: physical models for deposition of turbidites and their implications for reservoir prediction. In: Hartley A.J. & Prosser D. J. eds. *Characterization of deep-marine clastic systems*, Geological Society Special Publication 94, 31–49 (1995)

9) Cantero, M. I., Cantelli, A., Pirmez, C., Balachander, S., Mohrig, D., Hickson, T. A., Yeh, T., Naruse, H. & Parker, G. Emplacement of massive turbidites linked to extinction of turbulence in turbidity currents. *Nature Geoscience* 5, 42-45 (2015),

10) Mutti, E., Bernoulli, D., Ricci Lucchi, F. & Tinterri, R. Turbidites and turbidity currents from Alpine 'flysch' to the exploration of the continental margins. *Sedimentology* 56, 267-318 (2009)

11) Allen, J. R. L. Primary current lineation in the lower old red sandstone (Devonian), Anglo-Welsh basin. *Sedimentology* 3, 89-108 (1964)

12) Cheel R. J., & Middleton, G. V. Horizontal laminae formed under upper flow regime plane bed conditions. *Journal of Geology* 94, 489-504 (1986),

13) Greenwood, B., & Sherman, D. J. Hummocky cross-stratification in the surf zone: flow parameters and bedding genesis. *Sedimentology* 33, 33-45 (1986),

14) Bridge, J. S., & Best, J. L. Flow, sediment transport and bedforms dynamics over the transition from dunes to upper-stage plane beds: implications for the formation of parallel laminae. *Sedimentology* 35, 753-763 (1988)

15) Paola, C., Wiele, S. M. &Reinhart, M. A. Upper-regime parallel lamination as the result of turbulent sediment transport and low-amplitude bed forms. *Sedimentology* 36, 47-59 (1989)

16) Best, J., & Bridge, J. The morphology and dynamics of low amplitude bedwaves upon upper stage plane beds and the preservation of planar laminae. *Sedimentology* 39, 737-752 (1992),

17) Simons, D. B. & Richardson E. V. *The effect of bed roughness on depth-discharge relations in alluvial channels*, Geological Survey Water-Supply Paper 1498-E, U.S. Government Printing Office (1962)

18) Lowe, D. R. Sediment gravity flows: II. Depositional models with special reference to the deposits of high-density turbidity currents. *Journal of Sedimentary Research* 52 (1), 0279-0297 (1982)

19) Kneller, B. C. & Branney, M. J. Sustained high-density turbidity currents and the deposition of thick massive sands. *Sedimentology* 42, 607-616 (1995)

20) Breien, H., De Blasio, F. V., Elverhoi, A., Nystuen, J. P. & Harbitz, C. B. Transport mechanisms of sand in deep-marine environments – insights based on laboratory experiments. *Journal of Sedimentary Research* 80, 975-990 (2010)

21) Shanmugam, G. High-density turbidity currents: are they sandy debris flows? *Journal Sedimentary Research* 66 (1), 2-10 (1996),

22) Leclair, S. F. & Arnott, R. W. C. Coarse-tail, graded, structureless strata: indicators of an internal hydraulic jump, in Roberts, H.H., Rosen, N.C., Filion, R.H., & Anderson, J.B. eds., *Shelf Margin Deltas and Linked Down Slope Petroleum Systems: Global Significance and Future Exploration Potential*. SEPM, Gulf Coast Section, Houston, 817-836 (2003)

23) Cartigny, M. J. B., Ventra, D., Postma, G. & Van Den Berg, J. H. Morphodynamics and sedimentary structures of bedforms under supercritical-flow conditions: New insights from flume experiments. *Sedimentology* 61, 712-748 (2014)

24) Postma, G., Cartigny, M. & Kleverlaan, K. Structureless, coarse-tail graded Bouma Ta formed by internal hydraulic jump of the turbidity current? *Sedimentary Geology* 219, 1-6 (2009)

25) Baas, J. H. Conditions for formation of massive turbiditic sandstones by primary depositional processes. *Sedimentary Geology* 166, 293-310 (2004),

26) Marr, J. G., Harff, P. A., Shanmugam, G. & Parker, G. Experiments on subaqueous sandy gravity flows: the role of clay and water content in flow dynamics and

depositional structures. *Geological Society of America Bulletin* 113 (11), 1377-1386 (2001),

27) Vrolijk, P. J. & Southard, J. B. Experiments on rapid deposition of sand from high-velocity flows. *Geoscience Canada* 24 (1), 45-54 (1997)

28) Wilson, K. C. Bed-load transport at high shear stresses. *Journal of the Hydraulic Division* 92 (6), 49-59 (1966)

29) Dohmen-Janssen, C. M., & Hanes, D. M. Sheet flow dynamics under monochromatic nonbreaking waves. *Journal of Geophysical Research* 107 (C10), 3149, doi: 10.1029/2001JC001045 (2002)

30) Abrahams, A. D Bed-load transport equation for sheet flow. *Journal of Hydraulic Engineering* 129 (2), 159-163 (2003)

31) Middleton, G. V. Experiments on density and turbidity currents III. Deposition of sediment. *Canadian Journal of Earth Science* 4, 475-505 (1967)

32) Sohn, Y. H. On traction-carrpet sedimentation. *Journal of Sedimentary Research* 67(3), 502-509 (1997)

33) Parkash, B., & Middleton, G. V. Downcurrent textural changes in Ordovician turbidite greywackes *Sedimentology* 14, 259-293 (1970)

34) Gao, P. Transition between two transport regimes: saltation and sheet flow. *Journal of Hydraulic Engineering* 134 (3), 340-349 (2008)

35) Hassan, W. N. & Ribberink, J. S. Transport processes of uniform and mixed sands in oscillatory sheet flow. *Coastal Engineering* 52, 745-750 (2005)

36) Hernandez-Moreira, R. R., Huffman, B. J., Vautin, D., Kendal, C. G. St. C. & Viparelli, E. Bedload transport, bedform geometry and flow resistances of upper regime plane beds. *Journal of Geophysical Research – Earth Surface* (in review).

37) Abrahams, A. D. & Gao, P. A bed-load transport model for rough turbulent open-channel flows on plane beds. *Earth Surface Processes and Landforms* 31, 910-928 (2006)

38) Yokokawa, M., Takahashi, Y., Yamamura, H., Kishima, Y., Parker, G. & Izumi, N. Phase diagram for antidunes and cyclic steps based on suspension index, non-dimensional Chezy resistance coefficient and Froude number. *Proceedings River, Coastal and Estuarine Morphodynamics RCEM 2011* (2011)

39) Nnadi, F. N. & Wilson, K. C. Motion of contact-load particles at high shear stress. *Journal of Hydraulic Engineering* 118 (12), 1670–1684 (1992)

40) Pugh, F. J. & Wilson K. C. Velocity and concentration distributions in sheet flow above plane beds. *Journal of Hydraulic Engineering* 125 (2), 117–125 (1999)

41) Dohmen-Janssen, C. M., Hassan, W. N. & Ribberink, J. S. Mobile-bed effects in oscillatory sheet flow. *Journal of Geophysical Research: Oceans*, 106 (C11), 27,103–27,115 (2001),

42) Pirmez, C. & Imran, J. Reconstruction of turbidity currents in a meandering submarine channel. *Marine and Petroleum Geology* 20 (6-8), 823-849 (2003)

43) Sequeiros, O.E., Spinewine, B., Beaubouef, R. T., Sun, T., Garcia, M. H. & Parker, G. Bedload transport and bed resistance associated with density and turbidity currents. *Sedimentology* 57, 1463-1490 (2010),

44) Spinewine, B., Sequeiros, O.E., Garcia, M. H., Beaubouef, R. T., Sun, T., Savoye, B. & Parker, G. Experiments on wedge-shaped deep sea sedimentary deposits in minibasins and/or on channel levees emplaced by turbidity currents. Part II. Morphodynamic evolution of the wedge and of the associated bedforms. *Journal of Sedimentary Research* 79, 608-628 (2009)

45) Parker, G., Paola, C. & Leclair, S. Probabilistic Exner sediment continuity equation for mixtures with no active layer. *Journal of Hydraulic Engineering* 126 (11), 818-826 (2000)

46) Gray, J. M. N. T. & Ancey, C. Segregation, recirculation and deposition of coarse particles near two-dimensional avalanche fronts. *Journal of Fluid Mechanics* 629, 387-423 (2009)

47) Hill, K. M. & Tan, D. S. Segregation in dense sheared flows: gravity, temperature gradients, and stress partitioning. *Journal of Fluid Mechanics* 756, 54-88 (2014)

48) Babonneau, N., Savoye, B., Cremer, M. & Bez, M. Sedimentary architecture in meanders of a submarine channel: detailed study of the present Congo turbidite channel (Zaire Project). *Journal of Sedimentary Research* 80, 852-866 (2010)

49) Parker, G. 1D sediment transport morphodynamics with applications to rivers and turbidity currents. Copyrighted e-book freely downloadable at http://hydrolab.illinois.edu/people/parkerg/morphodynamics_e-book.htm (2004).

50) Dietrich, W. E. Settling velocity of natural particles. *Water Resources Research* 18(6), 1615–1626 (1982)

3.4. FIGURE CAPTIONS

Figure 3.1. Massive units in a) tempestite— Ordovocian Cincinnati Group, USA—, and b) turbidite— Aberystwyth Grits, South Wales—deposits (http://sepmstrata.org/)

Figure 3.2. Dip (left) and strike (right) stratigraphic sections for each experiment. The white lines represent the approximate location of the equilibrium deposit surface and the yellow arrows identify the two laminae deposited in the 6 kg/min experiment.

Figure 3.3. Vertical variation of the geometric mean diameter, D_g, in the deposit emplaced in the aggradation phase of the experiments. D_{go} denotes the geometric mean diameter of the original mixture, z is an upward oriented coordinate with origin on the equilibrium deposit and $\Delta\eta$ represents the thickness of the layer deposited in the aggradation phase of each experiment. The white diamonds refer to the 20 kg/min experiment, the white squares to the 16 kg/min experiment, the white triangles to the 10 kg/min experiment, the grey squares to the 6 kg/min experiment and the grey triangles to the 1.5 kg/min experiment.

3.5. FIGURES

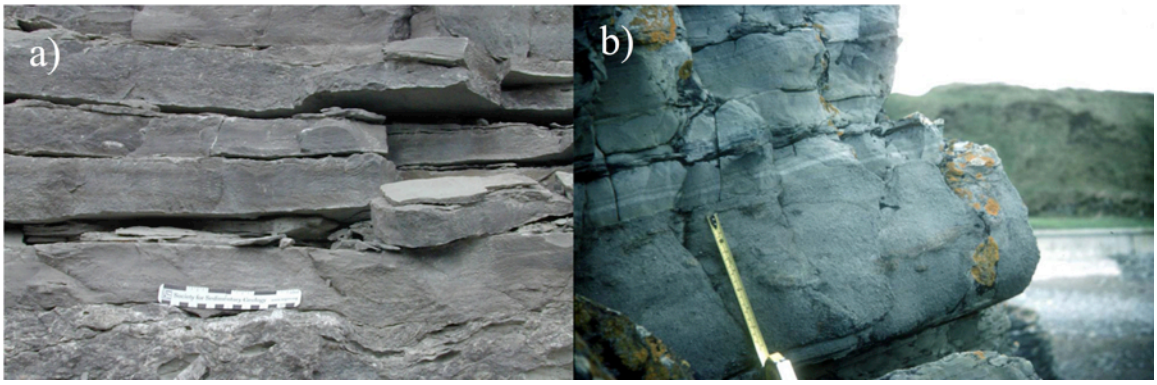

Figure 3.1. Massive units in a) tempestite —Ordovocian Cincinnati Group, USA—, and b) turbidite —Aberystwyth Grits, South Wales— deposits (http://sepmstrata.org/)

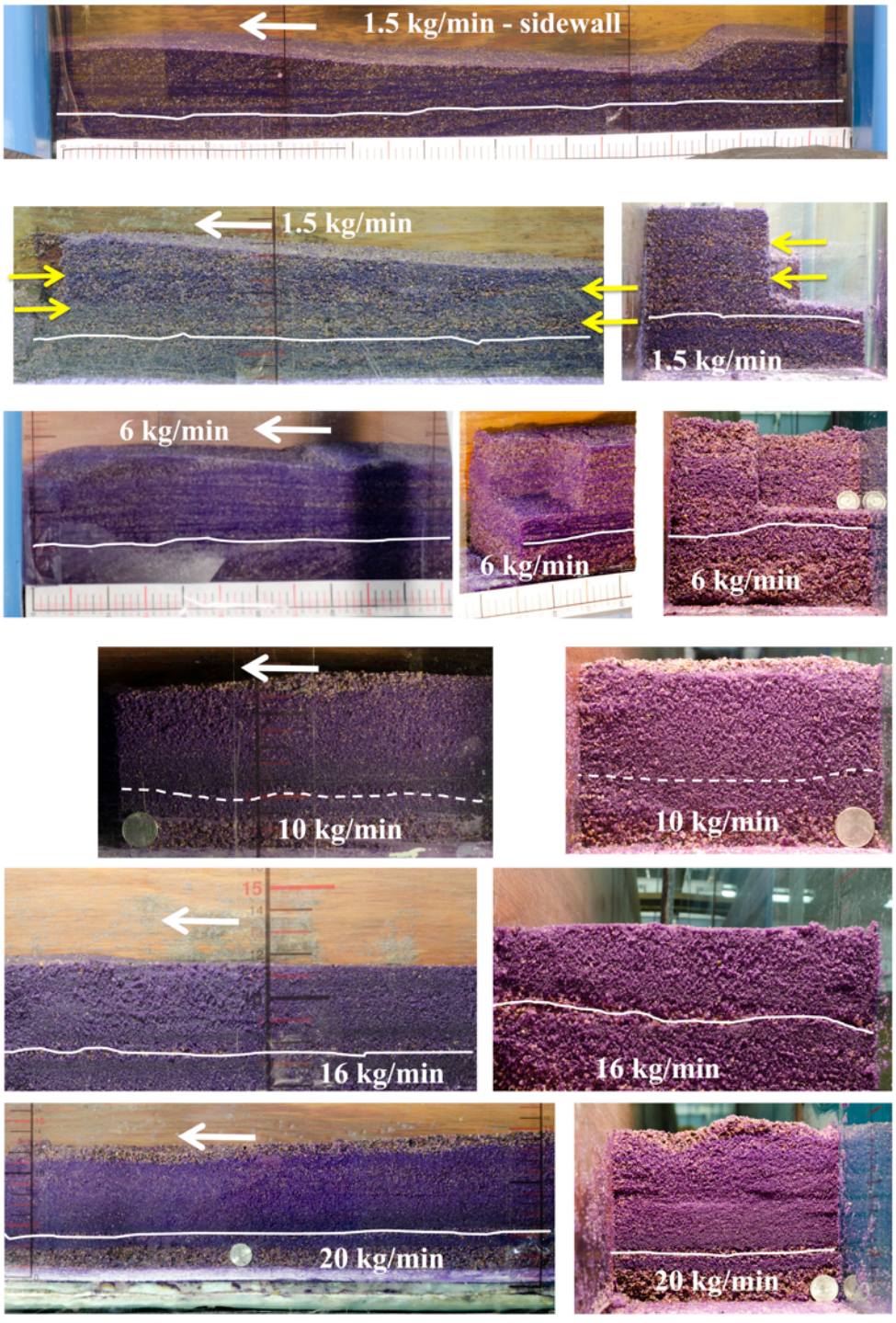

Figure 3.2 . Dip (left) and strike (right) stratigraphic sections for each experiment. The white lines represent the approximate location of the equilibrium deposit surface and the yellow arrows identify the laminae deposited in the 1.5 kg/min experiment.

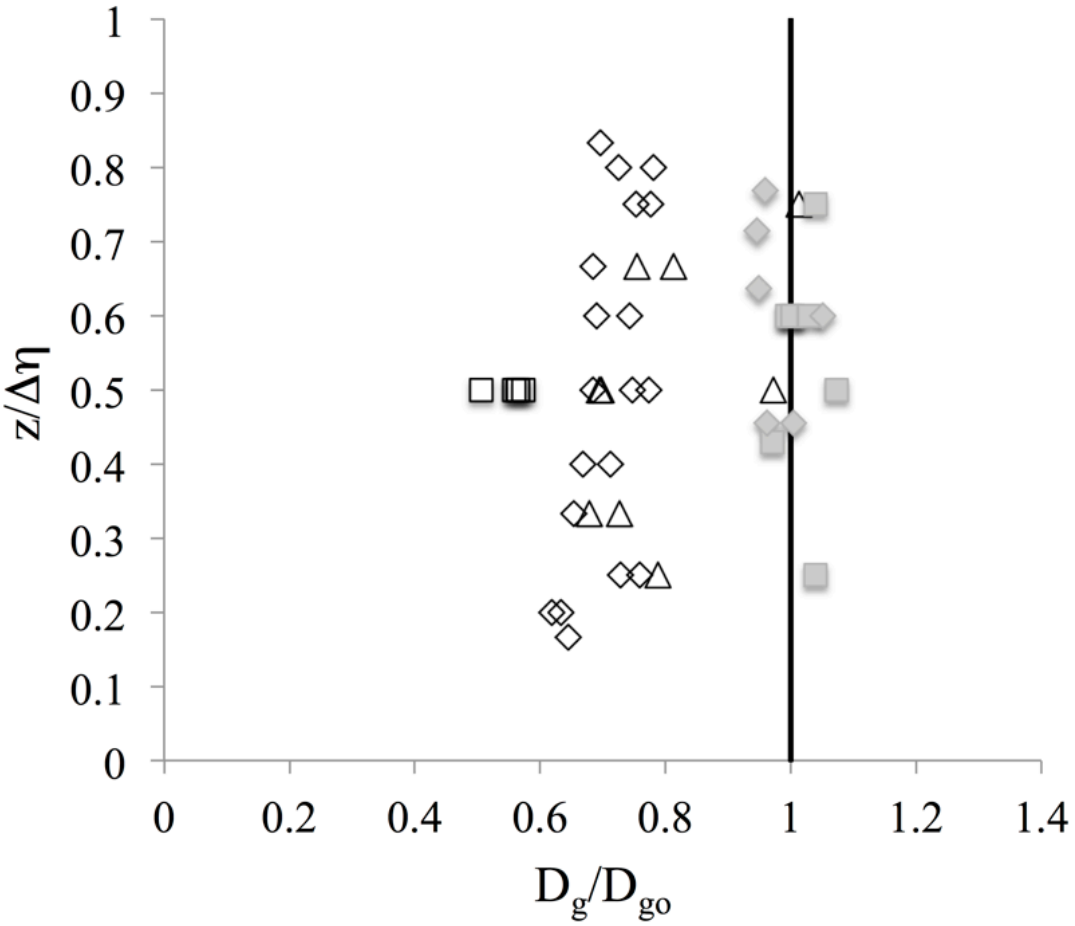

Figure 3.3. Vertical variation of the geometric mean diameter, D_g, in the deposit emplaced in the aggradation phase of the experiments. D_{go} denotes the geometric mean diameter of the original mixture, z is an upward oriented coordinate with origin on the equilibrium deposit and $\Delta\eta$ represents the thickness of the layer deposited in the aggradation phase of each experiment. The white diamonds refer to the 20 kg/min experiment, the white squares to the 16 kg/min experiment, the white triangles to the 10 kg/min experiment, the grey squares to the 6 kg/min experiment and the grey triangles to the 1.5 kg/min experiment.

3.6. TABLE

Table 3.1. Quantitative summary of the experimental results at mobile bed equilibrium. The flow rate was equal to 30 l/s. G_s = mass feed rate, H = water depth, S = bed slope, D_{sg} = geometric mean diameter of the bed surface, D_{s90} = diameter such that 90% of the bed surface is finer, τ_s^* = Shields number associated with skin friction, Δ = bedform height, λ = bedform wavelength and Lt = bedload layer thickness. In the last column of Table 3. 1 the equilibrium bed configuration (upper plane bed UP, downstream migrating antidune DA, and upper plane bed with sheet flow UPS) is reported.

G_s	H	S	D_{sg}	D_{s90}	τ^*_s	Δ	λ	Lt	Equilibrium
kg/min	cm		mm	mm		mm	cm	mm	configuration
1.5	21.2	0.0032	0.95	1.85	0.10	50	85	2.5	UP
6	12.8	0.0086	1.01	1.65	0.41	50	50	3	DA
10	11.8	0.0117	1.00	1.45	0.56	20	65	5	DA
16	10.2	0.0151	0.78	1.24	0.78	-	80	7.5	UPS
20	10.2	0.0168	1.09	1.63	0.66	-	90	15	UPS

3.7. METHODS

The experiments were performed in the 13 m long, 0.5 m wide and 0.9 m deep sediment feed flume of the hydraulic laboratory of the Department of Civil and Environmental Engineering at the University of South Carolina at Columbia. The flow rate was supplied from the head tank of the laboratory and was measured with a calibrated orifice plate and a wet-wet digital manometer.

The sediment trap was located 9 m downstream of the flume entrance. The flume cross section was narrowed to 0.19 m with marine plywood in the upstream most 9 m of the flume to reduce the likelihood of having three dimensional bedforms and to obtain sheet flow bedload transport with feasible sediment feed rates. The flume cross section was gradually narrowed in the upstream most 2 m of the flume, leaving a 7 m long test reach. The water surface elevation downstream of the sediment trap, i.e. the water surface base level, was controlled with a tailgate.

Experimental procedure

The experiments started with an empty flume. As the flow and the sediment feed were turned on a deltaic deposited formed with a downstream migrating delta front. When the delta front reached the sediment trap, periodic measurements of bed and water surface elevation were performed with rule readings from the glass flume sidewall. When the bed and the water surface elevation and slopes did not significantly change between consecutive readings, we assumed that the flow and the sediment transport reached conditions of mobile bed equilibrium[1,2]. Three-five readings of bed and water surface elevation were collected at equilibrium to estimate the equilibrium slopes and water

depths used to estimate the bed shear stresses. Thus, the equilibrium water depths, slopes and the other parameters reported in Table 3. 1 and used in the calculations have to be considered averages over a long series of bedforms.

Pictures and videos of the equilibrium deposit were taken from the glass flume sidewall to estimate the thickness of the bedload layer, the average bedform height and wavelength and the aggradation phase of the experiments started.

Aggradation of the bed deposit was then induced by slowly raising the tailgate at a constant rate. This caused the deposition of a layer of nearly uniform thickness on the entire test reach with a negligible change of the bed configuration. Depending on the sediment feed rate, the aggradation rate changed from one experiment to the other with higher rates of aggradation in the experiments with the highest feed rate. The aggradation phase of each experiment ended when a ~5 cm thick deposit was emplaced.

During the aggradation phase periodic measurements of bed and water surface elevation were collected to monitor that the water surface and the bed slopes did not significantly change from their equilibrium values. At the end of the aggradation phase, we took pictures of the deposit from the glass flume sidewall, one central dip and several strike stratigraphic sections were cut and photographed to characterize the internal fabric. Core samples were then collected and dried in the oven to measure the spatial (vertical and streamwise) variation of the grain size distribution in the emplaced deposit.

3.7.1. PROCEDURE TO REMOVE SIDEWALL EFFECTS

The experiments were performed in a narrow flume, i.e. the width was 0.19 m and the water depths ranged between 0.210 m and 0.102 m, thus a procedure to remove sidewall

effects was necessary to account for the different roughness between the smooth flume sidewalls (glass and plywood) and the mobile rough bed[3]. We followed the procedure to remove sidewall effects proposed by Vanoni and Brooks[3] and outlined in Chiew and Parker[4] and Viparelli et al.[1].

The main assumption is that the cross section can be divided in two non-interacting regions, the bed region and the wall region, and the Darcy–Weisbach resistance relation can be applied to the entire cross section and to each region. It is further assumed that in the entire cross section, in the bed and in the wall region 1) the streamwise component of gravity force is balanced by shear stresses acting on the wall and on the bed, and 2) the mean flow velocities, U, and energy gradients, S, are the same. Under these assumptions the equations of conservation of mass and momentum respectively take the form

$$A = A_b + A_w \tag{3.1}$$

$$C_f P = C_{fb} P_b + C_{fw} P_w \tag{3.2}$$

with A denoting the cross sectional area, P the wetted perimeter and C_f the non-dimensional friction coefficient equal to the Darcy-Weisbach friction coefficient f divided by 8. The absence of subscript indicates that the parameter refers to the entire cross section, and the subscripts b and w respectively denote the bed and wall region.

Recalling that the Darcy-Weisbach relation holds in the entire cross section and in each region, the condition that the energy gradients are assumed to be the same in the entire cross section and in each region is expressed as

$$\frac{C_f U^2}{gr} = \frac{C_{fb} U^2}{gr_b} = \frac{C_{fw} U^2}{gr_w} \tag{3.3}$$

where g represents the acceleration of gravity and r the hydraulic radius. Recalling that the Reynolds number is defined as $Re = rU/\nu$ with ν denoting the water kinematic viscosity, equation (3.3) can be rewritten as

$$\frac{C_f}{Re} = \frac{C_{fb}}{Re_b} = \frac{C_{fw}}{Re_w} \tag{3.4}$$

Equations (3.1), (3.2) and (3.4) represent a system of three equations in four unknowns, A_b, A_w, C_{fb}, C_{fw}. The equation used to close the problem is the Nikuradse equation for smooth pipes that takes the form

$$\frac{1}{\sqrt{f_w}} = 0.86\left(4Re_w\sqrt{f_w}\right) - 0.8 \tag{3.5}$$

Equations (3.1), (3.2), (3.4) and (3.5) are iteratively solved using the following form of the Blasius equation to estimate the Darcy-Weisbach friction coefficient for smooth pipes in the first iteration

$$f_w = 0.301\left(\frac{f}{Re}\right)^{\frac{1}{5}} \tag{3.6}$$

3.7.2. Partition between skin friction and form drag.

The friction coefficient for the bed region C_{fb} is used to compute the sidewall corrected bed shear stress τ^* as $\rho C_{fb} U^2$. When bedforms are not present the drag on the bed is only associated with the stresses acting tangentially to the bed (skin friction). In the presence of bedforms, part of the drag is primarily associated with the flow separation downstream of the lee faces (form drag) and does not contribute directly to the bedload transport[5]. It is thus necessary to partition between skin friction and form drag to perform bedload transport calculations[5].

In the case an ideal flow over a flat bed with the same microscopic roughness, energy gradient, S, and mean flow velocity, U, of the flow in the presence of bedforms, the roughness height, the bed friction and the associated water depth have to be smaller than the corresponding values for the original flow[5]. Thus, the friction coefficient and the water depth that characterize this ideal flow, i.e. the values associated with skin friction C_{fbs} and H_s, can be computed with a Manning-Strickler formulation with roughness height $k_s = 2D_{s90}$, with D_{s90} denoting the diameter of the bed surface such that 90% of the sediment is finer, and the depth slope product to compute the bed shear velocity associated with skin friction, u_s^*.

The system of equations used to compute C_{fbs} and H_s takes the form

$$C_{fbs}^{-0.5} = \frac{U}{u_s^*} = 8.1\left(\frac{r_{bs}}{k_s}\right)^{\frac{1}{6}} \tag{3.7}$$

$$u_s^* = \sqrt{r_{bs} g S} \tag{3.8}$$

$$r_{bs} = \frac{A_{bs}}{B} \tag{3.9}$$

with A_{bs} denoting the area of the bed region associated with skin friction and B the width of the rectangular flume cross section.

3.8. References to the Methods section

1) Viparelli, E., Solari, L. & Hill, K. M. Downstream lightening and upward heavying: Experiments with sediments differing in density. *Sedimentology* 62, 1384-1407 (2015).

2) Viparelli, E., Haydel, R., Salvaro, M., Wilcock, P.R. & Parker, G. River morphodynamics with creation/consumption of grain size stratigraphy 1: laboratory experiments. *Journal of Hydraulic Research* 48(6), 715-726 (2010).

3) Vanoni, V.A. ed. *Sedimentation engineering*. ASCE Manuals and Reports on Engineering Practice 54. ASCE, New York (1975).

4) Chiew, Y. and Parker, G. Incipient sediment motion on non-horizontal slopes. *Journal of Hydraulic Research* 32, 649–660 (1994).

5) Parker, G. *1D sediment transport morphodynamics with applications to rivers and turbidity currents*. Copyrighted e-book freely downloadable at http://hydrolab.illinois.edu/people/parkerg/morphodynamics_e-book.htm (2004).

3.9. ACKNOWLEDGMENT

The dataset has been made publicly available through the assistance of the Sediment Experimentalist Network (SEN) (NSF 1324660). The students participating in the experiments were supported by the NSF grant EAR-1250641, by the last author's start-up fund. The University of South Carolina Support for Minority Advancement in Research Training (SMART) Program supported Sydney Sanders.

3.10. AUTHOR CONTRIBUTIONS

Ricardo Hernandez Moreira designed the experiments, led experimental work, performed the analysis of the results and participated in the preparation of this manuscript.

Sadegh Jafarinik participated in the experiments and in the interpretation of the results and participated in the preparation of this manuscript.

Sydney Sanders participated in the experiments and performed the grain size distribution analysis.

Bradley Huffman participated in the experiments and was responsible for collecting images and videos during the experimental runs.

Christopher G. St. C. Kendall participated in the design of the experiments, in the interpretation of the results and in the preparation of this manuscript.

Gary Parker participated in the design of the preliminary experiments (not reported herein), in the interpretation of the preliminary results, in the analysis of the experiments presented herein, and helped with the preparation of this manuscript.

Enrica Viparelli designed and performed the preliminary experiments (not reported herein), participated in the design of the experiments presented herein, in the interpretation of the results and in the preparation of this manuscript.

3.11. SUPPLEMENTARY FIGURE

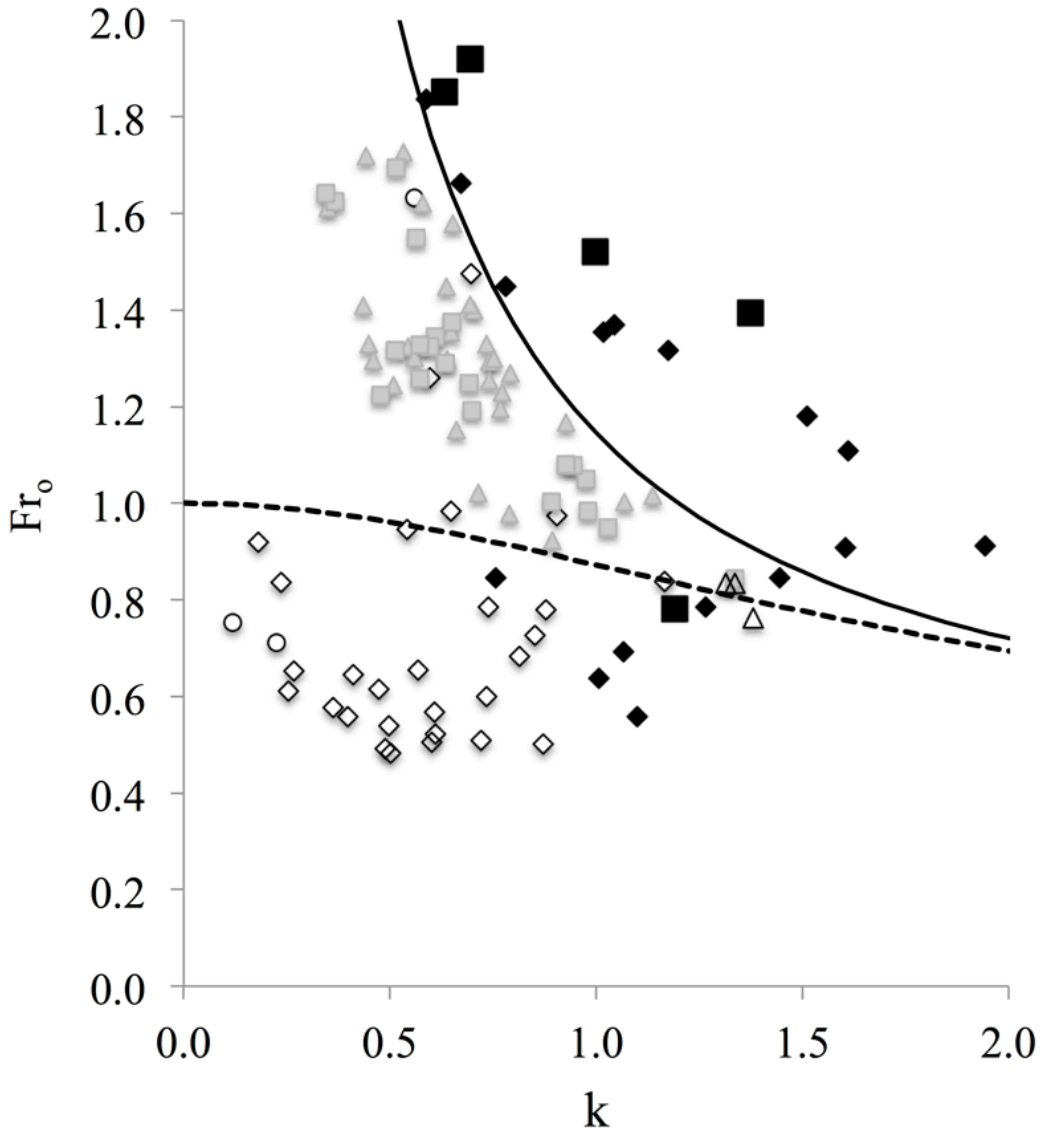

Figure 3.4. Bedform stability diagram[1]. The non-dimensional wave number k = $2\pi H_o/\lambda$ where H_o denotes the water depth of an idealized flow with the same flow rate, slope and mean velocity of the observed flow and a roughness height equal to the roughness height associated with skin friction, i.e. no form drag. The Froude number Fro is the Froude number of the associated idealized flow. The black squares are our experiments with mix-size sediment, the diamonds represent our experiments with uniform sediment[2], the white diamonds and triangles are the Guy et al.[3] and the Kennedy[4] transitional experiments, the white circles are the Guy et al.[3] upper plane bed experiments, the grey triangles are the Guy et al.[3] antidune experiments and the grey squares are the Kennedy[4] antidune experiments.

3.12. Supplementary Figure References

1) Engelund, F. Instability of erodible beds. *Journal of Fluid Mechanics* 42, 225–244 (1970).

2) Hernandez-Moreira, R. R., Huffman, B. J., Vautin, D., Kendal, C. G. St. C. & Viparelli, E. Bedload transport, bedform geometry and flow resistances of upper regime plane beds. *Journal of Geophysical Research – Earth Surface* (in review).

3) Guy, H., Simons, D. & Richardson E. *Summary of alluvial channel data from flume experiments, 1956-61*, Geological Survey Professional Paper no. 462-I (1966).

4) Kennedy, J. F. *Stationary waves and antidunes in alluvial channels*, Ph.D. thesis, California Institute of Technology (1960).

CHAPTER 4

PROBABILISTIC DESCRIPTION OF UPPER PLANE BED CONFIGURATIONS[3]

4.1. INTRODUCTION

Careful comparisons of active layer-based model predictions with field and laboratory data indicate that active layer-based models are useful tools to study transport, erosion and deposition of non-uniform material when the vertical sediment fluxes are primarily controlled by temporal changes in the mean channel bed elevation - aggradation or degradation. However, such comparisons also indicate that active layer-based models are inadequate to describe sediment transport processes in the presence of bedforms and to route sediment particles with different characteristics. In other words, active layer-based models cannot capture key details in certain systems, such as tracer and contaminant dispersal (e.g. Hassan and Church, 1994; Ferguson et al., 2002; Wong et al., 2007) and sediment sorting in the presence of bedforms (Blom and Parker 2004; Blom, 2008; Ganti et al., 2013). In these systems the sediment fluxes are primarily related to local changes in bed elevation that occur at time scales that are short compared to those associated with the changes in mean bed elevation. Finally, these models fail to capture the spatial

[3] Ricardo R. Hernandez Moreira and Enrica Viparelli. In preparation for submission to *Esurf*.

variation in sediment size distribution of alluvial channels due to changes in flow regime and sediment transport characteristics, such as the infiltration or winnowing of fine sediment in a coarse alluvial bed due to imposed changes in flow and sediment transport regime when channel bed aggradation or degradation are negligible (e.g. Viparelli et al., 2011).

The proposed model is based on a modified version of the continuous probabilistic modeling framework proposed by Parker, Paola, and Leclair (2000) – PPL framework - that describes the exchange of sediment between the bedload transport and the mobile bed in terms of probability density functions of bed elevation, entrainment and deposition. However, due to the lack of functional relations to predict 1) local entrainment rates of sediment in transport, 2) probability of bed elevation fluctuation, and 3) probabilities of entrainment and deposition, has never been fully implemented and tested against experimental results. Simplified versions of the PPL framework were implemented by Blom et al. (2006) and Blom et al. (2008) to describe the stratigraphy of dune deposits at laboratory scale, Parker and Perg (2005) to estimate on cosmogenic nuclides concentration based erosion rates in badlands and landscapes dominated by deepseated landslides, and Viparelli et al. (2016) to demonstrate that the implementation of the continuous approach is feasible at field scale and that, given appropriate boundary conditions, the model results are in reasonable agreement with field observations. In summary, the implementation of the continuous modeling framework with physically-based probability functions represents the first foundational step to overcome the well-know limitations of the ~50-year old active layer approximation.

Here we present the analysis of sonar based time series of bed elevation measurements to determine probability functions of bed elevation fluctuations around the mean elevation to statistically represent the short time scale fluctuations as a function of the flow hydrodynamics and the mode of bedload transport. This analysis represents the first step towards the implementation of a probabilistic model that is able to reproduce the internal fabric of the emplaced deposits. Here we illustrate the probabilistic model for the simplified case of tracer stone dispersal in uniform sediment.

4.2. UPPER REGIME PROBABILITY FUNCTIONS OF BED ELEVATION FLUCTUATIONS BEDLOAD DOMINATED SYSTEMS

In the experiments presented in Chapter 2 sonar-based time series of bed elevations were recorded for mobile bed equilibrium conditions at six equally spaced locations within the test reach. Descriptive statistics of the time series data are obtained from their frequency histograms with bin width of 2.5 mm. A complete statistical analysis of these time series goes well beyond the scope of the present chapter. Here the time series are used to 1) provide a preliminary characterization of the bed configuration in terms of time series of bed elevation (Parker, et al., 2000; Blom et al., 2006; Blom, 2008; Wong et al., 2007; Singh et al., 2009; Singh et al., 2011), 2) investigate if the variability of bed elevation in the upper regime can be represented in terms of probability functions, and if these probability functions can be parameterized to model the transition from upper regime plane bed with standard bedload transport to upper regime plane-bed with bedload transport in sheet flow mode as a function of the flow parameters, and 3) use the probability functions to estimate the bedform height.

4.2.1. DESCRIPTION OF THE TIME SERIES

Noting that the sonar measurements were performed at mobile bed equilibrium, when the bed elevation averaged over many bedforms did not change in time, the variability of bed elevation is represented in terms of fluctuations around the mean.

As schematically represented in Figure 4.1, if η denotes the instantaneous bed elevation and $\bar{\eta}$ denotes the average bed elevation (dashed black line), the bed elevation fluctuation η' equals $\eta - \bar{\eta}$. If $\eta' < 0$, $\eta < \bar{\eta}$. Similarly if $\eta' > 0$, $\eta > \bar{\eta}$ (Parker et al., 2000).

For example, the time series of bed elevation fluctuations measured in the 1.5_{30} experiment (i.e. the uniform sediment experiment with flow rate of 30 l/s and sediment feed rate of 1.5 kg/min) are presented in Figure 4.2, where the panels are ordered in the streamwise direction so that the topmost figure corresponds to measurements collected at x = 3.68 m (i.e. 3.68 m downstream of the flume entrance), the next panel refers to measurements performed at x = 4.68 m and the bottommost figure reports measurements performed at x = 8.68 m. The panels show that both the height and the period of the bedforms increased as they migrate downstream, suggesting the existence of a bedform development region in the upstream part of the test reach. The visual comparison between the time series suggests that in the 1.5_{30} experiment this development region ends around x = 5.68 m, corresponding to the location of the fourth sonar probe. A formal analysis to determine the length of the development region is not attempted herein.

To exclude the developing bedforms from the analysis and to avoid including possible bed deformations driven by the sudden flow expansion at x = 8.68 m, we used of the measurements of the probe located at x = 7.68 m as basis for the analysis presented

herein. Figure 4.3 shows time series of fluctuations of bed elevation and corresponding probability density functions for different feed rates at flume location x = 7.68 m. As the feed rate and thus the Shields number associated with skin friction increased, the fluctuations become more frequent and their height decreases. In other words, as previously reported from visual observations, as the Shields number associated with skin friction increases the bedform height decreases.

4.2.2. PROBABILITY FUNCTIONS OF BED ELEVATION FLUCTUATIONS

If we draw a horizontal line at the generic elevation z in one of the time series reported in Figures 2 and 3, the fraction of the line that falls within the bed deposit represents the average fraction of time that $\eta > z$. In other words, the fraction of the line that falls within the bed deposit at elevation z, $P_s(z)$, can be interpreted as the probability that $\eta > z$. Thus, $P_e = 1 - P_s$ represents the probability that the bed elevation is smaller or equal than z, i.e. the cumulative distribution function of the bed elevation fluctuations. Following Blom et al. (2006) in the analysis presented herein we use the upward oriented coordinate $y = z - \bar{\eta}$, which is a monotonically increasing function of z. Consequently, in the y coordinate system, $P_s(y) = P_s(z)$, $P_e(y) = P_e(z)$, the probability density function of bed elevation fluctuations $p_e = -\frac{\partial P_s}{\partial y}$ and the mean of the probability density of bed elevation fluctuation is known and equal to zero.

The cumulative distribution functions of bed elevation fluctuations of our experimental data are presented in the normal probabilistic charts of Figure 4.4, where the black grid lines denote the 90% interval around the mean and the experimental data have been grouped into four different plots for clarity. In each of the subfigures (a)–(d), the

points represent the cumulative probability function of bed elevation fluctuations around the mean estimated from the time series, and the dashed lines represent the normal distribution function fitted to each series.

As the feed rate, and thus the Shields number associated with skin friction, gradually increased, the distribution functions became less wide due to the reduction of bedform height observed in Chapter 2. Figure 4.4 also shows that the probability functions of bed elevation fluctuation around the mean can be reasonably approximated as normal within the 90% interval around the median.

A close look at the tails of the distributions, defined herein as the areas outside the 90% interval cantered on the median, revealed that in the experiments with feed rate smaller than 8 kg/min, corresponding to a Shields numbers associated with skin friction smaller than ~0.4, the distributions functions are heavy tailed, suggesting that fluctuations that are significantly larger than the average fluctuation occur frequently. In other words, the presence of heavy tails suggests a higher likelihood of having deep troughs and high crests than in the case of a normal distribution.

These results are consistent with previous experimental work performed in the lower regime with sediments in the pea gravel size range (Wong et al., 2007), in the sand range (Nakagawa and Tsujumoto, 1979 and references therein; Singh et al., 2009; Singh et al., 2011). In particular, Singh et al. (2011) noticed that 1) their distributions were preferentially asymmetric, and 2) at short time scales the probability density function of bed elevation increments had slightly thicker tails than a normal distribution, and it tended toward a normal distribution for relatively long time scales.

Noting that the probability functions of bed elevation fluctuations can be reasonably approximated as normal distributions with zero mean and standard deviation σ, a relation between σ and the flow parameters would allow us to parameterize these functions and model the transition from upper plane bed characterized by standard bedload transport, long wavelenght and small amplitude bedforms to upper plane bed with bedload transport in sheet flow mode.

The statistical parameters of the distributions are summarized in Table 4.1, where the first column identify the experiment with the same notation used in Chapter 2 (the full number identifies the sediment feed rate in kg/min and the subscript the flow rate in l/s), the Shields number associated with skin friction τ_{bs}^* is in the second column, s is reported in mm in the third column, the skewness β_1 and the coefficient of excess kurtosis β_2 are respectively in the fourth and fifth column, and the sonar-based estimate of bedform height $2A$ is reported in the sixth column.

Figure 4.5 shows the variation of the non-dimensional standard deviation made non-dimensional with the sediment geometric mean diameter D_g = 1.11 mm, σ/D_g, with the Shields number associated with skin friction τ_{bs}^*. The black diamonds represent the 30 l/s experiments, the black squares the 20 l/s experiments and the dashed lines the proposed lower and upper limits of the transition region from standard bedload transport to bedload transport in sheet flow mode. The black line is a linear fit to our data of equation

$$\frac{\sigma}{D_g} = \begin{cases} 18.7 - 29.6\tau_{bs}^* & \text{if} \quad \tau_{bs}^* < 0.56 \\ 2 & \text{if} \quad \tau_{bs}^* \geq 0.56 \end{cases} \tag{1}$$

and the dashed grey lines denote a ±30% interval around the proposed predictor.

The three points that fell outside this interval pertain to the 1.5_{20}, 6_{30} and the 8_{30} experiments. As observed in Chapter 2, the latter two experiments characterize the transition from upper plane bed with standard bedload transport to upper plane bed with bedload transport in sheet flow mode with increasing bedform height and thus flow resistances (Kishi, 1979). Finally, the grey line represents Wong et al. (2007) relation linking σ/D with τ_b^* , which is equal to τ_{bs}^* because the experiments were performed in lower-regime plane-bed.

The standard deviation of the distributions σ decreased for increasing values of τ_{bs}^* over the entire range of experiments, as previously observed in terms of the narrowing of the distributions with increasing feed rates in Figure 4.4. However, in the 20 l/s runs σ was consistently smaller than in the 30 l/s runs characterized by the same feed rates. The 30 l/s runs showed a slight increase of σ in the transition zone compared to the runs with $\tau_{bs}^* < 0.3$, while σ did not significantly changed in the 1.5_{20} and 8_{20} runs.

The prediction of a standard deviation of the bed elevation fluctuations that decreases with τ_{bs}^* is in contrasts with the results by Wong et al. (2007) who found that for the case of gravel transport in lower regime plane bed with $\tau_{bs}^* < 0.11$, higher τ_{bs}^* lead to higher variance in the bed elevation fluctuations (Figure 5). Wong et al. (2007) explained their result considering that σ scales with the characteristic particle grain size and is a measure of occupation and evacuation of individual particles on the surface of the bed. In our case, due to the presence of bedforms, σ decreases as the Shields number associated with skin friction increases and the bed tends to flatten out.

4.2.3. THE HIGH ORDER MOMENTS OF THE PROBABILITY DISTRIBUTION OF BED ELEVATION FLUCTUATION

When looking at the shape of the distribution, to attempt a meaningful parametric description, it is necessary to consider the higher moments of the distributions together and not piecewise, since both the skewness and kurtosis are needed together to establish peakedness and tailedness unambiguously. Figures 4.6a and 4.6b respectively show the variation of the skewness coefficient, β_1, and the coefficient of kurtosis excess—hereinafter referred to simply as kurtosis— β_2 with the Shields number associated with skin friction τ_{bs}^*. The black diamonds represent the 30 l/s experiments, the black squares the 20 l/s experiments. The vertical dashed black lines at τ_{bs}^* equal to 0.3 and 0.5 identify the transition region from standard bedload transport to bedload transport in sheet flow mode.

The skewness coefficient (Figure 4.6a) for the 30 l/s experiments are grouped such that far away from the transition region β_1 is positive and relatively large, while for values of τ_{bs}^* close to the transition region, β_1 is small and oscillates around zero. These results suggest that the bed elevation tends to be preferentially smaller than mean due to the presence of deep bedform troughs for values of τ_{bs}^* significantly smaller than 0.3, while the distribution of bed elevation tends to become symmetrical as the mode of bedload transport transitions from standard bedload transport to sheet flow. In the 20 l/s experiments β_1 maintains negative, almost constant values of β_1 = ~0.17, across the range of experiments, denoting a nearly symmetrical distribution in the presence of bedforms with a poorly defined brinkpoint. Due to the relatively small size of the time series, we

cannot confidently comment on the sign of β_1 in the experiments with bedload transport in sheet flow mode.

Figure 4.6b shows that the kurtosis β_2 follows similar behaviors for both sets of experiments, i.e. does not seem to be dependent of the flow depth. For $\tau_{bs}^* < 0.5$, β_2 = ~0.8, denoting a tendency to obtain distributions that may be flatter than normal. As τ_{bs}^* approaches 0.5, corresponding to the onset of bedload transport in sheet flow mode, β_2 becomes positive denoting that the distributions tend to have higher peaks than a normal distribution.

Positive skewness, $\beta_1 > 0$ suggest bedforms exhibiting deep troughs and long stosses, resulting in long and slow local net erosional processes on the stoss of the bedform and relatively rapid and intense local net depositional processes on the lee faces of the bedforms. Negative skewness $\beta_1 < 0$ conversely suggests the presence of relatively symmetrical bedforms, with local net erosional and net depositional processes that occur at similar rates. Noting that the skewness is relatively small (smaller than 1.7), except for the lowest and highest range of experiments, the distributions may be considered symmetrical.

The kurtosis is associated with a movement of mass of the distribution that does not affect its variance (De Carlo, 1997). Negative kurtosis is related to light tails and flat, low peaks (Balanda and Mac Gillivray, 1988; De Carlo, 1997), if present, in the distributions. Referring to Figure 4.6b and the probability density functions in Figure 4.4 we note the absence of peaks in the experimental runs with negative kurtosis, suggesting a relatively flat distribution for the large variability in the bedform heights.

Positive kurtosis, paired up with positive skewness may be indicative of fat tailed distributions, suggesting that most of the bedforms exhibit approximately the same height fluctuating about the mean bed elevation, while the remaining few are infrequent enough and far away enough from the mean to qualify as relatively frequent extreme events and impact the variability of the distribution.

Summarizing, the study of the variability of β_1 and β_2 with the Shields number associated with skin frictions further confirms the experimental observations presented in Chapter 2. As τ_{bs}^* approaches 0.3, the bedforms tend to become more symmetrical with the consequent reduction in skewness and the kurtosis remains negative due to the relatively frequent migration of large bedforms with deep throughs. In the transition region with $0.3 < \tau_{bs}^* < 0.5$, the bedform height decreases with a movement of the mass towards the center of the distribution, i.e. big bedforms are less frequent than at lower values of τ_{bs}^*. Due to this change in bedform height, β_2 changes sign denoting a high concentration of fluctuations near and around the mean. Finally, in the upper plane bed region with bedload transport in sheet flow mode, $\tau_{bs}^* > 0.5$, the bed elevation fluctuations are very fast and with height on the order of $2D_g$. Consequently, the probability density functions of bed elevation fluctuations become very narrow with peaks that may be higher than in the normal distribution case. Predictive relations of β_1 and β_2 as a function of the flow and the sediment parameters are not fitted to the calculated coefficients because they are not needed to parameterize the probability distribution functions of bed elevation fluctuation.

4.3. PROBABILISTIC-BASED PREDICTIONS OF BEDFORM HEIGHT AND IMPLICATIONS TO ESTIMATE THE ACTIVE LAYER THICKNESS

A representative sonar-based bedform height was defined as the difference in elevation between the fluctuations around the mean bed elevation with cumulative probabilities equal to 0.05 and 0.95. In other words, the sonar based bedform height was characterized by the 90% interval around the mean bed elevation. This interval was chosen after comparing sonar-based estimates of bedform height for different interval amplitudes with the observed heights and the 90% interval showed the best agreement between sonar-based heights and observations.

The best agreement was determined based on the number of points contained within a ±25% interval in a sonar-based vs. observed bedform height, as presented in Figure 4.7a. In Figure 4.7a the points corresponding to the 10_{30} and the 12_{30} runs are both characterized by sonar-based bedform heights that are significantly smaller than the visual observations identifying the possibility of errors in the visual observations.

Figure 4.7b shows the sonar-based bedform heights $2A$ as functions of the Shields number associated with skin friction τ_{bs}^{*}, with the black squares and black diamonds denoting the 20 l/s and 30 l/s experiments respectively and the dashed lines marking the apparent lower and upper bounds of the transition region between standard bedload transport and sheet flow transport. The variation of sonar based bedform height with skin friction shows a similar behaviour as that of the observed bedform heights discussed in Chapter 2. Bedform heights decrease with increasing feed rate, first gradually and then sharply, as the mode of sediment transport transitions from standard bedload transport to bedload transport in sheet flow mode. As for the visual observations, two transitional

paths are captured in the transition region: one in which the bedform height decreases continuously as τ_{bs}^* increases, and one in which the bedform height grows with τ_{bs}^* before sharply decreasing. These two paths are in agreement with the analysis by Kishi (1979) based on data collected in experiments with finer material.

4.4. Towards the implementation of a continuous model of sediment mass conservation for tracer stones in uniform material

The two-dimensional equation of sediment conservation at location x and elevation z in the bed deposit in the case of uniform bed material takes the form (Parker et al., 2000)

$$c_b \frac{\partial P_s}{\partial t} = D_z - E_z \qquad (2)$$

with z denoting an upward oriented vertical coordinate, x a streamwise longitudinal coordinate and t a temporal coordinate; c_b represents the volume fraction of the deposit that is solid at elevation z and it is equal to $1 - \lambda_p$, where λ_p is the bed porosity, assumed constant for simplicity. $P_s = P_s(x, z, t)$ denotes the probability that the bed elevation is higher than z, thus $c_b P_s$ represents the volume of sediment at elevation z per unit area of the bed deposit. D_z and E_z respectively represent the deposition and entrainment of sediment at location x and elevation z.

Following the same procedure illustrated in section 2, we introduce the upward oriented vertical coordinate with origin on the channel bed $y = z - \bar{\eta}$ with $\bar{\eta}$ denoting the bed elevation averaged over a series of bed fluctuations, i.e. the mean bed elevation at location x and time t. In the y reference system $P_s(x, z, t) = P_s(x, y, t)$ represents the probability that the bed elevation fluctuation $\eta' = \zeta - \bar{\eta}$, with ζ denoting an instantaneous

realization of bed elevation, is higher than y. The probability that the bed elevation fluctuation is smaller or equal than y will thus be $P_e(x, y, t) = 1 - P_s$. In other words, P_e is the cumulative probability function of bed elevation fluctuations and $p_e = -\partial P_s/\partial y$ is the probability density function of bed elevation fluctuations.

It is important to note here that the y coordinate is attached to the mean bed elevation and it is a function of time because the average bed elevation $\bar{\eta}$ can change in time for channel bed aggradation and degradation. Thus, in the y coordinate system the elevation specific equation of conservation of bed material takes the form (Parker et al., 2000)

$$c_b \left(\frac{\partial P_s}{\partial t} + p_e \frac{\partial \bar{\eta}}{\partial t} \right) = D_y - E_y \tag{3}$$

where $p_e \frac{\partial \bar{\eta}}{\partial t}$ represents a convective flux of sediment associated with the changes in mean bed elevation, and D_y and E_y respectively represent the deposition and the entrainment rate of sediment at elevation y. Parker et al. (2000) propose to evaluate D_y and E_y as a function of the total, i.e. integrated in the y direction over the entire deposit, deposition and entrainment rates of sediment D and E times elevation specific probability functions of deposition p_D and entrainment p_E.

In equation (3) the time rate of change of mean bed elevation $\bar{\eta}$ is computed with the Exner equation of conservation of bed material that takes the form

$$c_b \frac{\partial \bar{\eta}}{\partial t} = D - E = -\frac{\partial q_b}{\partial x} \tag{4}$$

with q_b denoting the volumetric bed material load per unit channel width. Equation (4) expresses the equivalency between the entrainment (D – E) and the divergence ($-\partial q_b/\partial x$) form of the Exner equation. For a complete derivation of equation (4) we refer to Parker et al. (2000) and the references therein.

The elevation specific equation of conservation of tracer stones at location x and elevation z takes the form (Parker, Paola, and Leclair, 2000)

$$c_b \frac{\partial f P_s}{\partial t} = D_z f_{tr} - E_z f \tag{5}$$

where $f = f(x, z, t)$ denotes the volume fraction content of tracer stones at location (x, z) and time t in the bed deposit and $f_{tr} = f_{tr}(x, t)$ is the volume fraction content of tracer stones in transport. In the y coordinate system the equation of conservation of tracer stones takes the form (Parker et al., 2000)

$$c_b \left[f \left(\frac{\partial P_s}{\partial t} + p_e \frac{\partial \eta}{\partial t} \right) + P_s \left(\frac{\partial f}{\partial t} - \frac{\partial f}{\partial y} \frac{\partial \eta}{\partial t} \right) \right] = D p_D f_{tr} - E p_E f \tag{6}$$

With the aid of equation (3), the above equation reduces to

$$c_b P_s \left(\frac{\partial f}{\partial t} - \frac{\partial f}{\partial y} \frac{\partial \eta}{\partial t} \right) = D p_D (f_{tr} - f) \tag{7}$$

To implement equation (7) functional relations expressing the elevation specific probabilities of entrainment and deposition should be available. Unfortunately these relations are not available in the literature and cannot be derived from the time series of bed elevations.

To overcome this problem, we note that the elevation specific probabilities of net entrainment and net deposition can be estimated from the time series of bed elevation. Thus, if the right hand sides of the equations of conservation of sediment mass are expressed in terms of net deposition ΔD and entrainment ΔE, we should be able to use the continuous framework to model the dispersal of tracer stones.

In a time series of bed elevation net deposition occurs when the bed elevation increases in time, and net erosion occurs when the bed elevation decreases in time. At the generic elevation y in the bed deposit, the average fraction of time that the bed elevation increases in time represents the absolute probability of net deposition $p_{a,netD}$, and the

average fraction of time that the bed elevation decreases in time can be interpreted as the absolute probability of net erosion $p_{a,netE}$.

To obtain the elevation specific probabilities of net entrainment and deposition, the absolute probabilities $p_{a,netD}$ and $p_{a,netE}$ have to be multiplied for the probability that the bed is at elevation y, p_e. Thus, the elevation specific probabilities of net deposition, p_{ND} and p_{NE} are defined as

$$p_{ND} = p_{a,netD} p_e \tag{8a}$$

$$p_{NE} = p_{a,netE} p_e \tag{8b}$$

It is important to note here that the integrals of p_{ND} and p_{NE} over the entire bed deposit are not equal to 1. They are respectively equal to F_{ND} and $F_{NE} = 1 - F_{ND}$, respectively representing the average fractions of time that the system is net depositional or net erosional. Examples of elevation specific probabilities of net deposition and net entrainment estimated from the time series of bed elevation fluctuations recorded in the uniform sediment experiments of Chapter 2 with vertical bins of 5 mm are presented in Figure 4.8 for the experiments 1.5_{30}, 8_{30} and 16_{30} corresponding to upper plane bed with standard bedload transport (Figure 4.8a), downstream migrating antidunes (Figure 4.8b) and upper regime with bedload transport in sheet flow mode (Figure 4.8c) respectively.

The conservation of sediment mass at location x and elevation y in terms of net deposition ΔD and entrainment ΔE takes the form

$$c_b \left(\frac{\partial P_s}{\partial t} + p_e \frac{\partial \eta}{\partial t} \right) = \Delta D p_{ND} - \Delta E p_{NE} \tag{9}$$

where

$$\Delta D = \frac{2A}{T_{ND}} \tag{10a}$$

$$\Delta E = \frac{2A}{T_{NE}} \tag{10a}$$

with T_{ND} denoting the average time in which there is net deposition over a wave period T and T_{NE} is the average time in which there is net erosion during a wave period T.

Following Nakagawa and Tsujimoto (1979), the wave celerity c can be computed from the relation

$$q_b = sc_b c2A \tag{11}$$

where c_b is assumed to be equal to 0.6, and s is a shape factor such that s = 0.5 for triangular bedforms and $s = 2/\pi$ for sinusoidal waves. When the wave celerity is known, the wave period T can be computed as

$$T = \frac{\lambda}{c} \tag{12}$$

The variability of c and T with the Shields number associated with skin friction for the uniform sediment experiments of Chapter 2 is presented in Figure 4.9 for s = 0.6. As τ_{bs}^* increases, the period of the fluctuations decreases and the celerity increases and the period of the fluctuations around the mean bed elevation decreases.

Having estimated 1) the average fraction of time in which the system is net depositional, F_{ND}, 2) the average fraction of time in which the system is net erosional $F_{NE} = 1 - F_{ND}$, and 3) the wave period T, the average time that the system is net depositional T_{ND} and the average time that the system is net erosional T_{NE} are defined as

$$T_{ND} = F_{ND}T \tag{13a}$$

$$T_{NE} = (1 - F_{ND})T \tag{13b}$$

The elevation specific equation of conservation of tracer stones at location x and elevation y in terms of net deposition and net entrainment takes the form

$$c_b\left[f\left(\frac{\partial P_s}{\partial t}+p_e\frac{\partial \eta}{\partial t}\right)+P_s\left(\frac{\partial f}{\partial t}-\frac{\partial f}{\partial y}\frac{\partial \eta}{\partial t}\right)\right]=\Delta D p_{ND} f_{ND}-\Delta E p_{NE} f_{NE} \quad (14)$$

With the aid of equation (9), the above equation reduces to

$$c_b P_s\left(\frac{\partial f}{\partial t}-\frac{\partial f}{\partial y}\frac{\partial \eta}{\partial t}\right)=\Delta D p_{ND}(f_{ND}-f)-\Delta E p_{NE}(f_{NE}-f) \quad (15)$$

The last step to implement equation (15) is to compute the net fluxes of tracers, $f_{ND}-f$ and fNE−f. We hypothesize that the net fluxes of tracers can be computed with a step length formulation to compute the entrainment and deposition rates integrated over the bed deposit and to link them with the net entrainment and deposition rates integrated over the bed deposit (Viparelli et al., 2016).

4.5. Conclusions

The analysis of the time series of bed elevation fluctuation shows that in upper regime normal bedload dominated systems, the probability distribution of bed elevation fluctuations around the mean can be reasonable well described in terms of a normal distribution function with zero mean and standard deviation that varies with the Shields number associated with skin friction. In particular, σ decreases for increasing values of τ_{bs}^* in the upper plane bed regime with standard bedload transport and in the downstream migrating antidune configuration - $\tau_{bs}^* < 0.56$. In the upper regime plane bed with bedload transport in sheet flow mode, σ/D is constant and equal to ~2.

The predictive functions that describe the evolution of the standard deviation of the bed elevation fluctuation can be implemented in models of river morphodynamics to quantitatively describe the vertical sediment fluxes that occur during high transport events.

Future work is needed to investigate the possibility of implementing a morphodynamic model that uses the probabilities of bed elevation fluctuations to capture the details of the erosion and deposition that cannot be described with the traditional approach based on the active layer approximation (Parker et al., 2000; Blom et al., 2006; Blom, 2008; Viparelli et al., 2016).

4.6. REFERENCES

Balanda, K. P and H. L. Mac Gillivray, 1988, Kurtosis: a critical review, The American Statistician 42.2, pp. 111–119.

Blom, A., 2008, Different approaches to handling vertical and streamwise sorting in modeling river morphodynamics, Water Resources Research 44.3.

Blom, A., J. S. Ribberink and G. Parker, 2008, Vertical sorting and the morphodynamics of bed form-dominated rivers: A sorting evolution model. Journal of Geophysical Research 113, F01019, doi: 10.1029/2006JF000618.

Blom, Astrid et al., 2006, Vertical sorting and the morphodynamics of bed-form dominated rivers: An equilibrium sorting model, Journal of Geophysical Research: Earth Surface 111.F1. F01006.

Blom, A. and G. Parker, 2004, Vertical sorting and the morphodynamics of bed form-dominated rivers: A modeling framework". In: Journal of Geophysical Research: Earth Surface 109.F2. F02007.

Blom, A., J. S. Ribberink, and H. J. de Vriend, 2003, Vertical sorting in bed forms: Flume experiments with a natural and a trimodal sediment mixture". Water Resources Research 39.2. 1025.

De Carlo, L. T. 1997, On the meaning and use of kurtosis, Psychological methods 2.3, p. 292.

Ferguson, R. I. et al., 2002, Mobility of river tracer pebbles over different time scales', Water Resources Research 38.5, pp. 31–38.

Ganti, V., C. Paola, and E. Foufoula-Georgiou, 2013, Kinematic controls on the geometry of the preserved cross sets". In: Journal of Geophysical Research: Earth Surface 118.3, pp. 1296–1307.

Hassan, M. A. and M. Church, 1994, Vertical mixing of coarse particles in gravel bed rivers: A kinematic model, Water Resources Research 30.4, 1173–1185.

Kishi, T. 1979, Bed forms and hydraulic relations for alluvial streams, Application of Stochastic Processes in Sediment Transport, H. W. Shen and H. Kikkawa. ISBN: 0918334314, 9780918334312. Littleton, CO: Water Resources Publications, LLC. Chap. 1, pp. 1–32.

Nakagawa, H. and T. Tsujimoto, 1979, Characteristics of sediment transport processes on duned beds analyzed by stochastic approach, Bulletin of the Disaster Prevention Research Institute 29.1, pp. 45–63.

Parker, G. and L. A. Perg, 2005, Probabilistic formulation of conservation of cosmogenic nuclides: effect of surface elevation fluctuations on approach to steady state, Earth Surface Processes and Landforms 30.9, pp. 1127–1144.

Parker, G., C. Paola, and S. Leclair, 2000, Probabilistic Exner sediment continuity equation for mixtures with no active layer, Journal of Hydraulic Engineering 126.11, pp. 818–826.

Singh, A. et al., 2009, Experimental evidence for statistical scaling and intermittency in sediment transport rates, Journal of Geophysical Research: Earth Surface 114.F1. F01025.

Singh, A. et al., 2011, Multiscale statistical characterization of migrating bedforms in gravel and sand bed rivers, Water Resources Research 47.12. W12526.

Viparelli, E., Blom, A. and Hernandez Moreira, R. R., Modeling stratigraphy-based GBR morphodynamics, J. Laronne and D. Tsutsumi eds. Gravel Bed River 8. In press.

Viparelli, E., D. Gaeuman, P.R. Wilcock and G. Parker, 2011, A model to predict the evolution of a gravel bed river under an imposed cyclic hydrograph and its application to the Trinity River, Water Resources Research 47, W02533, doi: 10.1029/2010WR009164.

Wong, M. et al., 2007, Experiments On Dispersion Of Tracer Stones Under Lower-Regime Plane-Bed Equilibrium Bed Load Transport, Water Resources Research 43.3.

4.7. FIGURE CAPTIONS

Figure 4.1. Schematic diagram of bed surface elevation variation with time, showing instantaneous realization of bed elevation η (black continuous line), average bed elevation $\bar{\eta}$ (dashed line), bed elevation fluctuation around the mean bed elevation η' (vertical distance separating solid and dashed lines), generic elevation z (horizontal grey line) and fraction of time generic elevation lines falls within the deposit (thick grey lines).

Figure 4.2. Example of the spatial variation of the time series of bed elevation fluctuations η', for the 1.5_{30} experiment.

Figure 4.3. Variation of bed elevation fluctuations with feed rate measured at x = 7.68 m for the 30 l/s experiments and corresponding probability density functions.

Figure 4.4. Cumulative probability distribution functions of bed elevation fluctuations P_e. Black grid lines denote the 90 % interval around the mean. Dashed lines represent normal distribution functions fitted to each series.

Figure 4.5. Variation of non dimensional standard deviation of the probability density of bed elevation fluctuations around the mean bed elevation σ/D_g as a function of the Shields number associated with skin friction τ_{bs}^*. Diamonds represent the 30 l/s experiments. Squares represent the 20 l/s experiments. Dashed lines indicate lower and upper limits of transition region from standard bedload transport. The black line is a linear fit given by Equation (1). Dashed grey lines denote a ±30% interval around the predictor.

Figure 4.6. Variation of the skewness and kurtosis around the mean bed elevation as a function of the Shields number associated with skin friction τ_{bs}^*. Diamonds represent the 30 l/s experiments. Squares represent the 20 l/s experiments. Dashed lines indicate lower and upper limits of transition region from standard bedload transport.

Figure 4.7. a) Relationship between visually observed and sonar-based bedform heights computed with the 90% interval around the mean bed elevation. b) Relationship between sonar-based bedform heights and the Shields number associated with skin friction.

Figure 4.8. Probability of net deposition and net erosion for the 1.5_{30}, 8_{30} and 16_{30} experiments. a) Absolute probabilities of net deposition, b) probability of net deposition, c) probability of net erosion.

Figure 4.9. Estimated bedform periods T (white diamonds) and celerities c (black diamonds) as functions of the Shields number associated with skin friction.

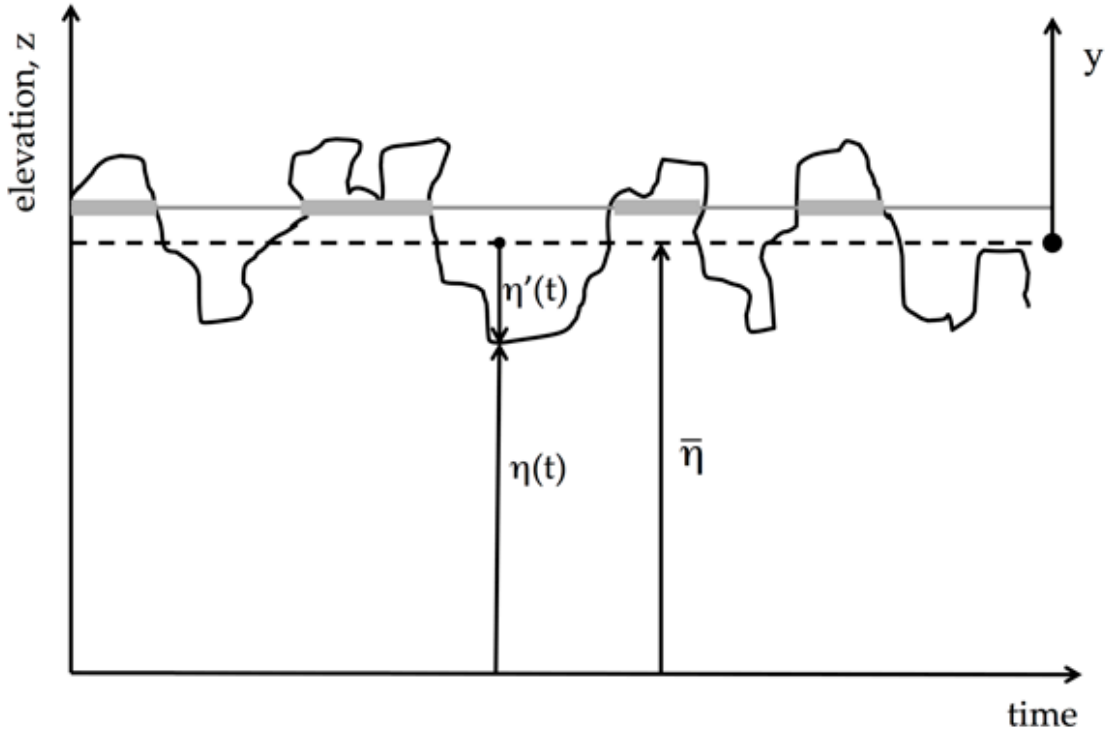

Figure 4.1. Schematic diagram of bed surface elevation variation with time, showing instantaneous realization of bed elevation η (black continuous line), average bed elevation $\bar{\eta}$ (dashed line), bed elevation fluctuation around the mean bed elevation η' (vertical distance separating solid and dashed lines), generic elevation z (horizontal grey line) and fraction of time generic elevation lines falls within the deposit (thick grey lines).

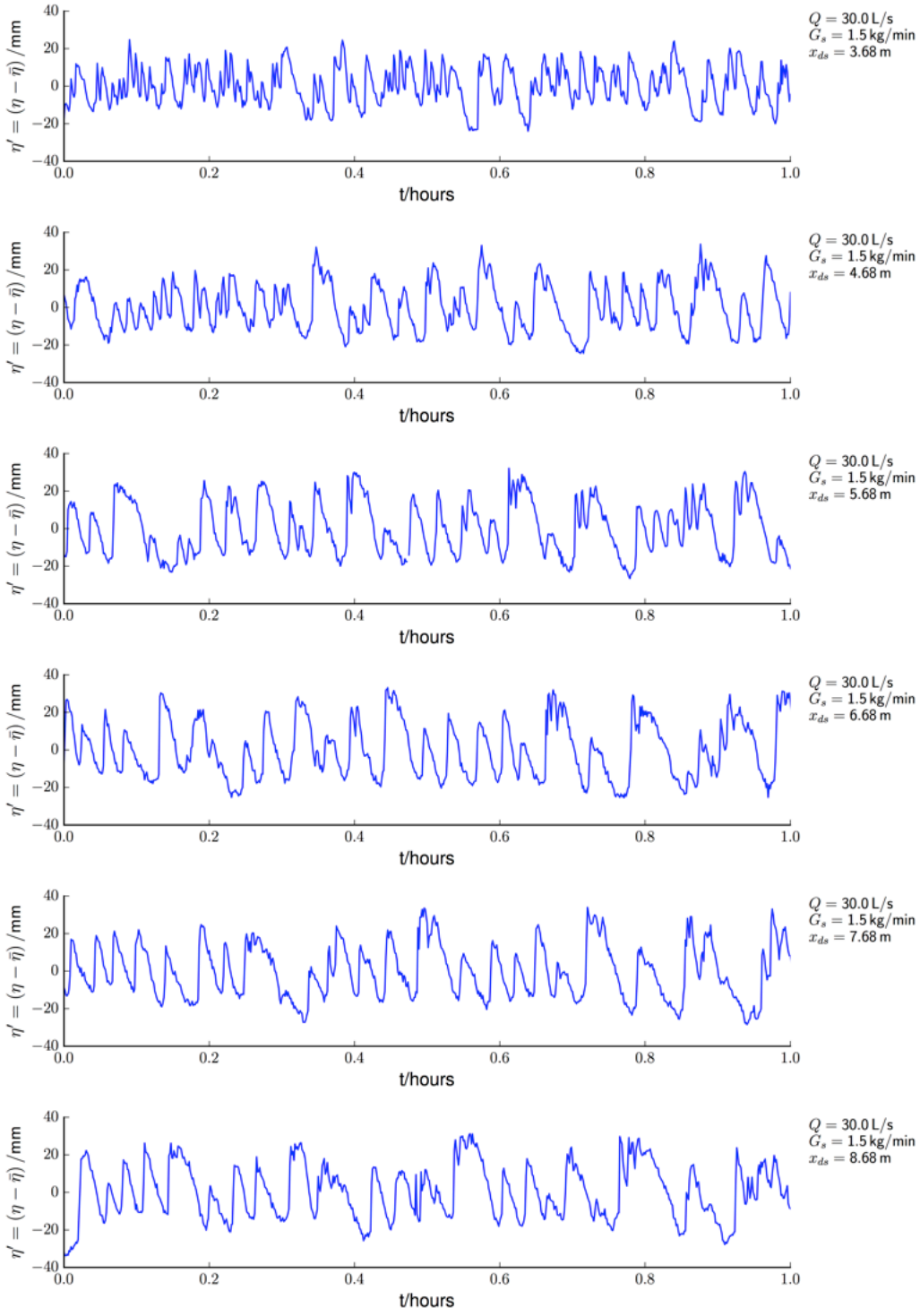

Figure 4.2. Example of the spatial variation of the time series of bed elevation fluctuations η′, for the 1.5_{30} experiment.

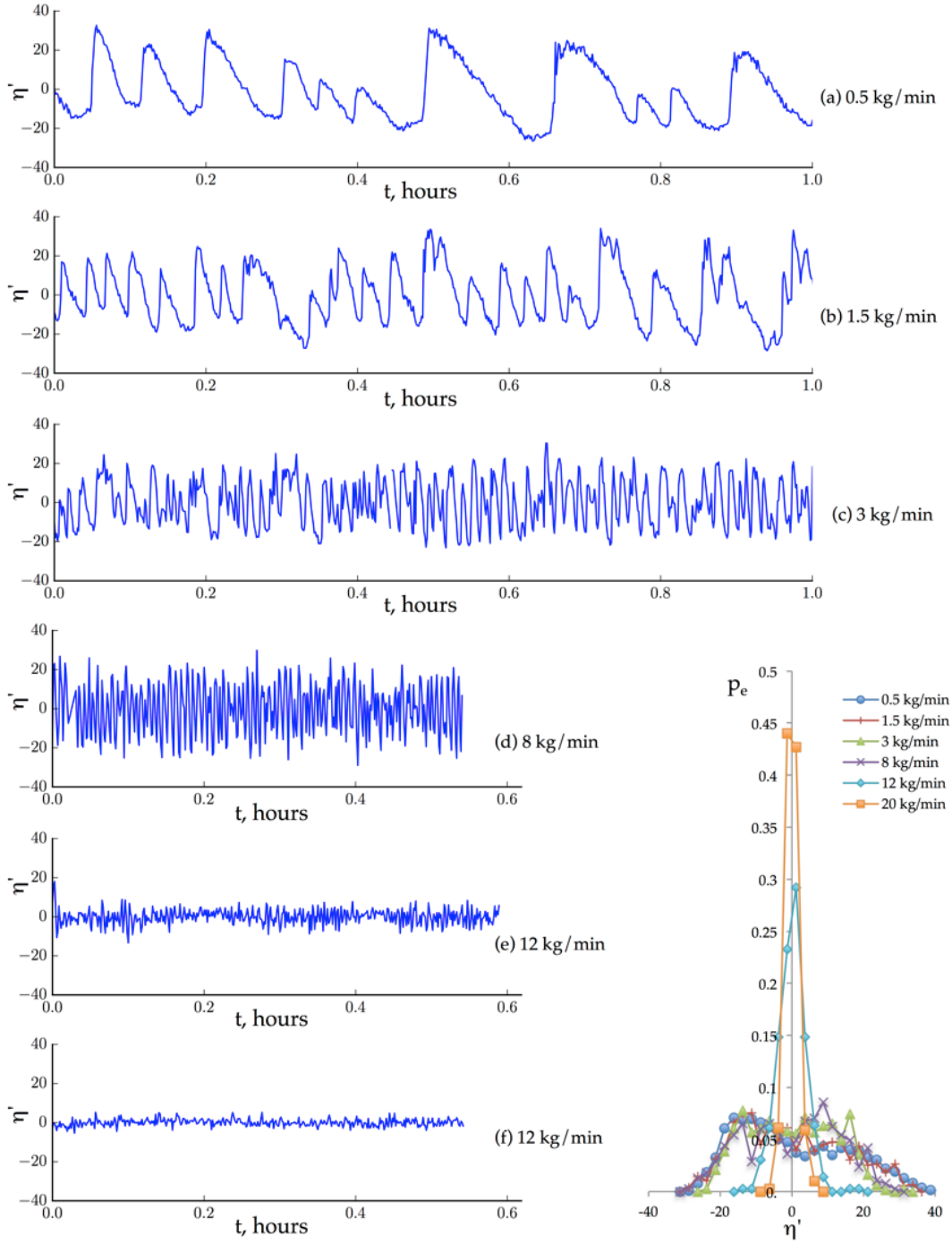

Figure 4.3. Variation of bed elevation fluctuations with feed rate measured at x = 7.68 m for the 30 l/s experiments and corresponding probability density functions.

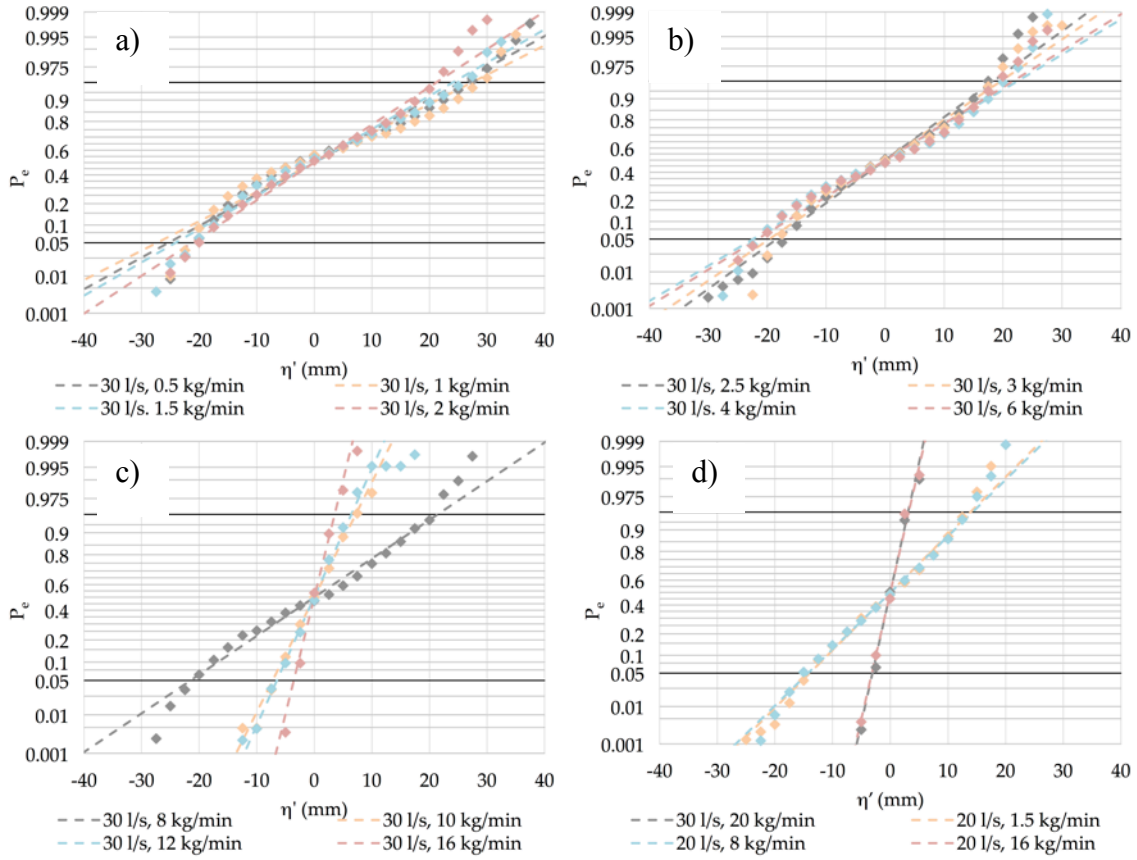

Figure 4.4. Cumulative probability distribution functions of bed elevation fluctuations P_e. Black grid lines denote the 90 % interval around the mean. Dashed lines represent normal distribution functions fitted to each series.

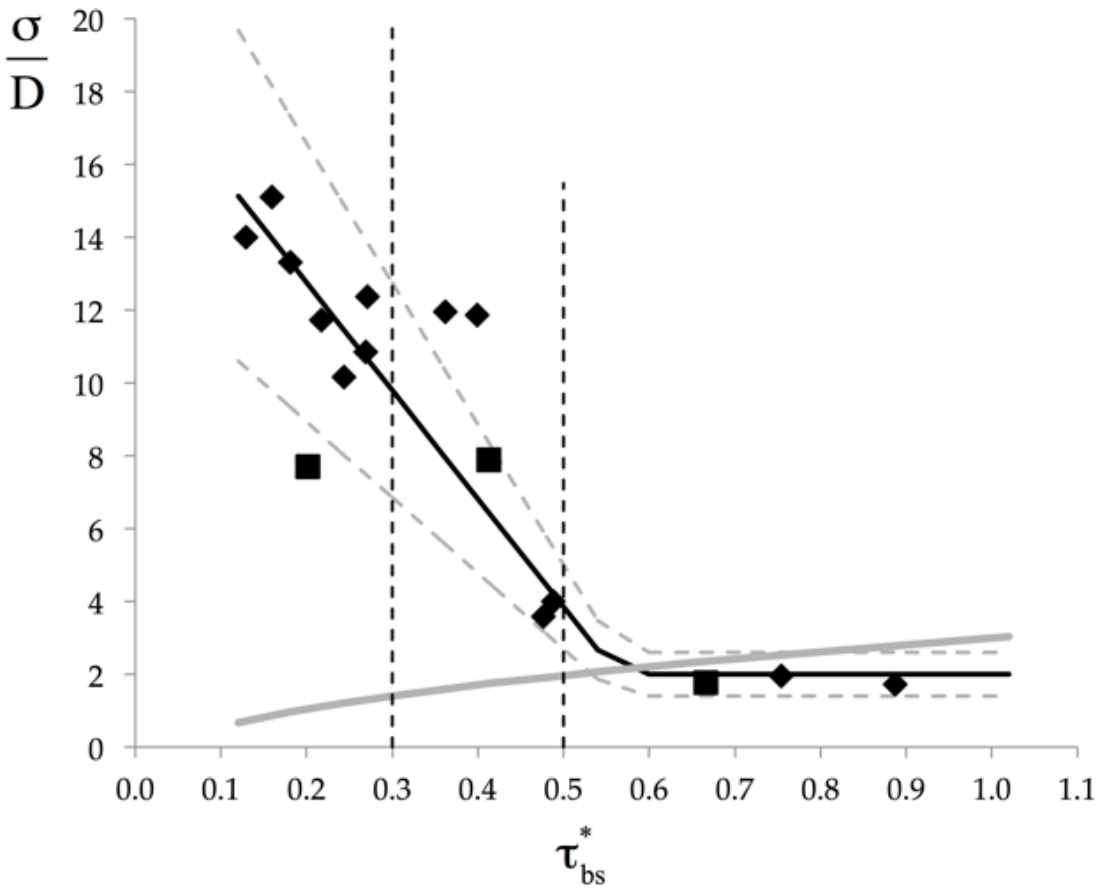

Figure 4.5. Variation of non dimensional standard deviation of the probability density of bed elevation fluctuations around the mean bed elevation σ/D_g as a function of the Shields number associated with skin friction τ^*_{bs}. Diamonds represent the 30 l/s experiments. Squares represent the 20 l/s experiments. Dashed lines indicate lower and upper limits of transition region from standard bedload transport. The black line is a linear fit given by Equation (1). Dashed grey lines denote a ±30% interval around the predictor.

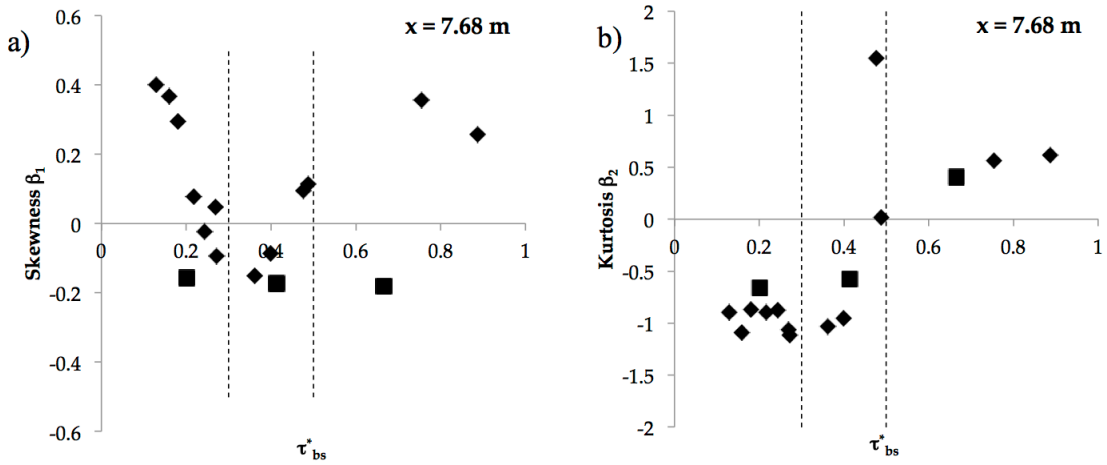

Figure 4.6. Variation of the skewness and kurtosis around the mean bed elevation as a function of the Shields number associated with skin friction τ^*_{bs}. Diamonds represent the 30 l/s experiments. Squares represent the 20 l/s experiments. Dashed lines indicate lower and upper limits of transition region from standard bedload transport.

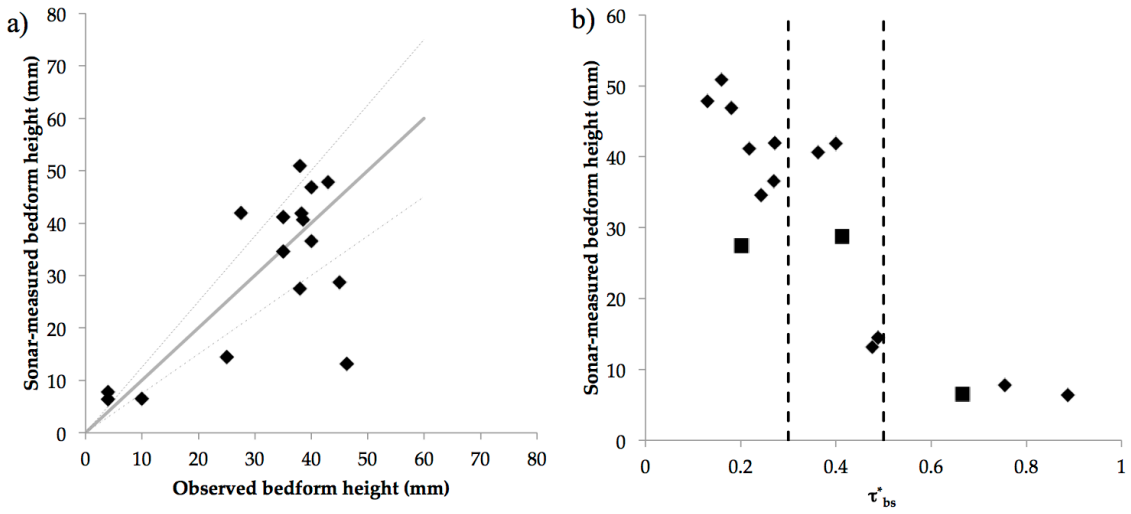

Figure 4.7. a) Relationship between visually observed and sonar-based bedform heights computed with the 90% interval around the mean bed elevation. b) Relationship between sonar-based bedform heights and the Shields number associated with skin friction.

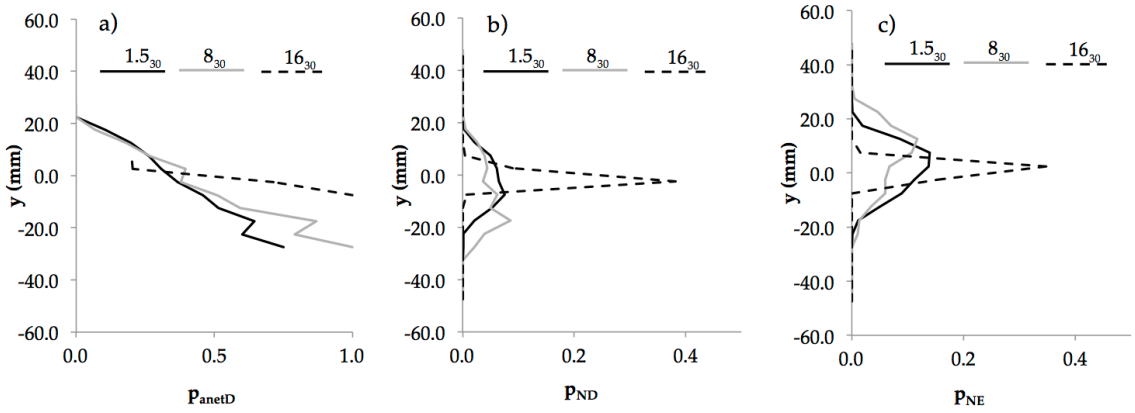

Figure 4.8. Probability of net deposition and net erosion for the 1.5_{30}, 8_{30} and 16_{30} experiments. a) Absolute probabilities of net deposition, b) probability of net deposition, c) probability of net erosion.

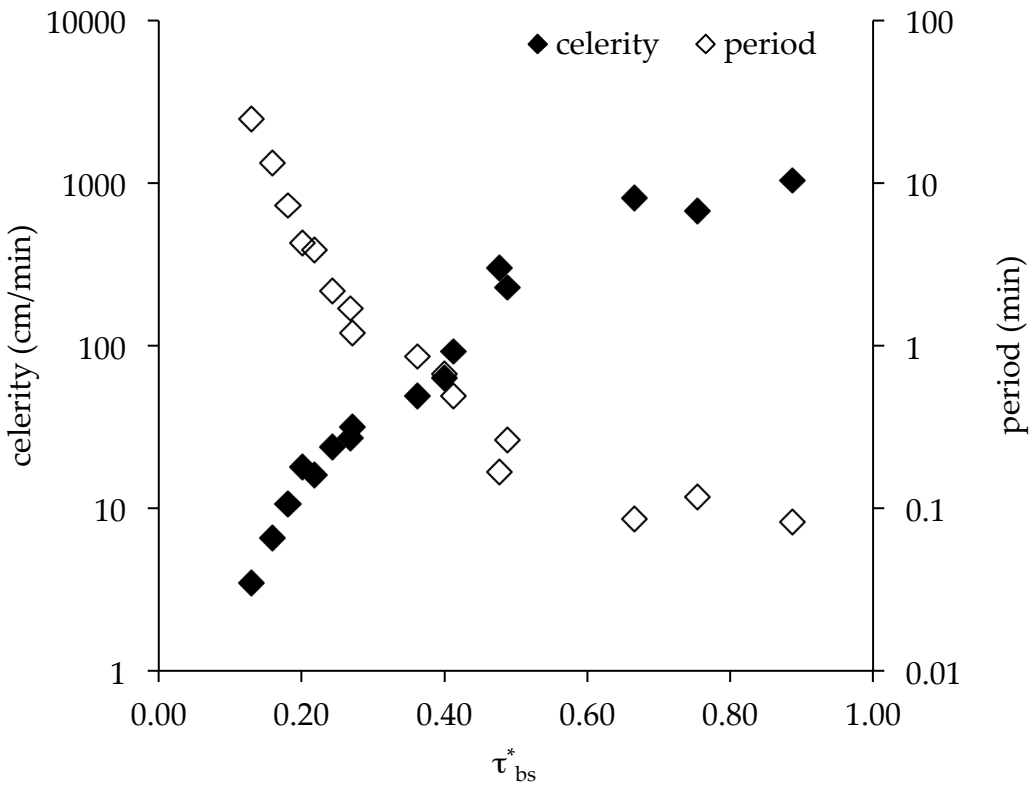

Figure 4.9 Estimated bedform periods T (white diamonds) and celerities c (black diamonds) as functions of the Shields number associated with skin friction.

4.9. TABLE

Table 4.1. Summary of the experimental observations at equilibrium with τ^*_{bs} denoting the Shields number associated with skin friction, σ the standard deviation in mm, β_1 the skewness coefficient, β_2 the coefficient of excess kurtosis, $2A$ the sonar-based bedform height.

Run	τ^*_{bs}	σ mm	β_1	β_2	2A mm
1.5_{20}	0.20	8.5	-0.16	-0.66	27.46
8_{20}	0.41	8.7	-0.17	-0.58	28.75
16_{20}	0.67	1.9	-0.18	0.41	6.50
0.5_{30}	0.13	15.4	0.40	-0.90	47.81
1_{30}	0.16	16.6	0.37	-1.09	50.87
1.5_{30}	0.18	14.7	0.29	-0.87	46.84
2_{30}	0.22	12.9	0.08	-0.90	41.16
2.5_{30}	0.24	11.2	-0.02	-0.87	34.57
3_{30}	0.27	11.9	0.05	-1.06	36.59
4_{30}	0.27	13.6	-0.09	-1.12	41.91
6_{30}	0.36	13.1	-0.15	-1.03	40.64
8_{30}	0.40	13.1	-0.09	-0.96	41.84
10_{30}	0.49	4.4	0.11	0.02	14.46
12_{30}	0.48	3.9	0.10	1.55	13.17
16_{30}	0.75	2.2	0.36	0.56	7.81
20_{30}	0.89	1.9	0.26	0.61	6.37

CHAPTER 5

SUMMARY OF THE RESULTS, CONCLUSIONS AND FUTURE RESEARCH NEEDS

5.1. HYPOTHESIS AND OBJECTIVES

Two research objectives motivated the research work presented herein, 1) testing the hypothesis that a basal massive unit overlying an erosional boundary and underlying a parallel laminated unit in turbidites and tempestites can be emplaced by bedload transport in sheet flow mode, and 2) developing physically-based probability functions of bed elevation fluctuations that can be implemented in vertically continuous morphodynamic models to predict the internal fabric of the deposits.

Two groups of laboratory experiments were performed to meet these research objectives.

The first group of experiments was conducted with uniform sediment to remove the complexities associated with the interactions between grains differing in size. Noting that previous research clearly demonstrated that the parallel laminated units are emplaced under upper regime plane bed with long wavelength and small amplitude bedforms and standard , and that the depositional sequence described above is emplaced by waning energy flows, the experiments were first conducted in upper plane bed configurations with long wavelength and small amplitude bedforms. The sediment transport capacity was then gradually increased to study the conditions that would have produced bedload

transport in sheet flow mode. During the experiments time series of bed elevations were measured with ultrasonic probes. These time series were then analyzed to determine the probability functions of bed elevation fluctuations.

The second group of experiments was performed with a mixture of sediments differing in size to characterize the internal fabric of deposits emplaced in the upper regime plane bed with long wavelength and small amplitude bedforms, in the upper regime plane bed with bedload transport in sheet flow mode and at the transition between the two upper plane bed regimes, which was characterized by downstream migrating antidunes.

5.2. MAIN RESULTS

Noting that bedload transport in the upper regime plane bed with long wavelength and small amplitude bedforms is characterized by a 2-3 grain diameter thick transport layer of non-colliding grains – *standard bedload transport*, and that bedload transport in sheet flow mode occurs with a 10s grain diameter thick near bed layer of colliding grains, the main results of this research effort can be summarized as follows:

1) the transition from upper regime plane bed with standard bedload transport to upper regime planed bed with bedload transport in sheet flow mode is characterized by

a) a gradual increase in the thickness of the bedload layer for $\tau_{bs}^{*} > 0.3$ corresponding to the development of the sheet flow layer,

b) the development of the sheet flow layer is associated with changes in bedform geometry. Bedform wavelengths gradually decrease when $\tau_{bs}^{*} \leq 0.3$, and

gradually increase for $\tau_{bs}^{*} > 0.3$. Bedform heights rapidly drop when the sheet flow layer is fully developed - $\tau_{bs}^{*} > 0.5$, and

c) a transition region, $0.3 < \tau_{bs}^{*} < 0.5$, in which downstream migrating antidunes represent a stable bed configuration when the suspended bed material transport is negligible;

2) in the upper plane bed regime with standard bedload transport, form drag should not be neglected in the calculations of flow resistances. The analysis of our data with previous experiments in the same bed configurations suggests that the form drag decreases as the product between the Froude number and the ratio H/D to the 0.25 power increases;

3) the comparison between downstream and upstream migrating antidunes in open channel flow experiments reveals that

a) they occur in the same range of Froude numbers,

b) they migrate downstream when suspended bed material transport is negligible,

c) downstream migrating antidunes are characterized by larger values of the ratio between flow depth and bedform height, and

d) the aspect ratio of the dowsntream migrating antidunes is smaller than in the case of upstream migrating bedforms. The same qualitative observations were performed in laboratory experiments on bedload transport driven by density currents;

4) upper regime plane bed with bedload transport in sheet flow mode can be interpreted as a stable bed configuration that separates upstream and downstream migrating antidunes in systems with relatively coarse bed material;

5) in the upper regime experiments the probability distribution functions of bed elevation fluctuations around the mean can be reasonably well described in terms of a normal distribution function with zero mean and standard deviation that varies with the flow conditions;

6) in the upper regime experiments the standard deviation of the bed elevation fluctuations, σ, varies with the bedload transport capacity and thus with the Shields number associated with skin friction,

a) σ decreases for increasing values of τ_{bs}^{*} in the upper plane bed regime with standard bedload transport and in the downstream migrating antidune configuration - $\tau_{bs}^{*} < 0.56$, and

b) in the upper regime plane bed with bedload transport in sheet flow mode, the ratio between σ and the characteristic sediment size is constant and equal to ~2.

6) parallel laminated deposit are emplaced in upper regime plane bed with standard bedload transport and with downstream migrating antidunes. As the Shields number associated with skin friction increases, the antidunes flatten out, the sheet flow layer develops and the deposits become massive. This observation is explained considering that the thin upper portion of the laminae is emplaced becasue of the upstream movement of fine sediment in the flow separation zone. As the bedforms are washed out and the sheet flow layer develops, the flow separation on the lee side of the bedforms becomes less evident (form drag decreases – point 2), the fine sediment is not trapped in the separation zone and the parallel laminae cannot form;

7) in the experiments the transition from a parallel laminated to a massive unit is associated with a change in the grain size distribution of the deposit with the massive

deposits being significantly finer than the laminated units. This is likely the result of particle segregation in the sheet flow layer, with the fine sediment preferentially transported near the bed and the coarse sediment preferentially transported in the upper part of the sheet flow layer.

5.3. New research questions

The experiments and the analysis of the time series of bed elevation fluctuations presented in this thesis motivated research questions that could not be answered in the present work due to the lack of experimental data and basic knowledge.

When plotted in the Engelund (1970) stability diagram, the points pertaining to the experiments with bedload transport in sheet flow mode fall near the curve separating upstream and downstream migrating antidunes, suggesting that the upper plane bed with bedload transport in sheet flow mode can be interpreted as a stable bed configuration separating the region with upstream migrating bedforms from the region with downstream migrating bedforms. Theoretical work and additional experiments are needed to investigate if the bedload transport in sheet flow mode can be interpreted as a stable bed configuration at the transition between upstream and downstream migrating upper regime bedforms in bedload dominated systems.

The comparison between the experiments presented herein on bedload transport and the experiments performed by Yokokawa et al. (2011) and Cartigny et al. (2014) reveal that upper regime bedforms evolve differently under increasing energy flows. In suspension dominated systems upstream migrating antidunes evolve into cyclic steps form. In bedload dominated systems downstream migrating antidunes evolve into a flat

bed with bedload transport in sheet flow mode. Experiments and theoretical analyses are necessary to investigate the role of suspended sediment transport on bedform morphodynamics. This work will also provide fundamental insights to differentiate between bed material and wash load in suspension dominated systems.

Finally, theoretical and numerical work is needed to investigate the possibility of implementing a continuous morphodynamic framework that uses the probabilities of bed elevation fluctuations, entrainment and deposition to model the sediment fluxes between the mobile bed and the bedload transport and reproduce the internal fabric of the emplaced deposits (Parker et al., 2000; Blom et al., 2006; Blom, 2008; Viparelli et al., 2016). The analysis of the time series can provide physically-based estimates of probability functions of bed elevation fluctuations, but cannot give information on the probabilities of entrainment and deposition. Fine scale granular physics models might be able to provide the probability functions of entrainment and deposition. The granular physics models, however, are too computationally intensive to reproduce the laboratory scales considered in this work. Thus, these models have to be carefully scaled up to laboratory and field conditions relevant for the problems studied herein.